ESD-TR-89-236

②

AD-A217 330

Algorithms for Optimal Processing
of Polarimetric Radar Data

L.M. Novak
M.B. Sechtin
M.C. Burl

6 November 1989

Lincoln Laboratory

MASSACHUSETTS INSTITUTE OF TECHNOLOGY

LEXINGTON, MASSACHUSETTS

90   03   091

The ESD Public Affairs Office has reviewed this report, and it is releasable to the National Technical Information Service, where it will be available to the general public, including foreign nationals.

This technical report has been reviewed and is approved for publication.

FOR THE COMMANDER

Hugh L. Southall

Hugh L. Southall, Lt. Col., USAF
Chief, ESD Lincoln Laboratory Project Office

MASSACHUSETTS INSTITUTE OF TECHNOLOGY
LINCOLN LABORATORY

ALGORITHMS FOR OPTIMAL PROCESSING OF POLARIMETRIC RADAR DATA

L.M. NOVAK
M.B. SECHTIN
M.C. BURL
Group 47

PROJECT REPORT TT-73

6 NOVEMBER 1989

Accession For	
NTIS GRA&I	☒
DTIC TAB	☐
Unannounced	☐
Justification	
By	
Distribution/	
Availability Codes	
Dist	Avail and/or Special
A-1	

LEXINGTON   MASSACHUSETTS

ABSTRACT

This report describes algorithms that make optimal use of polarimetric radar information to detect and classify targets in a ground clutter background. The optimal polarimetric detector (OPD) is derived; this algorithm processes the complete polarization scattering matrix (PSM) and provides the best possible detection performance from polarimetric radar data. Also derived is the best linear polarimetric detector, the polarimetric matched filter (PMF); the structure of this detector is shown to be related to simple polarimetric target types. Finally, the polarimetric whitening filter (PWF) is derived; this constant false alarm rate (CFAR) detector provides a simple alternative to the OPD for detecting targets in clutter. New K-distributed polarimetric target and clutter models are described; these models are used to predict the performance of the OPD, the PMF, and the PWF. The performance of these three algorithms is compared with that of simpler detectors that use only amplitude information to detect targets. The ability to classify target types by exploiting differences in polarimetric scattering properties is also discussed.

TABLE OF CONTENTS

LIST OF ILLUSTRATIONS

LIST OF TABLES

EXECUTIVE SUMMARY

Under DARPA sponsorship, M.I.T. Lincoln Laboratory is conducting a broad-based research effort to (1) develop an understanding of the phenomenology of polarimetric radar data and (2) relate this phenomenology to the performance achievable by target detection and classification algorithms that use polarimetric radar data. In order to develop the mathematical framework from which optimal polarimetric detectors and classifiers can be derived, a clear understanding of polarimetric radar returns is necessary. This understanding is also necessary for predicting and analyzing the performance of various polarimetric detectors and classifiers. This, in turn, will allow the development of viable stationary-target detection and classification systems. Such systems have application in surveillance, fire control, and target-seeker systems. This report summarizes some of the recent work in the area of stationary target detection and classification using polarimetric radar information.

To investigate the detection and classification performance improvement achievable through the use of fully polarimetric radar data, statistical models of targets and clutter were first developed based on available polarimetric target and clutter data. From these models, new algorithms were derived for optimal processing of the polarimetric radar data. These new algorithms--the optimal polarimetric detector (OPD), the polarimetric matched filter (PMF) and the polarimetric whitening filter (PWF)--were compared with a variety of non-polarimetric algorithms (i.e., algorithms that use only single-polarimetric-channel returns to detect targets). Also, detection performance for radars using circularly polarized data was investigated.

Based on a limited polarimetric clutter data base and a target data base of turntable measurements, our performance predictions suggest that the target detection performance achievable using the OPD or the PMF is not significantly better than that achievable using simpler, single-polarimetric-channel radar detectors. Furthermore, to implement the OPD or PMF requires prior knowledge of the target and clutter polarization covariances; this would be impractical, since clutter covariances vary widely and are highly unpredictable. Therefore, we developed a more practical algorithm (the adaptive polarimetric whitening filter, or APWF), which estimates the clutter covariance from the local clutter statistics.

Although polarization information may not improve detection performance significantly, it may be useful in target classification. Some target types have distinctive polarimetric scattering properties. Preliminary studies using an optimal polarimetric classifier suggest that these polarimetric properties could be exploited to discriminate among target types (e.g., armored targets vs. trucks).

It is again emphasized that the clutter data base which the results of this report are based on is very limited; a more comprehensive set of measurements of various clutter types (e.g., snow-covered terrain) must be obtained and analyzed. In the very near future we plan to collect this comprehensive clutter data base using the Advanced Detection Technology Sensor (ADTS), and to verify the tentative conclusions of this report using the new data base. The mathematical framework necessary to perform these future studies is provided in this report, along with the new polarimetric detection and classification algorithms for optimally processing the fully polarimetric radar data.

1.0 INTRODUCTION

The detection of stationary targets in ground clutter is an important problem for both strategic and tactical applications. In an earlier program, the Hostile Weapons Location System (HOWLS) Program [1,2], M.I.T. Lincoln Laboratory investigated the detection performance that could be achieved using a single-polarimetric-channel radar with a resolution on the order of the size of a typical target (10 m by 10 m). The radar employed pulse-to-pulse frequency diversity; this was used to obtain independent samples of targets and clutter which could then be noncoherently integrated. Statistical target and clutter models based on analysis of the collected radar data were developed. These models were used to develop performance predictions for various non-polarimetric detection algorithms. These predictions were found to agree reasonably well with the actual performance achieved by the algorithms.

Could HOWLS detection performance have been improved if the radar had been fully polarimetric, and if the full polarization scattering matrix (PSM) had been used in the detection algorithms? This report addresses that question.

To measure the full PSM, a radar must transmit two orthogonal polarizations at each frequency. In this report we assume that horizontal polarization is transmitted first and two linear orthogonal polarizations (denoted HH and HV) are received. Next, vertical polarization is transmitted and two linear orthogonal polarizations (denoted VV and VH) are received. By reciprocity VH = HV; therefore the three complex elements HH, HV, and VV comprise all the information contained in the polarization scattering matrix. For multi-look algorithms, successive independent PSM measurements are obtained using frequency diversity.

In order to investigate the possible contribution to detection from the fully polarimetric data, we extended the HOWLS target and clutter statistical models to the fully polarimetric case. Then we developed detection algorithms which use fully polarimetric information. Finally we developed formulas for predicting the performance of these algorithms, and used these formulas to evaluate and compare the various detection algorithms.

In Section 2 we introduce the basic polarimetric measurement model and develop homogeneous statistical models of targets and clutter. These statistical

3

models are used to predict the performance of various polarimetric and non-polarimetric detection algorithms.

In Section 3 we use these homogeneous target and clutter models to derive the optimal polarimetric detector (OPD). This algorithm reveals the structure of the detector which yields the best performance under ideal conditions; that is, it provides an upper bound on detection performance for the homogeneous case.

Section 4 develops a new detection algorithm, the polarimetric matched filter (PMF). This is a linear processor that processes the complex polarimetric returns (HH, HV, and VV) so as to provide maximum target-to-clutter ratio to the detector. A useful interpretation of the solution of the PMF is shown to correspond to simple dihedral and trihedral reflector types.

Several alternative, suboptimal detection algorithms are presented in Section 5. These algorithms are suboptimal because they ignore some of the polarimetric information; they are, however, independent of the polarimetric parameters of the target and clutter whereas the OPD and the PMF require exact knowledge of the target and clutter covariances. The algorithms considered include the polarimetric span and various single-polarimetric-channel detectors.

Section 6 develops more realistic target and clutter models. In this section it is assumed that clutter is spatially nonhomogeneous and that target returns vary with aspect angle. Random polarimetric target and clutter models having a product-model structure are post·'ated; such models are consistent with these more realistic assumptions. The exact pr·'bability density function (PDF) for both product-model targets and clutter is derived; this PDF is used to obtain the optimal-likelihood-ratio detector for product-model targets and clutter.

The formulas for predicting the performance of the detection algorithms introduced in Sections 3, 4, and 5 are derived in Section 7. The analysis uses the product-model characterizations of targets and clutter developed in Section 6. The detection algorithms analyzed include the OPD, the PMF, and single-polarimetric-channel detectors. In these analyses the performance predictions for homogeneous targets and clutter are obtained as a special case of the more general product-model solution.

Section 8 investigates the performance of a radar that uses a single-transmit, dual-receive configuration with a circular polarization basis. This scheme is predicated on the empirical observation that armored targets tend to have a significant amount of even-bounce (LL) return whereas clutter tends to have mostly odd-bounce (LR) return. A circular polarization configuration could take advantage of this difference. Section 8 parallels the previous Sections 3 through 7. That is, for this circular polarization case, an OPD and PMF are derived, as well as alternative suboptimal detectors. Then the product-model characterizations of targets and clutter are used to derive formulas for performance predictions of the various algorithms.

The algorithms derived in Sections 3 through 8 assume that the frequency-diverse radar obtains uncorrelated samples of both clutter and targets. In practice there may be some correlation between the frequency samples, due to insufficient frequency-diversity step size. Ignoring this correlation produces overly optimistic performance predictions. Section 9 modifies the clutter and target models to take into account the correlation between the elements of the PSM obtained at different frequencies.

In Section 10, a comparison of the detection performance of various polarimetric and non-polarimetric detectors is presented. The performance comparisons presented include (1) a comparison of the OPD, span, and single-channel $|HH|^2$ detectors, (2) a comparison of the PMF and single-channel $|HH|^2$ and $|LL|^2$ detectors, and (3) a comparison of the OPD, PMF, and dual-circular detectors. Also, the performance degradation due to using correlated measurement data is evaluated.

Once a target has been detected, polarimetric information may be useful for classification of target types (e.g., tank versus truck). Section 11 presents some preliminary performance predictions for the OPD when it is used as a target classifier.

Speckle is a major cause of degradation in synthetic aperture radar (SAR) imagery. It is possible to use the three complex elements (HH, HV, VV) of the polarization scattering matrix to reduce this speckle. In Section 12 we derive the optimal method of combining the elements of the scattering matrix to minimize image speckle; the solution is shown to be a polarimetric whitening filter (PWF). A simulation of spatially correlated, K-distributed, fully polarimetric clutter is developed; it is used to compare the optimal speckle reduction method with other, suboptimal methods. Finally, the target detection performance of the PWF was compared with that of other detectors.

Section 13 summarizes the findings of these studies and describes some possible future study efforts.

5

2.0 THE BASIC POLARIMETRIC MEASUREMENT MODEL

This section describes the basic mathematical modeling of targets and clutter used in our studies. These models are used in the later sections to derive the optimal polarimetric detector and the polarimetric matched filter.

We express the radar ret...n as the polarimetric feature vector $\underline{X}$, where

$$\underline{X} = \begin{bmatrix} HH_i & + & jHH_q \\ HV_i & + & jHV_q \\ VV_i & + & jVV_q \end{bmatrix} = \begin{bmatrix} HH \\ HV \\ VV \end{bmatrix} \tag{1}$$

Each complex element HH, HV, and VV is modeled as having a complex-Gaussian probability density function (PDF). The joint PDF of vector $\underline{X}$ is given by the expression

$$f(\underline{X}) = \frac{1}{\pi^3 |\Sigma|} \exp\left\{-\underline{X}^t \Sigma^{-1} \underline{X}\right\} \tag{2}$$

where $\Sigma = E\{\underline{X}\,\underline{X}^\dagger\}$ is the covariance of the polarimetric feature vector. The data have a zero-mean ($E\{\underline{X}\} = \underline{0}$). Thus, the complete characterization of the jointly Gaussian complex elements HH, HV, and VV is given in terms of an appropriate covariance matrix Σ. The covariance matrices which we use for target and clutter data (in a linear polarization basis) are [3, 4] of the form

$$\Sigma = \sigma \begin{bmatrix} 1 & 0 & \rho\sqrt{\gamma} \\ \hline 0 & \varepsilon & 0 \\ \hline \rho^*\sqrt{\gamma} & 0 & \gamma \end{bmatrix} \tag{3}$$

where $\sigma = E\{|HH|^2\}$, $\varepsilon = \dfrac{E\{|HV|^2\}}{E\{|HH|^2\}}$, $\gamma = \dfrac{E\{|VV|^2\}}{E\{|HH|^2\}}$ $\qquad$ (4)

and $\rho\sqrt{\gamma} = \dfrac{E\{HH\,VV^*\}}{E\{|HH|^2\}}$

The clutter covariance is specified by four parameters $(\sigma_c,\,\varepsilon_c,\,\gamma_c,\,\rho_c)$ and the target covariance is also specified by four parameters $(\sigma_t,\,\varepsilon_t,\,\gamma_t,\,\rho_t)$. Also, since the target is in a clutter background, the measured target data are modeled (by superposition) as

$$\underline{X}_{t+c} = \underline{X}_t + \underline{X}_c \tag{5}$$

This implies that the target-plus-clutter data are also zero-mean and complex-Gaussian with covariance

$$\Sigma_{t+c} = \Sigma_t + \Sigma_c \tag{6}$$

and thus has the same structure as given in Equation (3) above, with

$$\sigma_{t+c} = \sigma_t + \sigma_c$$

$$\varepsilon_{t+c} = \frac{\sigma_t \varepsilon_t + \sigma_c \varepsilon_c}{\sigma_{t+c}}$$

$$\gamma_{t+c} = \frac{\sigma_t \gamma_t + \sigma_c \gamma_c}{\sigma_{t+c}}$$

$$\rho_{t+c}\sqrt{\gamma_{t+c}} = \frac{\sigma_t \rho_t \sqrt{\gamma_t} + \sigma_c \rho_c \sqrt{\gamma_c}}{\sigma_{t+c}} \tag{7}$$

Finally, the input target-to-clutter ratio is defined

$$(T/C)_{in} = \frac{\sigma_t}{\sigma_c} \tag{8}$$

3.0 THE OPTIMAL POLARIMETRIC DETECTOR

In this section we will derive the optimal polarimetric detector (OPD) for the ideal situation, that is, assuming the parameters ($\sigma, \varepsilon, \gamma, \rho$) and the target-to-clutter ratio (T/C) in are known exactly. The algorithm we obtain will reveal the structure of the detector that provides the best possible detection performance achievable under ideal conditions. The performance of this ideal optimal detector will provide an upper bound against which other polarimetric and non-polarimetric detection schemes can be compared. For our two-class problem (i.e., target-plus-clutter versus clutter) the likelihood ratio test for the presence of a target is [5]

$$\frac{f\left(\underline{X}\mid\omega_{t+c}\right)}{f\left(\underline{X}\mid\omega_c\right)} > T \tag{9}$$

where we denote the target-plus-clutter class by ω_{t+c} and the clutter only class by ω_c. T is the detection threshold. The likelihood ratio has been shown [5] to be a quadratic detector of the form

$$\underline{X}^{t}\left(\Sigma_c^{-1} - \Sigma_{t+c}^{-1}\right)\underline{X} + \ln\frac{|\Sigma_c|}{|\Sigma_{t+c}|} > \ln\ T \tag{10}$$

Substituting particular covariance matrices defining two classes (target-plus-clutter and clutter in our examples) into the above algorithm yields an interesting result. Rewriting the above solution in a slightly different form, the optimal detector uses the distances to the target-plus-clutter class and the clutter class in the following test:

$$d_c(\underline{X}) - d_{t+c}(\underline{X}) > \ln\ T \tag{11}$$

where
$$d_c(\underline{X}) = \underline{X}^{t}\Sigma_c^{-1}\underline{X} + \ln|\Sigma_c| \tag{12}$$

and
$$d_{t+c}(\underline{X}) = \underline{X}^{t}\Sigma_{t+c}^{-1}\underline{X} + \ln|\Sigma_{t+c}| \tag{13}$$

Evaluating the above distance measures, one obtains an expression for the detection statistic [3]

$$d_i(\underline{X}) = -\frac{|HH|^2}{\sigma_i\left(1-|\rho_i|^2\right)} + \frac{|VV|^2}{\sigma_i\left(1-|\rho_i|^2\right)\gamma_i} + \frac{|HV|^2}{\sigma_i\,\varepsilon_i}$$

$$- \frac{2\,|\rho_i|}{\sigma_i\left(1-|\rho_i|^2\right)\sqrt{\gamma_i}}|HH||VV|\cos\left(\phi_{HH}-\phi_{VV}-\phi_{\rho_i}\right)$$

$$+ \ln\left[\sigma_i^3\,\varepsilon_i\,\gamma_i\left(1-|\rho_i|^2\right)\right]\,;\quad i = c, t + c \tag{14}$$

where ϕ_{HH}, ϕ_{VV}, and $\phi_{\rho i}$ are the phase terms of the complex quantities HH, VV, and ρ_i, respectively. The fundamental structure of the optimal polarimetric detector is revealed in Equation (14); the detector makes use of the polarimetric amplitude information (|HH|, |HV|, |VV|) and the polarimetric phase difference (ϕ_{HH} - ϕ_{VV}), which is the difference in phase between the HH and VV returns. The OPD applies optimal weighting [as shown in Equation (14) above] to the observed radar measurement data prior to making its detection decision.

4.0 THE POLARIMETRIC MATCHED FILTER

In the previous section of the report we defined the two-class target detection problem and derived the detection algorithm which makes optimal use of the observed polarimetric return. This algorithm is optimal in the likelihood-ratio sense; that is, it yields the best possible probability of detection (P_D) for a given false alarm probability (P_{FA}). An alternative approach is to design a linear processor or matched filter, which processes the polarimetric return so as to provide maximum target-to-clutter ratio to the radar detector. We will call this algorithm a polarimetric matched filter (PMF); it is easily derived using the approach given in Reference 7. A brief derivation of this detector is given below.

Again the assumption is that we have two classes (the target-plus-clutter class and the clutter class) but we now seek the best set of linear weighting coefficients for processing the polarimetric data vector. That is, we seek the linear combination $y = \underline{h}^t \underline{x}$ which provides the maximum target-to-clutter ratio at the filter output. This ratio is given by

$$(T/C)_{out} = \frac{\underline{h}^t \Sigma_t \underline{h}}{\underline{h}^t \Sigma_c \underline{h}} \tag{15}$$

The polarimetric matched filter makes use of the target and clutter covariances Σ_t and Σ_c. This implies a design which is independent of the actual input target-to-clutter ratio; i.e., the PMF is a constant-coefficient filter.

It is well known [7] that the optimal weight vector, denoted $\underline{h}^*$, is obtained as the solution to the generalized eigenvalue problem

$$\Sigma_t \underline{h}^* = \lambda^* \Sigma_c \underline{h}^* \tag{16}$$

where $\underline{h}^*$ is the eigenvector corresponding to the maximum eigenvalue, λ^*. Also, the maximum eigenvalue λ^* is actually the optimal target-to-clutter ratio out of the filter which is obtained as a result of using the optimal $\underline{h}^*$. Equivalently, one may obtain the (λ^*, $\underline{h}^*$) solution by solving the following simpler eigenvalue-eigenvector problem:

$$\Sigma_c^{-1} \Sigma_t \underline{h}^* = \lambda^* \underline{h}^* \tag{17}$$

It is more convenient to solve this equivalent eigenvalue problem since the structure of the matrix $\Sigma_c^{-1} \Sigma_t$ is simple and easily leads to an exact analytical solution.

Specifically, we find

$$\Sigma_c^{-1}\Sigma_i = \frac{\left[\begin{array}{c|c|c} \varepsilon_c\left(\gamma_c - \sqrt{\gamma_c}\sqrt{\gamma_i}\rho_c\rho_i\right) & 0 & \varepsilon_c\left(\gamma_c\sqrt{\gamma_i}\rho_i - \gamma_i\sqrt{\gamma_c}\rho_c\right) \\ \hline 0 & \varepsilon_i\left(1-\rho_c^2\right)\gamma_c & 0 \\ \hline \varepsilon_c\left(\rho_i\sqrt{\gamma_i} - \rho_c\sqrt{\gamma_c}\right) & 0 & \varepsilon_c\left(\gamma_i - \sqrt{\gamma_c}\sqrt{\gamma_i}\rho_c\rho_i\right) \end{array}\right]}{\sigma_c\left(1-\rho_c^2\right)\varepsilon_c\gamma_c}\sigma_t$$

(18)

Although the above matrix is not symmetric, it has been shown [7] that the eigenvalues are all positive. In evaluating the eigenvalues and eigenvectors of Equation (18), we first simplify the solution by omitting the scale factor $\sigma_t/\sigma_c (1-\rho_c^2)\varepsilon_c\gamma_c$ since the eigenvectors are independent of this scale factor. We then determine the (normalized) eigenvalues and their corresponding eigenvectors. The results of this analysis are summarized as follows:

1. The (normalized) eigenvalue $\lambda_1 = \varepsilon_i\gamma_c(1-\rho_c^2)$ has the eigenvector

$$h_1 = \begin{bmatrix} 0 \\ 1 \\ 0 \end{bmatrix}$$

(19)

2. The remaining (normalized) eigenvalues λ_2, λ_3 are found to be

$$\lambda_2 = 0.5\varepsilon_c\left[-\sqrt{\gamma_c\gamma_i 4\rho_i^2 + 4\rho_c^2 - 2 - 4\sqrt{\gamma_c}\,\gamma_i^{3/2}\rho_c\rho_i - 4\sqrt{\gamma_i}\,\gamma_c^{3/2}\rho_c\rho_i + \gamma_i^2 + \gamma_c^2} \right.$$
$$\left. -2\sqrt{\gamma_c}\sqrt{\gamma_i}\rho_c\rho_i + \gamma_i + \gamma_c\right]$$

(20)

$$\lambda_3 = 0.5\varepsilon_c\left[+\sqrt{\gamma_c\gamma_i 4\rho_i^2 + 4\rho_c^2 - 2 - 4\sqrt{\gamma_c}\,\gamma_i^{3/2}\rho_c\rho_i - 4\sqrt{\gamma_i}\,\gamma_c^{3/2}\rho_c\rho_i + \gamma_i^2 + \gamma_c^2} \right.$$
$$\left. -2\sqrt{\gamma_c}\sqrt{\gamma_i}\rho_c\rho_i + \gamma_i + \gamma_c\right]$$

(21)

Thus the three eigenvectors obtained for the above matrix are of the form

$$\underline{h}_1 = \begin{bmatrix} 0 \\ 1 \\ 0 \end{bmatrix}, \ \underline{h}_2 = \begin{bmatrix} 1 \\ 0 \\ \beta_2 \end{bmatrix}, \ \underline{h}_3 = \begin{bmatrix} 1 \\ 0 \\ \beta_3 \end{bmatrix}$$

(22)

where the parameters β_2 and β_3 are given by the expression

$$\beta_{2,3} = \pm \frac{\sqrt{\left[4\gamma_c\gamma_t\rho_t^2 - 4\sqrt{\gamma_c}\gamma_t^{3/2}\rho_c\,\rho_t - 4\sqrt{\gamma_t}\gamma_c^{3/2}\rho_c\,\rho_t + 4\gamma_c\gamma_t\rho_c^2 + \gamma_t^2 - 2\gamma_c\gamma_t + \gamma_c^2\right]} + \gamma_t - \gamma_c}{2\gamma_c\sqrt{\gamma_t}\rho_t - 2\sqrt{\gamma_t}\gamma_t\rho_c}$$

(23)

The optimal polarimetric matched filter corresponds to one of the three solutions in Equation (22); in particular, it corresponds to the solution defined by the maximum of the three eigenvalues $\lambda_1, \lambda_2, \lambda_3$. Thus the polarimetric matched filter is one of the three possible linear combinations of the polarimetric measurements, namely

(i) $y_1 \;=\; HV$

(ii) $y_2 \;=\; HH + \beta_2 VV$

(iii) $y_3 \;=\; HH + \beta_3 VV$

(24)

To gain further insight into the above solution, we will consider the behavior of the solution for the cases $\beta = \pm 1$. These solutions are related to simple types of radar reflectors. For the special case when $\gamma_t = \gamma_c = 1$, the optimal polarization combinations become

(i) $y_1 \;=\; HV$

(ii) $y_2 \;=\; HH + VV$

(iii) $y_3 \;=\; HH - VV$

(25)

These three solutions correspond to the following simple target-in-clutter situations

(i)   HV is the polarization measurement that has the maximum signal return for a dihedral reflector oriented at $\pm 45°$ relative to the horizontal.

(ii) HH + VV is the polarization measurement combination that has the maximum signal return for a trihedral reflector.

(iii) HH - VV is the polarization measurement combination that has the maximum signal return for a dihedral reflector oriented horizontally or vertically.

5.0 ALTERNATIVE DETECTION ALGORITHMS

Sections 3 and 4 discussed two approaches (the optimal polarimetric detector and the polarimetric matched filter) to detecting targets in clutter. Both of these approaches are dependent on the parameters of the target and clutter classes. There are other approaches to detecting targets in clutter that are independent of the parameters of the target and clutter classes. These detection algorithms are suboptimal because they ignore some of the polarimetric information. We will consider several of these methods.

The first scheme (used extensively in various radar applications by numerous researchers) processes the complex radar return by computing the polarimetric span according to the relation

$$y = |HH|^2 + 2|HV|^2 + |VV|^2 \tag{26}$$

The span detection statistic makes use of the total power in the polarimetric return and has the property of being invariant with respect to the polarization basis used by the radar. The span is actually a suboptimal quadratic detector, since it is obtained from the simplified algorithm

$$y = (HH^*, HV^*, VV^*) \begin{bmatrix} 1 & 0 & 0 \\ 0 & 2 & 0 \\ 0 & 0 & 1 \end{bmatrix} \begin{bmatrix} HH \\ HV \\ VV \end{bmatrix} > T \tag{27}$$

Note that the span detector does not make use of the polarimetric phase ($\phi_{HH} - \phi_{VV}$). Since the span detector utilizes only the polarimetric amplitude information, using it will provide some insight from the comparison of performance results for the various algorithms as to the usefulness of polarimetric phase in our target detection application. We will also consider single polarimetric channel radars (specifically, HH, LL, and LR) and will compare the performance of these simpler algorithms to that of the more complex algorithms. Finally, we will evaluate the performance of a single circular transmit, dual circular receive radar system. This scheme makes use of both LL and LR polarimetric returns and we will compare the performance of this system to the performance achieved using the full PSM system.

6.0 NON-GAUSSIAN TARGET AND CLUTTER MODELS

The previous sections presented a number of polarimetric and non-polarimetric detectors, namely,

1. The optimal polarimetric detector (OPD)
2. The polarimetric matched filter (PMF)
3. The span detector
4. Single-channel (non-polarimetric) detectors

This section develops more realistic target and clutter models; these will be used in the next section to evaluate the detection performance of these algorithms and their sensitivity to non-Gaussian distributions of targets and clutter.

Until now we have assumed a homogeneous clutter background; as a result each clutter pixel in the scene had the same average polarimetric power and the same covariance between the polarimetric returns. Also, we assumed the target-plus-clutter samples to be from a single Gaussian PDF (probability density function) with a constant average power and covariance. It is more realistic to assume that (a) the clutter background is spatially nonhomogeneous, and (b) the target returns vary with aspect angle. To this end, in this section we postulate random polarimetric target and clutter models consistent with these more realistic assumptions. Specifically, we postulate random polarimetric target and clutter models having a product-model structure. This enables us to evaluate the effects of spatial variability of clutter and aspect angle variability of targets on the performance of the optimal polarimetric detector, the polarimetric matched filter, and the other, simpler detectors. To compare these detectors, we also need an optimal likelihood-ratio detector for the product models of targets and clutter. Therefore, we also derive the exact PDF for the product model polarimetric feature vectors and implement the likelihood ratio detector for the product model problem.

Since we are interested in a product model for both targets and clutter, we take the model to be of the form

$$\underline{Y} = \sqrt{g}\,\underline{X} \tag{28}$$

where $\sqrt{g}$ represents an arbitrary scale factor. Our basic assumptions are (1) that the feature vectors $\underline{X}$ have a specified covariance matrix Σ and (2) that the vectors $\underline{X}$ are scaled according to some random variable $\sqrt{g}$. This defines our product model for polarimetric data measurements and represents a simple extension of the single-polarimetric-channel product models of targets and clutter derived in Reference 2. Determining the PDF of random vector $\underline{Y}$ is straightforward and proceeds as described below.

For a given value g, we have

$$E\{\underline{Y} / g\} = \sqrt{g} E\{\underline{X}\} = \underline{0} \tag{29}$$

$$COV\{\underline{Y} / g\} = g\Sigma \tag{30}$$

Since the vector $\underline{X}$ is assumed to be complex-Gaussian, the conditional PDF of random vector $\underline{Y}$ is also complex-Gaussian

$$f(\underline{Y} / g) = \frac{1}{\pi^3 g^3 |\Sigma|} \exp\left\{-\frac{\underline{Y}^\dagger \Sigma^{-1} \underline{Y}}{g}\right\} \tag{31}$$

Next, we compute the unconditional PDF of random vector $\underline{Y}$ which is obtained from the integral

$$f(\underline{Y}) = \int_0^\infty f(\underline{Y} / g) f(g) \, dg \tag{32}$$

where f(g) is the PDF of the scalar product multiplier. In References 8, 9, and 10, a Gamma (or chi-square) distributed cross-section model was assumed having density

$$f_G(g) = \frac{1}{\bar{g}} \left(\frac{g}{\bar{g}}\right)^{v-1} \frac{1}{\Gamma(v)} \exp\left\{\frac{-g}{\bar{g}}\right\} \tag{33}$$

In this two-parameter cross-section model, v is the order parameter and $\bar{g}$ is related to the mean radar cross-section. This has been shown [8, 9, 10] to yield the K-distribution for single polarimetric-channel ground clutter and sea clutter. We have shown that this distribution is a reasonable model for both radar ground clutter and targets similar to that data collected using the HOWLS [1] radar. We will apply this cross-section model to the polarimetric feature vector problem and will show that this leads to a generalized K-distribution for the PDF of random vector $\underline{Y}$.

In the fully polarimetric case, it has been found that tree clutter agrees less well with this product model than does meadow clutter. We anticipate future work in clutter modeling in order to generalize the product model so that it agrees with both meadow clutter and tree clutter. Substituting Equations (31) and (33) into Equation (32), we obtain the result

$$f(\underline{Y}) = \frac{1}{\pi^3 \bar{g}^v \Gamma(v) |\Sigma|} \int_0^\infty g^{3-v-1} \exp\left\{-g\underline{Y}^\dagger \Sigma^{-1} \underline{Y}\right\} \exp\left\{-\frac{1}{g\bar{g}}\right\} dg \tag{34}$$

18

Using tabulated integrals from Reference 11, we obtain the result

$$f(\underline{Y}) = \frac{2}{\pi^3 \overline{g}^\upsilon \Gamma(\upsilon) \, |\Sigma|} \frac{K_{3-\upsilon}\left(2\sqrt{\dfrac{\underline{Y}^t \Sigma^{-1} \underline{Y}}{\overline{g}}}\right)}{\left(\overline{g}\underline{Y}^t \Sigma^{-1}\underline{Y}\right)^{(3-\upsilon)/2}} \tag{35}$$

Given this exact PDF for the product model characterization of targets and clutter, we next obtain the corresponding optimal log-likelihood ratio detector. Omitting the details, we obtain the distance measures $D_{t+c}(\underline{Y})$ and $D_c(\underline{Y})$

$$D_i(\underline{Y}) = (\nu_i - 3)\ln\left(d_i^2 / 2\overline{g}_i\right) + \ln K_{\nu_i-3}\left(2\sqrt{\frac{d_i^2}{2\overline{g}_i}}\right)$$
$$-\ln\Gamma(\nu_i) - \ln|\Sigma_i| - \nu_i \ln \overline{g}_i$$
$$\text{where} \quad d_i^2 = \underline{Y}^t \Sigma_i^{-1}\underline{Y} \; ; \; i = c, \, t + c \tag{36}$$

The optimal polarimetric detector for product-model targets and clutter determined by Equation (36) has the same form as Equation (11); i.e., the optimal test for the presence of a target is

$$D_c(\underline{Y}) - D_{t+c}(\underline{Y}) > \ln T \tag{37}$$

We will use this detector in the ideal situation-where the parameters ($\sigma, \epsilon, \gamma, \rho$) and the target-to-clutter ratio are known exactly and the parameters ($\nu, \overline{g}$) are also known exactly. The performance of this detector therefore will provide an upper bound against which we can compare the performance of our other detectors. In this way, we may judge the relative degradation in performance which occurs when the detectors are designed for some nominal target and clutter parameters but tested against product model input data.

7.0 SENSITIVITY ANALYSIS OF POLARIMETRIC DETECTION ALGORITHMS

In the previous sections, we derived polarimetric and non-polarimetric detectors for homogeneous (Gaussian) target and clutter statistics. In this section, the actual test inputs will be assumed to have a product model structure, and the sensitivity of the detectors to the effects of clutter spatial variability and target aspect-angle variability will be determined.

7.1 ANALYSIS OF THE OPD - SINGLE-LOOK SOLUTION

For the optimal polarimetric detector, we write

$$y = \underline{X}^\dagger \left(\Sigma_c^{-1} - \Sigma_{t+c}^{-1} \right) \underline{X} + C \tag{38}$$

where

$$C = \ln \frac{|\Sigma_c|}{|\Sigma_{t+c}|} - \ln T \tag{39}$$

Taking the approach of References 12 and 13, we evaluate the conditional characteristic function of random variable y:

$$\phi_{y/g}(jw) = \int_{-\infty}^{\infty} ... \int_{-\infty}^{\infty} \exp\left\{ jw\left(\underline{X}^\dagger [\Sigma_c^{-1} - \Sigma_{t+c}^{-1}]\underline{X} + C \right) \right\} \frac{\exp\left\{ \frac{-\underline{X}^\dagger \Sigma^{-1} \underline{X}}{g} \right\} d\underline{X}}{\pi^3 g^3 |\Sigma|} \tag{40}$$

The above expression implies that we have designed the detector using nominal Σ_{t+c} and Σ_c for our target-plus-clutter and clutter classes, but are testing the algorithm with measurement data that have a product model structure by appropriately selecting Σ and g. For now, however, we assume a given g and evaluate the exact characteristic function to be of the form

$$\phi_{y/g}(jw) = e^{jwC} \prod_{i=1}^{3} \frac{1}{(1 - j2g\lambda_i w)} \tag{41}$$

where the eigenvalues λ_1, λ_2, λ_3 are obtained from the simultaneous diagonalization of the matrices

$$\Sigma_c^{-1} - \Sigma_{t+c}^{-1} \text{ and } \Sigma^{-1} \tag{42}$$

A FORTRAN program which computes the eigenvalues λ_1, λ_2, and λ_3 is included in the Appendix. The eigenvalues are given as analytical closed-form expressions; these expressions were obtained using MACSYMA [14].

21

Expanding Equation (41) by partial fractions yields

$$\phi_{y/g}(jw) = e^{jwC} \sum_{i=1}^{3} \frac{A_i}{(1 - j2g\lambda_i w)} \tag{43}$$

where the residues A_i are simple functions of λ_1, λ_2, and λ_3. Taking the inverse transform yields the conditional probability density

$$f_{y/g}(y) = \sum_{i=1}^{3} A_i f_i(y) \tag{44}$$

where

$$f_i(y) = F^{-1}\left\{ \frac{e^{-jwC}}{(1 - j2g\lambda_i w)} \right\} \tag{45}$$

Detection and false alarm probabilities are obtained by integrating:

$$P_{D/FA}(g) = \int_0^7 f_{y/g}(g)dg \tag{46}$$

The result is the sum of three integrals

$$P_{D/FA}(g) = \sum_{i=1}^{3} A_i P_i(g) \tag{47}$$

where

$$
\begin{aligned}
P_i(g) &= 1 - \exp\left\{\frac{C}{2g\lambda_i}\right\} &; \lambda_i > 0, C < 0 \\
P_i(g) &= 0 &; \lambda_i > 0, C > 0 \\
P_i(g) &= \exp\left\{\frac{C}{2g\lambda_i}\right\} &; \lambda_i < 0, C > 0 \\
P_i(g) &= 1 &; \lambda_i < 0, C < 0
\end{aligned} \tag{48}
$$

The above expressions (47) and (48) are valid for any particular value of g. When g is modeled as a random variable (as it is for the product model), the detection probability is likewise a random variable. An average probability is obtained by averaging with respect to g:

$$\overline{P}_{D/FA} = E_g\left\{P_{D/FA}(g)\right\} = \sum_{i=1}^{3} A_i E_g\left\{P_i(g)\right\} \tag{49}$$

22

where

$$E_g\{P_i(g)\} = 1 - \left(\frac{-C\bar{g}}{2\lambda_i}\right)^{v/2} \frac{K_v\left(2\sqrt{\frac{-C}{2\lambda_i\bar{g}}}\right)}{\bar{g}^v\Gamma(v)} \qquad ; \lambda_i > 0, C < 0$$

$$E_g\{P_i(g)\} = 0 \qquad\qquad\qquad ; \lambda_i > 0, C > 0$$

$$E_g\{P_i(g)\} = \left(\frac{-C\bar{g}}{2\lambda_i}\right)^{v/2} \frac{K_v\left(2\sqrt{\frac{-C}{2\lambda_i\bar{g}}}\right)}{\bar{g}^v\Gamma(v)} \qquad ; \lambda_i < 0, C > 0$$

$$E_g\{P_i(g)\} = 0 \qquad\qquad\qquad ; \lambda_i < 0, C < 0 \qquad (50)$$

The exact $P_{D/FA}$ performance of the OPD for homogeneous target and clutter models is obtained from Equations (47) and (48) by setting the random multiplier $g = 1$. The exact solution for the detection performance of the OPD involves calculation of the three eigenvalues λ_1, λ_2, λ_3 from simultaneous diagonalization of the covariance matrices of Equation (42) above; this is true for both homogeneous and non-homogeneous inputs. The exact solution to this simultaneous diagonalization problem is given in the Appendix.

7.2 ANALYSIS OF THE OPD - MULTI-LOOK SOLUTION

We are interested in evaluating the performance of the OPD when two or more independent measurements of the polarimetric data, X, are processed in an optimal manner. In this subsection, the extension of the analysis to the multi-look case is presented. The assumptions we make are (i) that each observed polarimetric measurement vector from class wc has the same mean and covariance statistics (Q, Σ_c) and (ii) that each polarimetric measurement vector from class ω_{1+c} has the same statistics (Q, Σ_{1+c}). With these assumptions, it is easy to show that the likelihood ratio test for m independent observations is equivalent to sequentially processing each observed vector X_i, $i=1,2,...m$ in the single-look quadratic classifier [15]. The single-look detection statistics y_i are then summed and compared with the detection threshold T. Finally, since the characteristic function of a sum of independent random variables is the product of the individual characteristic functions, we obtain for the m-look case

$$\phi_{y/g}^{(m)}(jw) = e^{jwC} \prod_{i=1}^{3} \frac{1}{(1-j2g\lambda_i w)^m} \qquad (51)$$

From this, one may obtain the exact formulas for detection and false alarm probabilities. The solution is lengthy and only the final results will be given here. Using the partial fraction expansion technique of Reference 16, we obtain the solution

$$P_{D/FA}^{(m)}(g) = \sum_{i=1}^{3} \sum_{\ell=1}^{m} A_{i\ell}^{(m)} P_{i\ell}^{(m)} \qquad (52)$$

23

where

$$
\begin{aligned}
P_{u}^{(m)} &= G_{u}(g) &&; \lambda_i > 0, C < 0 \\
P_{u}^{(m)} &= 1 &&; \lambda_i > 0, C > 0 \\
P_{u}^{(m)} &= 1 - G_{u}(g) &&; \lambda_i < 0, C > 0 \\
P_{u}^{(m)} &= 0 &&; \lambda_i < 0, C < 0
\end{aligned}
\tag{53}
$$

where

$$
G_{u}(g) = \int_{-C/g\lambda_i}^{-} \frac{X^{\ell-1} e^{-X/2}}{2^{\ell}(\ell-1)!}\, dx
\tag{54}
$$

and

$$
A_{u} = \frac{(-2\lambda_i)^{\ell}}{(m-\ell)! \prod_{k=1}^{3}(-2\lambda_k)^{m}} \sum_{n=0}^{m-\ell} \binom{m-\ell}{n}
$$

$$
\frac{\left[(-m-n+1)(-m-n+2)....(-m)\right]\left[(-2m+\ell+n+1)........(-m)\right]}{\left[\dfrac{1}{2\lambda_i} - \dfrac{1}{2\lambda_{i_1}}\right]^{m+n}\left[\dfrac{1}{2\lambda_i} - \dfrac{1}{2\lambda_{i_2}}\right]^{2m-\ell-n}}
\tag{55}
$$

where $\quad i_1 = \text{modulo}_3(i) + 1$

$\qquad\quad i_2 = \text{modulo}_3(i+1) + 1$

Finally, when the test inputs have the product multiplier, g, which is characterized by the Gamma distribution of Equation (33), we take the expectation with respect to this variable and obtain

$$
E_{g}\left\{P_{D/FA}^{(m)}(g)\right\} = \sum_{i=1}^{3} \sum_{\ell=1}^{m} A_{u} E_{g}\left\{P_{u}^{(m)}\right\}
\tag{56}
$$

where

$$
\begin{aligned}
E_{g}\left\{P_{u}^{(m)}\right\} &= E_{g}\left\{G_{u}(g)\right\} &&; \lambda_i > 0, C < 0 \\
E_{g}\left\{P_{u}^{(m)}\right\} &= 1 &&; \lambda_i > 0, C > 0 \\
E_{g}\left\{P_{u}^{(m)}\right\} &= 1 - E_{g}\left\{G_{u}(g)\right\} &&; \lambda_i < 0, C > 0 \\
E_{g}\left\{P_{u}^{(m)}\right\} &= 0 &&; \lambda_i < 0, C < 0
\end{aligned}
\tag{57}
$$

and

$$E_t\{G_{\nu}(g)\} = \frac{1}{\bar{g}^{\nu}\Gamma(\nu)} \sum_{k=0}^{\ell-1} \frac{\left(-\frac{C}{\lambda_i}\right)^{\nu+k}\left(\frac{\bar{g}}{2}\right)^{\nu-k}}{2^{k-1}k!} K_{\nu-k}\left(2\sqrt{\frac{-C}{2\bar{g}\lambda_i}}\right)$$

(58)

7.3 ANALYSIS OF THE PMF - GENERAL SOLUTION

Compared to the analysis of the OPD, discussed above, analysis of the matched filter algorithm is simpler because the algorithm is linear. We will briefly summarize here the solution for the multi-look case.

The output of the filter is a complex-Gaussian random variable comprised of the optimal weighted sum of the HH, HV, and VV data. This output is noncoherently detected and summed prior to being compared with the detection threshold T. Mathematically, the algorithm is represented as

$$y = \sum_{k=1}^{m} |\underline{h}^t\underline{X}_k|^2 > T$$

(59)

Random variable y is chi-square, since it is the sum of m-independent exponential variables; therefore, in order to calculate the detection performance of the algorithm, we need only compute $E\{|\underline{h}^t\underline{X}|^2\}$. We obtain

$$E\{|\underline{h}^t\underline{X}|^2\} = gd^2(\underline{h})$$

where

$$d^2(\underline{h}) = \underline{h}^t\Sigma\underline{h}$$

(60)

and g is the product multiplier

The conditional detection and false alarm probabilities, for a given value of the multiplier, g, are

$$P_{D/FA}^{(m)}(g) = \sum_{k=0}^{m-1} \frac{\left(\frac{T}{gd^2(\underline{h})}\right)^k}{k!} \exp\left\{-\frac{T}{gd^2(\underline{h})}\right\}$$

(61)

As with the OPD, the homogeneous target and clutter case is obtained by setting g = 1 in the above expression.

When the product multiplier is modeled as a Gamma random variable with parameters $\{(\nu_i, \bar{g}_i)\ i = t+c,c\}$, the average detection performance is calculated to be

$$E\{P_{D/FA}(g)\} = \frac{2}{g\Gamma(v)} \sum_{k=0}^{m-1} \frac{\left(T/d^2(\underline{h})\right)^k}{k!} \left(\frac{T\overline{g}}{d^2(\underline{h})}\right)^{(v-k)/2} K_{v-k}\left(2\sqrt{\frac{T}{d^2(h)\overline{g}}}\right) \tag{62}$$

7.4 ANALYSIS OF SUBOPTIMAL DETECTORS

Two suboptimal polarimetric detectors which are under investigation use simpler detection statistics based on the polarimetric span ($|HH|^2 + 2 |HV|^2 + |VV|^2$) and the single channel, $|HH|^2$. Analysis of each of these algorithms is a special case of a previous analysis. The single $|HH|^2$ channel detector is a special case of the matched filter. Its detection performance is evaluated by letting

$$\underline{h}^t = (1 \ 0 \ 0) \tag{63}$$

in Equations (61) and (62).

Similarly, the detection statistic based on the polarimetric span is a special case of the OPD. Evaluation of its detection performance is easy because this detector is quadratic and of the form

$$y = \underline{X}^t \begin{bmatrix} 1 & 0 & 0 \\ 0 & 2 & 0 \\ 0 & 0 & 1 \end{bmatrix} \underline{X} + C > 0 \tag{64}$$

Thus, we modify Equation (40) to obtain the following:

$$\phi_{y/s}(jw) = \int...\int \exp\left\{ jw\underline{X}^t \begin{bmatrix} 1 & 0 & 0 \\ 0 & 2 & 0 \\ 0 & 0 & 1 \end{bmatrix} \underline{X} + C \right\} \frac{\exp\left\{\frac{-\underline{X}^t \Sigma^{-1} \underline{X}}{g}\right\} d\underline{X}}{\pi^3 g^3 |\Sigma|} \tag{65}$$

and use our previously developed solution to evaluate detection performance for this algorithm.

26

8.0 DUAL CHANNEL LL, LR DETECTION ALGORITHMS

Previous sections presented descriptions of detectors which used the full PSM (in a linear HH, HV, and VV polarization basis). An interesting alternative to the use of the full PSM for detection of targets has been proposed, namely dual channel LL, LR detection algorithms. In this scheme, left circular polarization is transmitted and both LL and LR polarizations are received simultaneously. As was done previously for algorithms using the full PSM, a number of algorithms for processing the LL and LR data will be discussed: (1) the optimal detector using both LL and LR data, (2) a matched filter detector using the LL and LR data, and (3) suboptimal detectors which use only the LL and LR power; one uses LL only, one LR only, and one sums the LL and LR power.

We describe the polarimetric feature vector comprised of the complex LL and LR returns by

$$\underline{Z} = \begin{bmatrix} LL_i + jLL_q \\ LR_i + jLR_q \end{bmatrix} = \begin{bmatrix} LL \\ LR \end{bmatrix} \tag{66}$$

Note that to be consistent with our previous definitions and for purposes of comparing results with the OPD, we express the LL and LR returns in terms of the linear basis by

where

$$\underline{Z} = T \begin{bmatrix} HH \\ HV \\ VV \end{bmatrix}$$

$$T = \begin{bmatrix} 0.5, & j, & -0.5 \\ & & \\ 0.5j, & 0, & 0.5j \end{bmatrix} \tag{67}$$

From the polarization covariance matrix in the linear basis given by Equation (3), the covariance matrix of $\underline{Z}$ is found to be

$$\Sigma_z = \frac{\sigma}{4} \begin{bmatrix} 1 - 2\text{Re}\{\rho\sqrt{\gamma}\} + \gamma + 4\varepsilon & 2\text{Im}\{\rho\sqrt{\gamma}\} - j(1-\gamma) \\ 2\text{Im}\{\rho\sqrt{\gamma}\} + j(1-\gamma) & 1 + 2\text{Re}\{\rho\sqrt{\gamma}\} + \gamma \end{bmatrix} \tag{68}$$

The optimal detector using LL and LR data can be derived in the same manner as the OPD. That is, the optimal detector for LL and LR data, assuming that the feature vectors are jointly Gaussian with zero mean, is one which applies the test

$$\underline{Z}^{\dagger}\left(\Sigma_{Z_{t}}^{-1} - \Sigma_{Z_{t+c}}^{-1}\right)\underline{Z} + \ln\frac{|\Sigma_{Z_{t}}|}{|\Sigma_{Z_{t+c}}|} > \ln T \tag{69}$$

where $\Sigma_{Z_{t+c}}$ is the covariance matrix of the target-plus-clutter vector Z_{t+c}, which is defined by

$$Z_{t+c} = Z_t + Z_c \tag{70}$$

where

$$\Sigma_{Z_{t+c}} = \Sigma_{Z_t} + \Sigma_{Z_c} \tag{71}$$

The feature vectors $\underline{Z}$ comprised of LL and LR data are zero-mean and complex-Gaussian because they are obtained through the linear transformation (67) and because the feature vectors $\underline{X}$ comprised of HH, HV, and VV data were assumed to be zero-mean and complex-Gaussian.

The calculation of the performance of this detector, assuming the product target and clutter models described previously, is very similar to the calculation of the OPD. For the single-look case

$$P_{D/FA}(g) = \sum_{i=1}^{2} A_i E_s\{P_i(g)\} \tag{72}$$

where $E_g\{P_i(g)\}$ is given by (50) where the eigenvalues $(\lambda_1\ \lambda_2)$ are obtained by the simultaneous diagonalization of $\Sigma^{-1}z_t - \Sigma^{-1}z_{t+c}$ and Σ_z^{-1}, the covariance matrix of the test vector. For the multi-look case

$$E_s\left\{P_{D/FA}^{(m)}(g)\right\} = \sum_{i=1}^{2}\sum_{\ell=1}^{m} A_{i\ell} E_s\left\{P_{i\ell}^{(m)}\right\} \tag{73}$$

where $E_s\left\{P_{i\ell}^{(m)}\right\}$ is given by (57) and (58) and

$$A_{i\ell} = \frac{(-2\lambda_i)^\ell}{(m-\ell)!\ \prod\limits_{k=1}^{2}(-2\lambda_k)^m}\ \frac{[-2m+\ell+1]\,[-2m+\ell+2]...[-m]}{\left[\dfrac{1}{2\lambda_i} - \dfrac{1}{2\lambda_{i1}}\right]^{2m-\ell}} \tag{74}$$

where $i_1 = \mathrm{modulo}_2(i) + 1$

In Section 4, a polarimetric matched filter was derived using the full PSM. In a similar manner, a matched filter detector which optimizes the target-to-clutter ratio at the filter output can be defined using LL and LR data. As was shown for the detector using the PSM, the filter which maximizes T/C is the

eigenvector which corresponds to the maximum eigenvalue of $\Sigma_{z_t}^{-1} \Sigma_{z_t}$. The performance of the matched filter that uses LL and LR data can be calculated in the same fashion as for the matched filter that uses HH, HV, and VV data [see Equations (59) through (62)].

One suboptimal algorithm we studied calculates the sum of the powers in the LL and LR channels

$$y = |LL|^2 + |LR|^2 \tag{75}$$

Like the span detector, this algorithm is a suboptimal quadratic classifier since the detection statistic y can be obtained from

$$y = \left(LL^* \ LR^* \right) \begin{bmatrix} 1 & 0 \\ 0 & 1 \end{bmatrix} \begin{bmatrix} LL \\ LR \end{bmatrix} \tag{76}$$

The performance of this algorithm can be determined in the same manner as the performance of the span detector using the PSM.

Finally, since the LL and LR responses can be determined from a linear combination of the HH, HV, and VV returns as shown in Equation (67), the performance of the |LL| only or |LR| only detectors can also be determined using Equations (61) and (62).

9.0 CORRELATION BETWEEN PSM MEASUREMENTS

In the previous sections, optimal multi-look detectors were derived for processing independent PSM measurements. These multi-look algorithms (OPD, PMF, etc.) merely sum the detection statistics obtained at each frequency and compare this sum with the detection threshold. When the PSM measurements at different frequencies are correlated (due to insufficient frequency step size) these multi-look detectors are not optimal; the performance analysis of these detectors must be modified to include the effects of correlated measurements. In this section of the paper, we derive the mathematical formulas for calculating the performance of multi-look polarimetric detectors which were designed assuming independent PSM measurements but tested using correlated measurements.

If the test vectors are not independent, the characteristic equation corresponding to the multi-look OPD algorithm can be written

$$\phi_{y_{m/s}} = \int ... \int \exp\left\{ jw\left[\underline{X}_m^t\left(\Sigma_{m_c}^{-1} - \Sigma_{m_{t+c}}^{-1} \right)\underline{X}_m + C \right] \right\} \frac{\exp\left\{ \frac{-\underline{X}_m^t \Sigma_m^{-1} \underline{X}_m}{g} \right\}}{\pi^{3m} g^{3m} |\Sigma_m|} \, d\underline{X}_m \tag{77}$$

where the design covariance matrices Σ_{m_c} and $\Sigma_{m_{t+c}}$ are block diagonal

$$\Sigma_{m_i} = \begin{bmatrix} \Sigma_i & 0 & ... & 0 \\ 0 & \Sigma_i & ... & 0 \\ \vdots & \vdots & \vdots & \vdots \\ 0 & 0 & ... & \Sigma_i \end{bmatrix} \; ; \; i = c, t+c \tag{78}$$

The test covariance matrix is assumed to be

$$\Sigma_m = \begin{bmatrix} \Sigma & r\Sigma & ... & r^{(m-1)}\Sigma \\ r^*\Sigma & \Sigma & ... & r^{(m-2)}\Sigma \\ \vdots & \vdots & \vdots & \vdots \\ r^{*(m-1)}\Sigma & r^{*(m-2)}\Sigma & ... & \Sigma \end{bmatrix} \tag{79}$$

and r is, in general, the complex correlation between PSM measurements at any two adjacent frequencies.

The conditional characteristic function can be shown to be

$$\phi_{y_{m/s}}(jw) = e^{jwC} \sum_{i=1}^{3m} \frac{A_i}{\left(1 - j2g\lambda_i w \right)} \tag{80}$$

31

where λ_i are the eigenvalues of $\Sigma_m (\Sigma_{m_c} - \Sigma_{m_{t+c}})$.

If the eigenvalues are all distinct (which is not the case when $r = 0$) then P_D and P_{FA} can be shown to be

$$P_{D/FA} = \sum_{i=1}^{3m} A_i E_g \{P_i(g)\} \tag{81}$$

where $E_g\{P_i(g)\}$ is given in Equation (50) and the residues are

$$A_i = \prod_{\substack{j=1 \\ i \neq j}}^{3m} \frac{1}{\left(1 - \dfrac{\lambda_j}{\lambda_i}\right)} \tag{82}$$

It can be shown that $\Sigma_m\left(\Sigma_{m_c}^{-1} - \Sigma_{m_{t+c}}^{-1}\right)$ is of the form

$$\Sigma_m\left(\Sigma_{m_t}^{-1} - \Sigma_{m_{t+c}}^{-1}\right) = \left[\begin{array}{c|c|c|c} A & rA & \cdots & r^{(m-1)}A \\ \hline r^*A & A & \cdots & r^{(m-2)}A \\ \hline \vdots & \vdots & \vdots & \vdots \\ \hline r^{*(m-1)}A & r^{*(m-2)}A & \cdots & A \end{array}\right] \tag{83}$$

where
$$A = \Sigma\left(\Sigma_c^{-1} - \Sigma_{t+c}^{-1}\right) \tag{84}$$

If we define

$$
R = \begin{bmatrix} 1 & r & \cdots & r^{(m-1)} \\ r^{*} & 1 & \cdots & r^{(m-2)} \\ \vdots & \vdots & \vdots & \vdots \\ r^{*(m-1)} & r^{*(m-2)} & \cdots & 1 \end{bmatrix} \tag{85}
$$

then the eigenvectors of $\Sigma_m\left(\Sigma_{m_c}^{-1} - \Sigma_{m_{i+c}}^{-1}\right)$ can be shown to be of the form

$$
\begin{bmatrix} h_R(1) & \underline{h}_\Sigma \\ \vdots \\ h_R(m) & \underline{h}_\Sigma \end{bmatrix} \tag{86}
$$

where $\underline{h}_\Sigma$ is an eigenvector of $\Sigma\left(\Sigma_c^{-1} - \Sigma_{i+c}^{-1}\right)$ and $\underline{h}_R$ is an eigenvector of R

$$
\underline{h}_R = \begin{bmatrix} h_R(1) \\ h_R(2) \\ \vdots \\ h_R(m) \end{bmatrix} \tag{87}
$$

Also, the 3m eigenvalues of $\Sigma_m\left(\Sigma_{m_c}^{-1} - \Sigma_{m_{i+c}}^{-1}\right)$ can be shown to be the product of an eigenvalue of R with an eigenvalue of $\Sigma\left(\Sigma_c^{-1} - \Sigma_{i+c}^{-1}\right)$. Since we have obtained the eigenvalues of $\Sigma\left(\Sigma_c - \Sigma_{i+c}\right)$, using MACSYMA [14], we only require the eigenvalues of R in order to find the eigenvalues of $\Sigma_m\left(\Sigma_{m_c}^{-1} - \Sigma_{m_{i+c}}^{-1}\right)$. Note also that the complex matrix R, for which $r = |r|e^{j\phi}$, can be factored as

$$
\Phi^{-1}R\Phi = \begin{bmatrix} 1 & |r| & \cdots & |r|^{m-1} \\ |r| & 1 & \cdots & |r|^{m-2} \\ \vdots & \vdots & \vdots & \vdots \\ |r|^{m-1} & |r|^{m-2} & \cdots & 1 \end{bmatrix} \tag{88}
$$

33

where

$$
\Phi = \begin{bmatrix} e^{-j\phi} & 0 & \ldots & \ldots \\ 0 & e^{-j2\phi} & \ldots & 0 \\ \vdots & \vdots & \vdots & \vdots \\ 0 & 0 & \ldots & e^{-jm\phi} \end{bmatrix}
$$

(89)

Thus two matrices of the form described in Equation (85) whose elements have the same magnitudes but different phases share the same eigenvalues. This implies that the detection performance of the multi-look OPD algorithm is independent of the phase of the correlation between frequencies. The eigenvalues of the matrix R must be computed numerically.

Other polarimetric detectors such as the span, the LL, LR optimal detector and the $|LL|^2 + |LR|^2$ algorithms are also quadratic detectors. Thus, the detection performance of these algorithms for multiple correlated looks can be solved in the same manner as above.

For the PMF, the optimal processing of independent multiple looks is to sum the magnitude-squared of the matched filter output from each look. Clearly, this algorithm is also sensitive to the correlation between PSM measurements at different frequencies.

Using the multi-look model described above where the covariance of the vector $\underline{X}_m$ is described by Equation (79), the outputs of the PMF for multiple correlated looks are jointly Gaussian random variables. Because of this, the detection performance of the PMF can be solved in a similar manner similar to the OPD. Thus, for m-looks we obtain

$$
P_{D/FA} = \sum_{i=1}^{m} A_i E_g \{ P_i(g) \}
$$

(90)

where

$$
A_i = \prod_{\substack{j=1 \\ i \neq j}}^{m} \frac{1}{(1 - \lambda_j / \lambda_i)}
$$

(91)

and $E_g\{Pi(g)\}$ is given by Equation (50). The λ_i in the above expression are the eigenvalues of the matrix $\sigma_m^2 R$ where σ_m^2 is the variance of the single-frequency matched filter output, for a given scale factor g. Other algorithms such as the $|HH|^2$-only, $|LL|^2$-only, and $|LR|^2$-only can also be evaluated in the same way.

10.0 DETECTION ALGORITHM PERFORMANCE PREDICTIONS

The information presented in the previous sections includes the following: (1) a discussion of a number of detection algorithms, (2) development of homogeneous (Gaussian) and non-homogeneous (non-Gaussian) product target and clutter models, (3) derivations of the formulas necessary for evaluating the performance of various detectors for: single-look and multi-look cases, and for homogeneous and non-homogeneous targets and clutter. This section predicts the performance of the various detection algorithms in different situations. It does so by using parameters $(\sigma, \epsilon, \gamma, \rho)$ from measured target and clutter data to construct polarization covariance matrices of targets and clutter. These covariance matrices are used to calculate predicted detection performance of the various detectors. The subjects discussed in this section are

1. OPD, Span and $|HH|^2$ Performance Predictions
2. PMF Detection Performance Predictions
3. Detection Performance Using Circular Polarization
4. Discrimination Performance of the OPD

The performance predictions presented in this section of the report are based on polarimetric measurement data from typical ground targets and meadow clutter. Detection performance predictions presented in this section are for an armored target (target 1) versus clutter. Target discrimination results presented are for target 1 versus target 2 (a truck).

The polarimetric parameters of these targets and clutter are presented in Table I.

TABLE I

Polarimetric Parameters of Targets and Clutter

	σ	ϵ	γ	$\rho\sqrt{\gamma}$
TARGET 1	58.5	0.19	1.0	0.28
TARGET 2	618.3	0.02	1.1	0.83
CLUTTER	4.75	0.18	1.6	0.63

10.1 OPD, SPAN, AND $|HH|^2$ PERFORMANCE PREDICTIONS

This section compares performance predictions of three different detectors; (1) the optimal polarimetric detector (OPD) which uses all the information contained in the PSM, (2) the polarimetric span which uses the amplitude information but not the phase information in the PSM, and (3) the single-channel $|HH|^2$ detector which is the simplest radar detection scheme. This is the type of detector used in the HOWLS [1] program.

Single-Look Predictions: We have compared the performance of the OPD with the performance of both span and single-channel $|HH|^2$

algorithms. Both OPD and span processing require two pulses per look, whereas $|HH|^2$ processing requires only one. A fair comparison among the three algorithms requires the use of the same number of pulses. Therefore, we assumed that (1) the "extra" pulse for $|HH|^2$ processing would be used to provide a second, independent sample at a second frequency, and (2) the two independent $|HH|^2$ samples were noncoherently averaged.

For single-look processing with homogeneous targets and clutter, Figure 1 shows that the OPD outperformed span processing; this is to be expected, since the OPD uses all the polarimetric information in an optimally weighted fashion. The $|HH|^2$ processing also outperformed span processing, even though span processing uses all three polarimetric amplitudes; presumably this is due to the use of two independent samples in the $|HH|^2$ processing.

The OPD performed somewhat better than $|HH|^2$ processing. However, achievement of this improvement in detection performance requires exact knowledge of the target-to-clutter ratio as well as the target and clutter covariance statistics, since the optimal weighting coefficients are computed from this information. Since these target and clutter statistics are difficult to predict a priori, implementing the OPD in a real system would be difficult.

Contribution of Polarimetric Phase Information: The contribution of the polarimetric phase term, $|HH|\ |VV|\cos(\phi_{HH} - \phi_{VV})$, in target detection does not appear to be significant. In the first place, it can be shown that the distance measures of Equations (12)-(14) are dominated by the radar cross-section terms ($|HH|^2, |VV|^2, |HV|^2$). Another way to show this is to evaluate detection performance using amplitude-normalized feature vectors. The optimal processor of normalized data (OPDN) [17] provides the best possible performance for normalized Gaussian feature vectors. The optimal performance for the normalized data is shown in the curves of Figure 2. A comparison of the performance of the optimal processor for normalized data (Figure 2) with that of the OPD which processes unnormalized data (Figure 1) clearly shows that it is the polarimetric amplitude information which provides the good detection performance results of the OPD.

Multi-Look Processing: Figure 3 summarizes the performance predictions for the 6-dB target-to-clutter ratio case using multi-look processing for homogeneous targets and clutter. $|HH|^2$ detection performance is again superior to detection using the span statistic. An optimally weighted combination of the $|HH|^2, |VV|^2$ and $|HV|^2$ amplitudes might improve performance of the span detector somewhat; however, the span performance is bounded above by the OPD, and HH processing is not significantly worse than OPD performance.

Product Model Effects: The results of Figure 3, which correspond to multi-look processing of statistically independent PSM samples, are very optimistic because idealized homogeneous target and clutter models were used. With more realistic product model representations of targets and clutter,
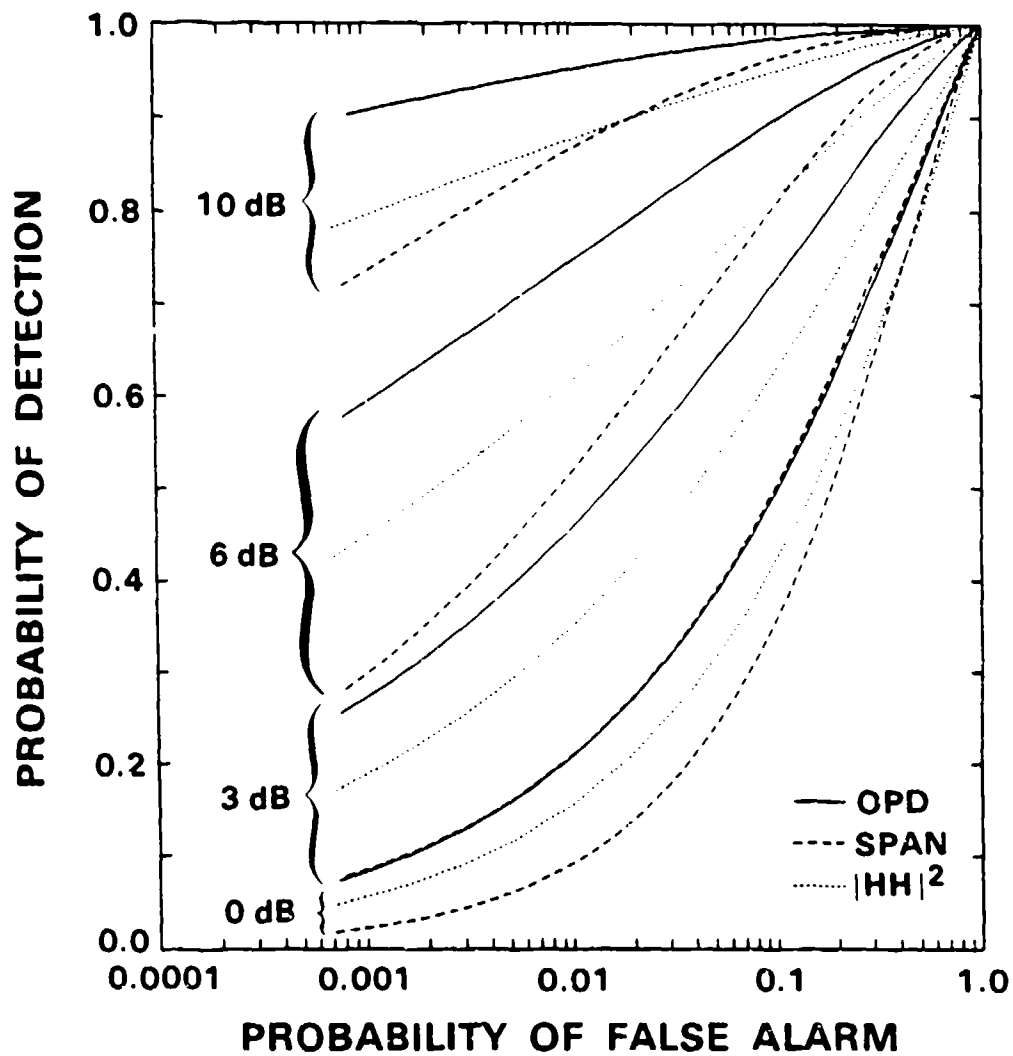
Figure 1. Algorithm performance comparison vs T/C ratio
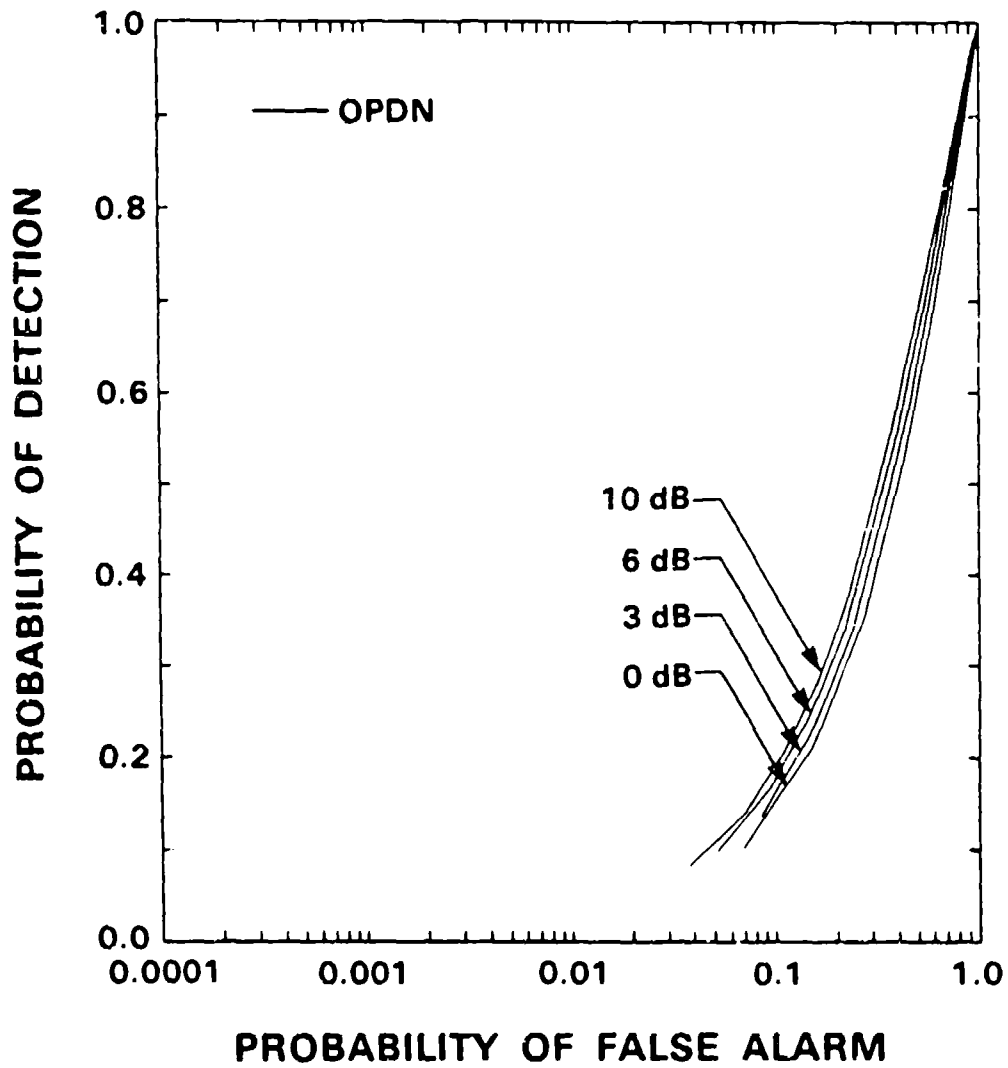(single-look homogeneous models).

Figure 2. Performance of optimal normalized polarimetric detector
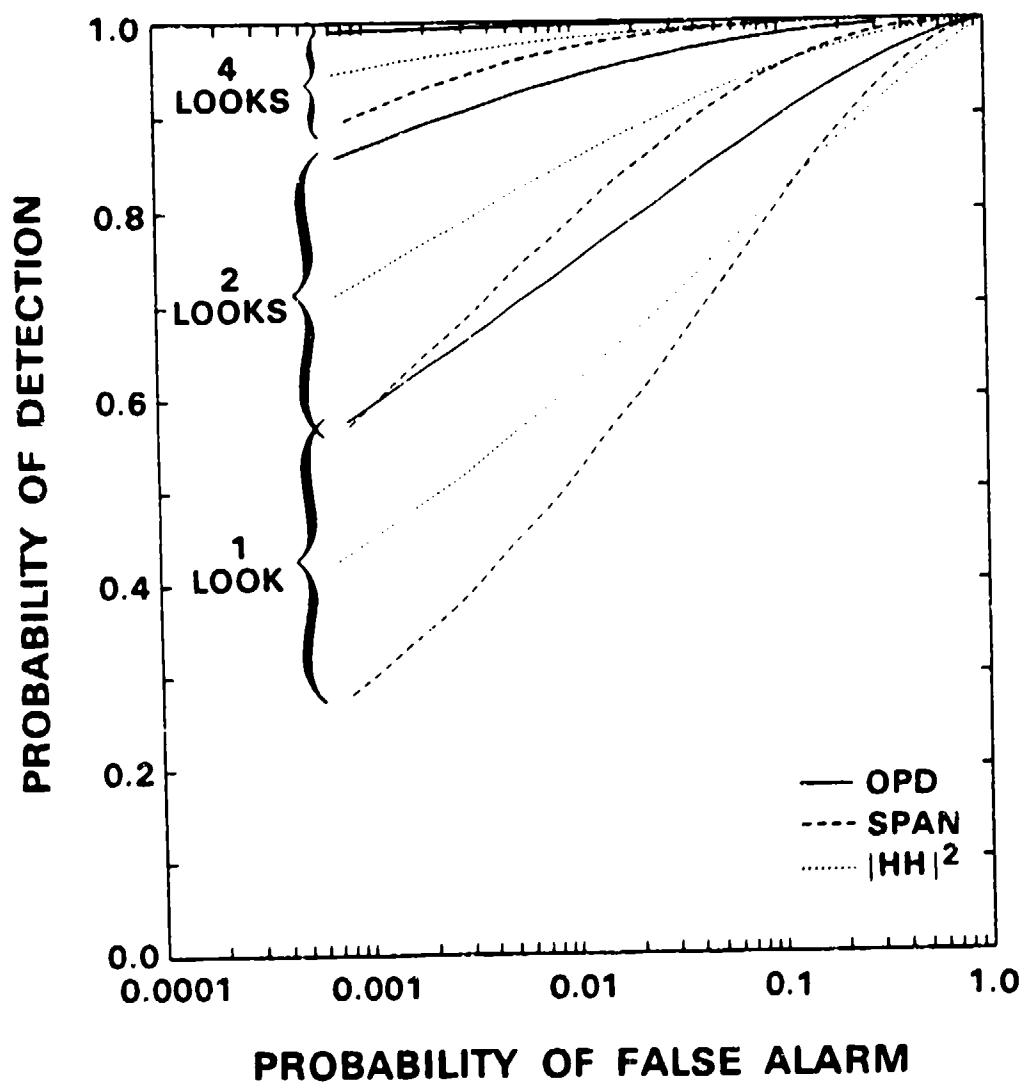vs T/C ratio (single-look, homogeneous models).

Figure 3. Algorithm performance comparison vs N looks
(T/C = 6 dB, homogeneous models).

we obtain performance results for HH processing which are consistent with those achieved using the HOWLS [1] radar data.

The curves of Figures 4 and 5 show more realistic algorithm performance predictions based on the product target and clutter models. These figures show the performance of the OPD designed for homogeneous target and clutter models but tested against nonhomogeneous product target and clutter model inputs. Comparing Figure 4 with Figure 1 (and Figure 5 with Figure 3) shows the deleterious effect of nonhomogeneous targets and clutter on the performance of all three algorithms. For example, for $P_{FA} = 10^{-3}$ the detection performance of the OPD with 10-dB target-to-clutter ratio is degraded from 90 percent to less than 70 percent. Similar reductions can be observed for the other algorithms and at other target-to-clutter ratios.

Furthermore, the performance improvement achieved through multi-look processing is considerably reduced when the more realistic (nonhomogeneous) target and clutter models are used (compare Figure 5 with Figure 3). Thus, the benefits of frequency averaging of independent PSM samples are reduced due to nonhomogeneity of the target and clutter models. These observations are consistent with results obtained previously using HOWLS data [1]. Also, the performance advantage of the OPD relative to $|HH|^2$ processing is reduced in this case since the OPD detector was designed to be optimal for homogeneous target and clutter models.

Sensitivity to Product Model Parameters: In a previous study [1], we showed that the nonhomogeneity of ground clutter and aspect angle variability of targets were dominant factors in the reduction of detection performance of a single-channel $|HH|^2$ detector; that is, the sensitivity of detection performance to the target and clutter standard deviation parameters, α_t and α_c, is quite severe. To verify that this effect also applies to polarimetric detection algorithms we have evaluated the performance of the OPD over a reasonable range of α_c (1, 1.5, 2, 2.5, and 3 dB). Figure 6 shows the OPD performance predictions for single-look and 4-look processing. The top curves (denoted as $\alpha_c = 0$ dB) correspond to the homogeneous clutter model and are included as an upper bound on performance. From the curves, it is clear that detection performance is degraded rapidly with the increasing nonhomogeneity of clutter.

We have also evaluated the performance of the OPD over a reasonable range of α_t (0, 1, 2, 3, and 4 dB). Figure 7 shows the resulting performance predictions. From these curves, it is seen that the single-look results are less affected by a change in α_t than the 4-look results. Nevertheless, there is, in general, a fairly strong dependence on α_t.

Comparison of OPD with Product-Model Likelihood Ratio Test: The product-model likelihood ratio test is the optimal detector for product-model targets and clutter. This algorithm was defined in Equation (37). Since the OPD (designed for homogeneous models) exhibits degraded performance when tested with nonhomogeneous models, it is of interest to compare the
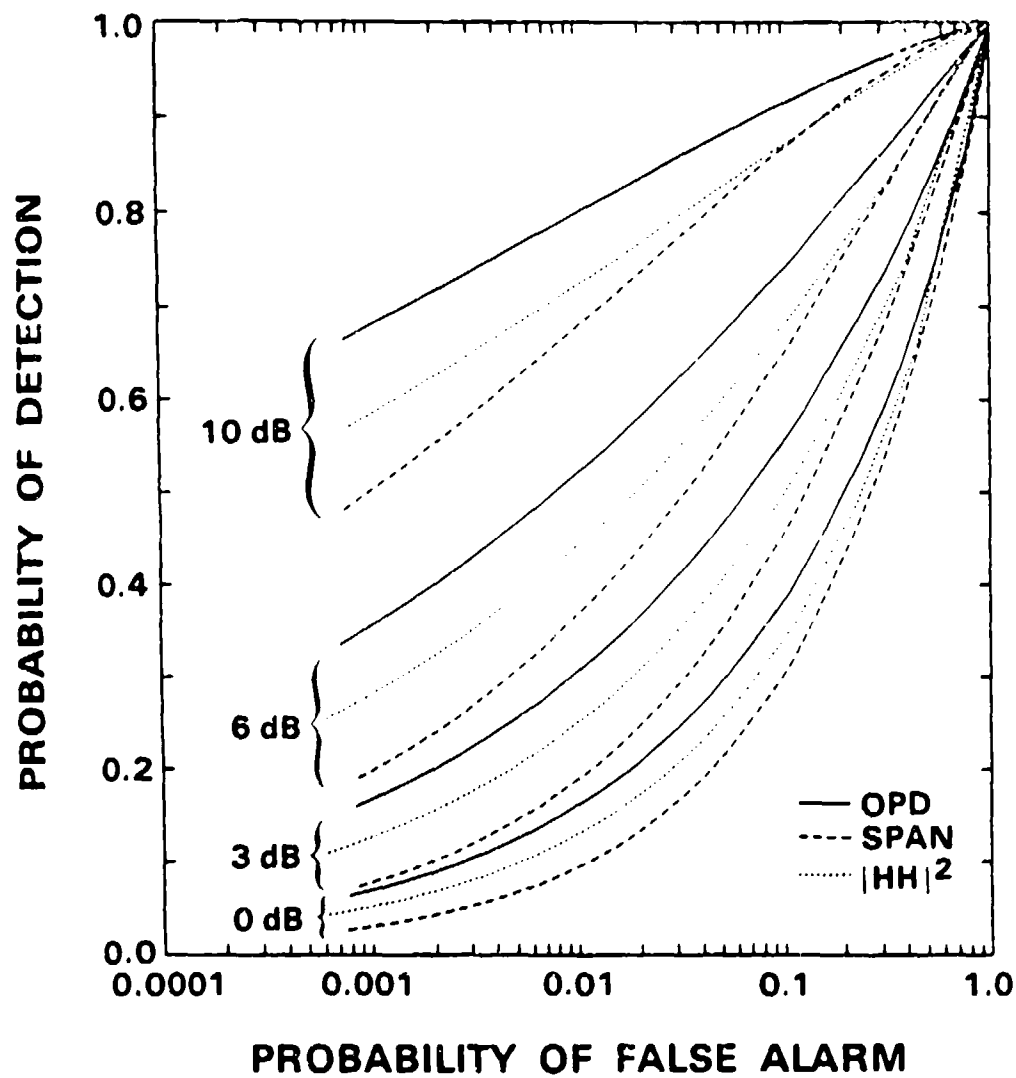
Figure 4. Algorithm performance comparison vs T/C ratio
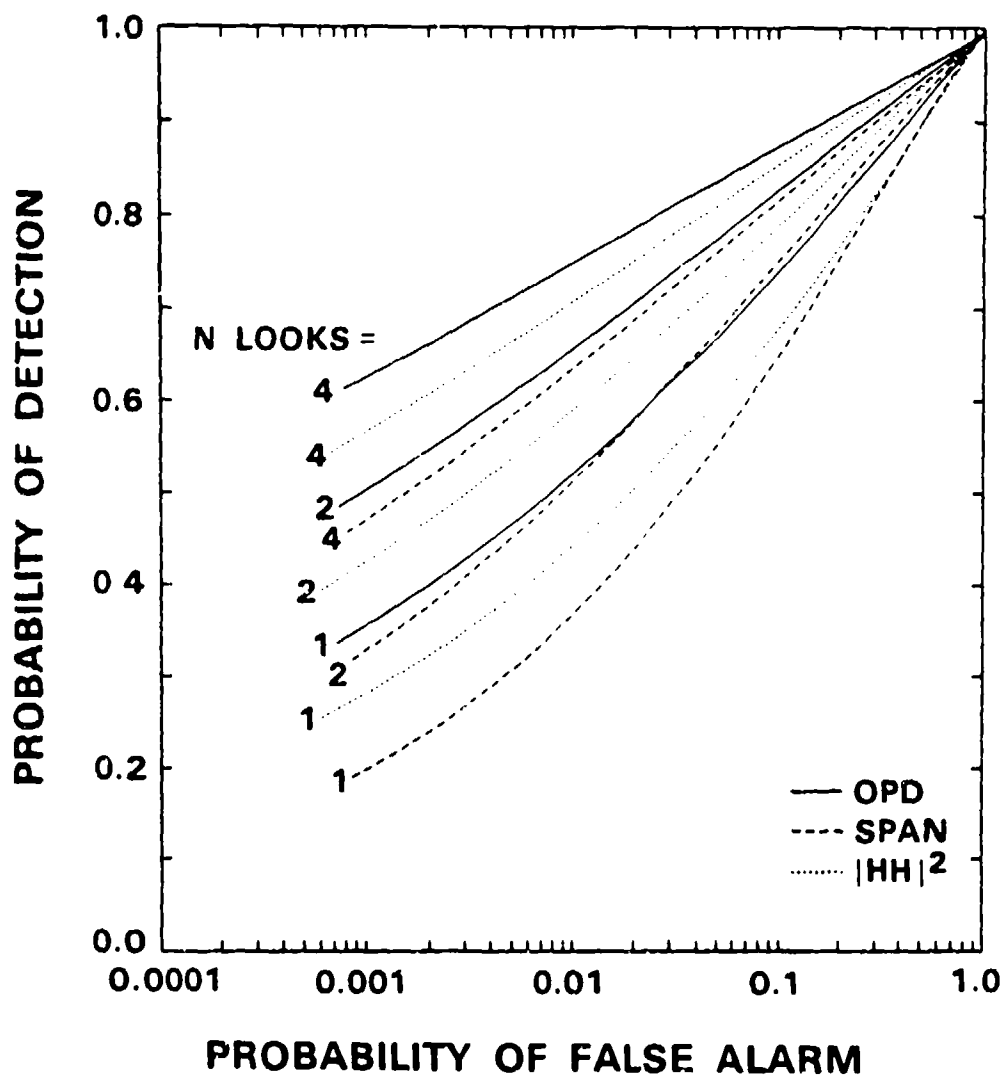[single-look product rnodel (α_t = 3 dB, α_c = 1.5 dB)].

41

Figure 5. Algorithm performance comparison vs N looks [T/C = 6 dB, product models (α_t = 3 dB, α_c = 1.5 dB)].
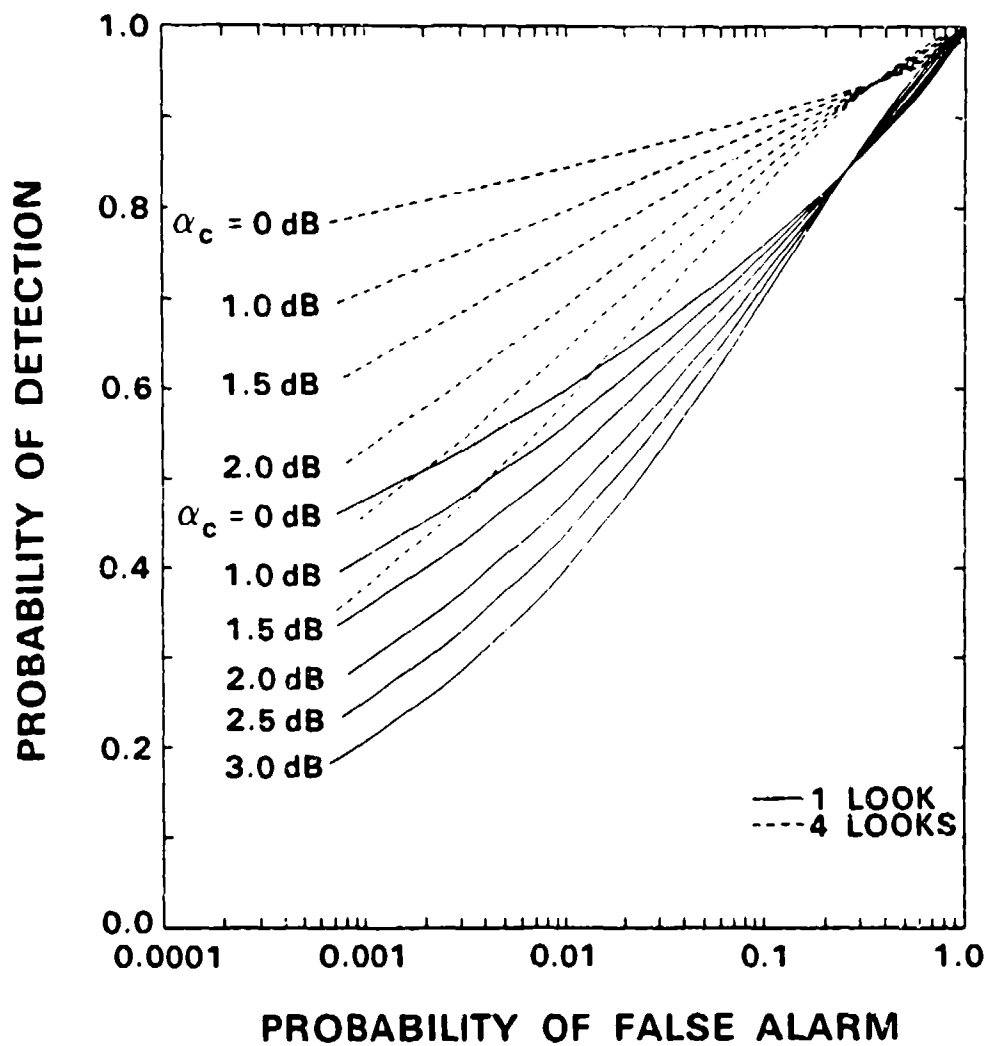
Figure 6. Sensitivity of OPD to clutter St. Dev.
[T/C = 6 dB, product model (α_t = 3 dB)].
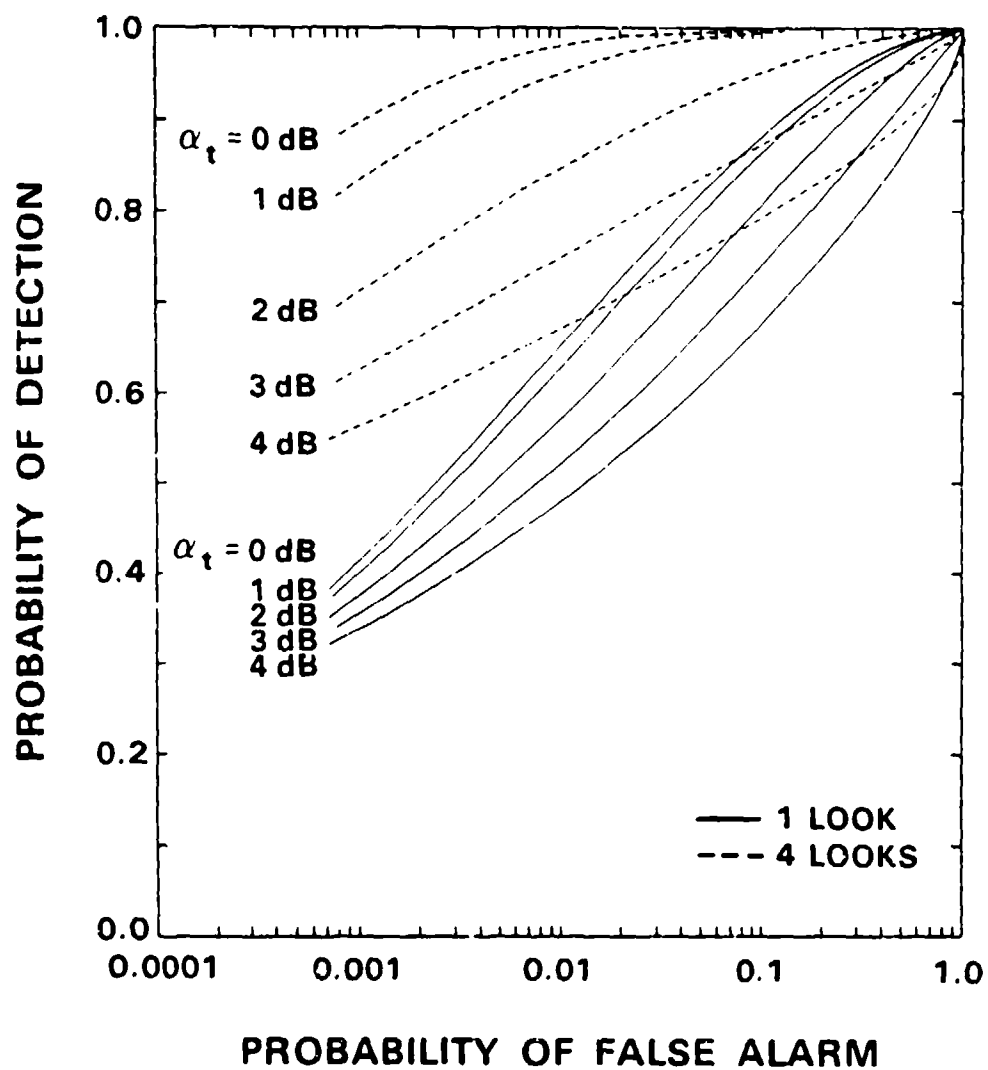
43

Figure 7. Sensitivity of OPD to target St. Dev.
[T/C = 6 dB, product model (α_c = 1.5 dB)].

performance of the OPD with that of the LRT algorithm. Our studies indicate that over the range of parameter variations of interest the OPD performs almost as well as the LRT algorithm.

10.2 PMF DETECTION PERFORMANCE PREDICTIONS

The OPD discussed in previous sections is the optimal processor assuming Gaussian statistics; however, it is nonlinear, and requires a priori knowledge of both the target and clutter covariances and the target-to-clutter ratio. The PMF on the other hand is a linear processor which also requires a priori knowledge of the target and clutter covariances. However, the PMF (a constant-coefficient filter) does not require a priori knowledge of the target-to-clutter ratio.

This section presents the results of our polarimetric matched filter studies. We designed the PMF based on the target and clutter covariances specified earlier [see Equations (18)-(23)]. Evaluating the eigenvalues and eigenvectors of the matrix $\Sigma_c^{-1} \Sigma_t$, yields the following solutions:

$$(i) \quad \lambda_1 = 12.78 \leftrightarrow \underline{h}_1 = \begin{bmatrix} 0 \\ 1 \\ 0 \end{bmatrix}$$

$$(ii) \quad \lambda_2 = 7.54 \leftrightarrow \underline{h}_2 = \begin{bmatrix} 1 \\ 0 \\ 3.6 \end{bmatrix}$$

$$(iii) \quad \lambda_3 = 15.58 \leftrightarrow \underline{h}_3 = \begin{bmatrix} 1 \\ 0 \\ -0.5 \end{bmatrix}$$

The best PMF is, therefore, specified by solution (iii) above. Note, however, that solution (i) is also a good solution. We have compared the detection performance of the optimal PMF (solution (iii)) with that of the single-channel $|HH|^2$ detector. One of our objectives was to make a direct comparison of the PMF with the results of the HOWLS radar [1], so for these comparisons we have used product target and clutter models with standard deviation parameters $\alpha_t = 3$ dB, $\alpha_c = 2$ dB and $(T/C) = 6$ dB. Equations (61) and (62) were used to obtain the performance predictions. Figure 8 summarizes the results, showing detection performance of the PMF with 1, 2, 4, 8, and 16 independent polarimetric samples processed. Since these polarimetric samples require transmitting 2, 4, 8, 16, and 32 radar pulses, we show the comparison with $|HH|^2$ processing using these same numbers of transmitted pulses.

The PMF (with an equivalent number of transmitted pulses) does not perform as well as $|HH|^2$ processing until we process about 8 independent fully polarimetric measurements. With 8 independent looks (16 pulses transmitted)
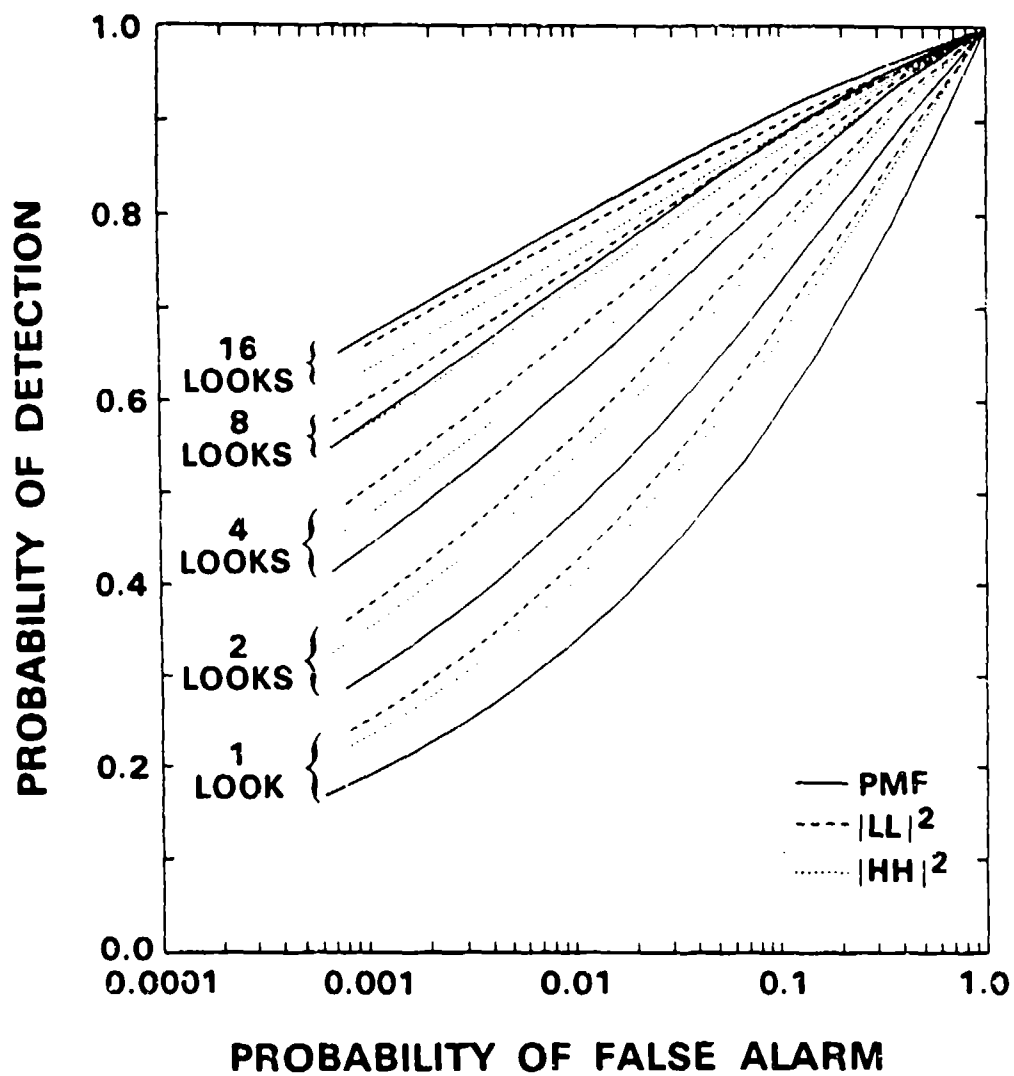
Figure 8. Algorithm performance comparison
[T/C = 6 dB, product models (α_t = 3 dB, α_c = 2 dB)].

the two algorithms provide essentially the same performance. The performance predictions with 16 pulses transmitted agree closely with the HOWLS measurements (i.e., $P_D \sim 50$ percent and $P_{FA} \sim 10^{-3}$ with 6 dB target-to-clutter ratio). As more independent looks are processed, the PMF begins to out perform the $|HH|^2$ detector.

We have also made a performance comparison of the best PMF design with a detector using a circular transmit, circular receive $|LL|^2$ system. It has been reported that this algorithm achieves a better target-to-clutter ratic than the linear transmit, linear receive $|HH|^2$ system. Also, a single $|LL|^2$ measurement requires only 1 pulse transmission. For the actual target and clutter data used in this study, the $|LL|^2$ (even-channel) T/C was 6.3 dB, and the $|HH|^2$ T/C was 6.0 dB. Correspondingly,Figure 8 shows that the even channel $|LL|^2$ detection performance is slightly better than the $|HH|^2$ detection performance. All three detectors are essentially equivalent in performance with 16 pulses transmitted.

10.3 DETECTION PERFORMANCE WITH CIRCULARLY POLARIZED DATA

In this section we evaluate the performance of detectors that use circularly polarized radar data. We compare the performance of the OPD (which uses all the information contained in the PSM but requires two orthogonal transmit pulses) with that of simpler detectors that use a single circular transmit polarization. The detection algorithms we examine are:

(i) the OPD

(ii) the optimal quadratic detector using complex LL, LR data

(iii) a polarimetric matched filter using complex LL, LR data

(iv) a detector using the sum of the powers $|LL|^2 + |LR|^2$

(v) detectors using either $|LL|^2$ or $|LR|^2$ data

The curves in Figure 9 compare the results using the OPD, the optimal quadratic detector using complex LL and LR data, and the suboptimal detector which uses the sum of the powers $|LL|^2 + |LR|^2$, for the situation where two pulses are transmitted (which is the minimum required by the OPD). It is assumed that the dual-circular detectors obtain and process two independent looks of LL, LR data whereas the OPD uses the two transmit pulses to obtain LL, LR, and RR returns. The analysis used product-model target and clutter inputs. Figure 9 shows performance predictions versus target-to-clutter ratio. Figure 10 shows the detection performance of these same algorithms for a fixed target-to-clutter ratio of 6 dB, for 1-, 2-, and 4-look data, where each look consists of two transmitted pulses. These figures show that optimal processing of two independent measurements of complex LL, LR data provides better detection performance than the OPD (which requires two pulses to construct the PSM).
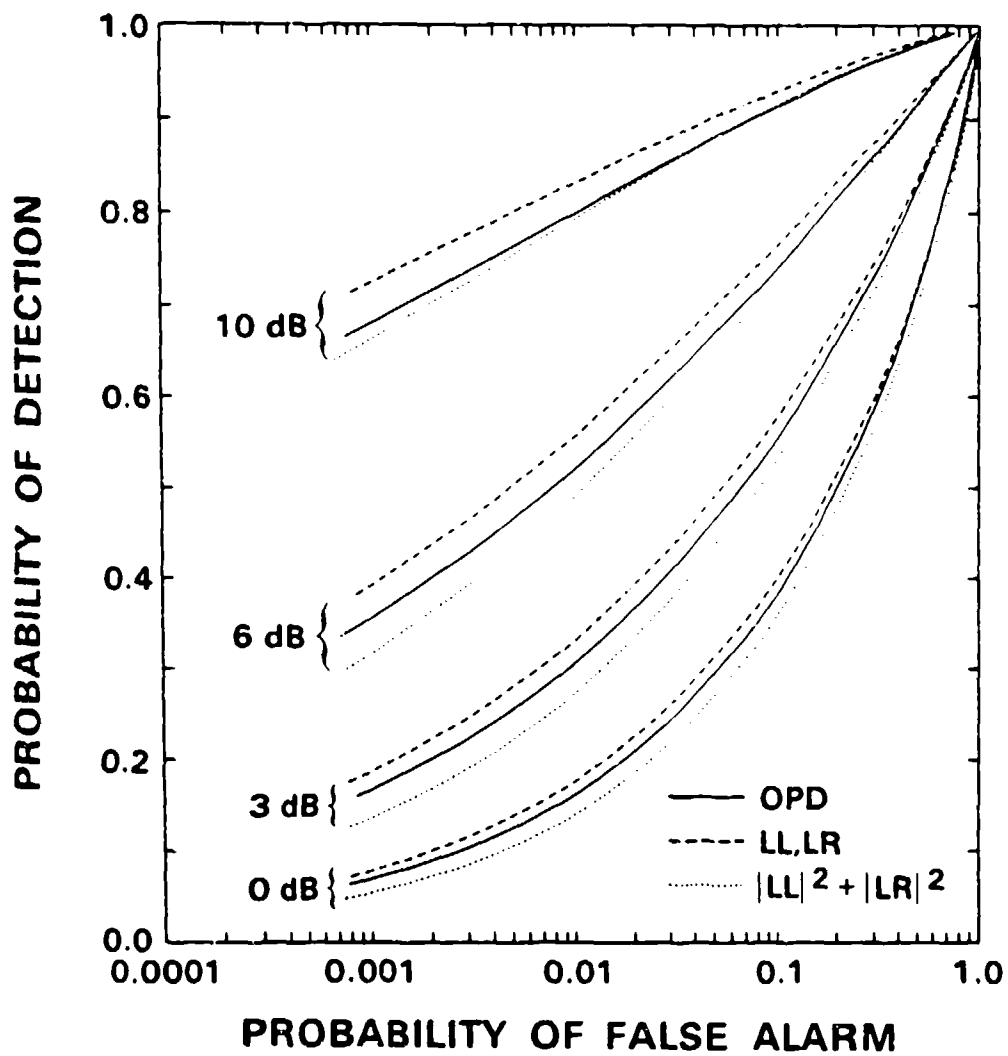
Figure 9. Algorithm performance comparison vs T/C ratio [single-look product model (α_t = 3 dB, α_c = 1.5 dB)].
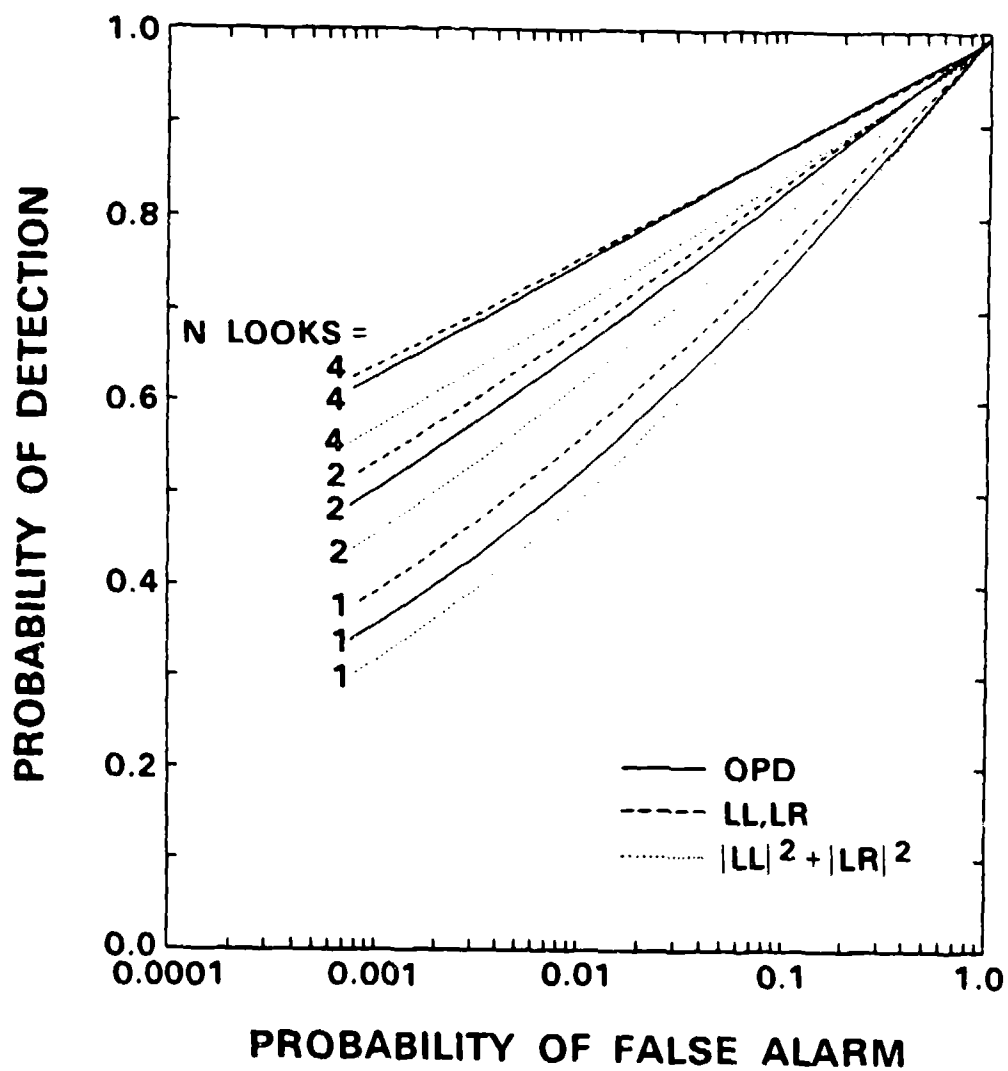
Figure 10. Algorithm performance comparison vs N looks
[T/C = 6 dB, product models ($\alpha_t = 3$ dB, $\alpha_c = 1.5$ dB)].

They also show that the $|LL|^2 + |LR|^2$ detector (which , unlike the other two algorithms, requires no previous information concerning the target and clutter covariances or the target-to-clutter ratio) provides slightly less performance than the OPD.

Figure 11 compares the performance of four detection algorithms that require only one transmit pulse per look, the LL, LR matched filter, the $|LL|^2 + |LR|^2$ detector, the $|LL|^2$-only detector, and the $|LR|^2$-only detector. The LL, LR PMF was designed based on the target and clutter covariances specified in Table I. Evaluating the eigenvalues and eigenvectors of the matrix $\Sigma_{Z_c}^{-1} \Sigma_{Z_t}$ yields the following solution

(i) $\lambda_1 = 7.715 \quad \leftrightarrow \quad \underline{h}_1 = \begin{bmatrix} 1 \\ -2.182 \end{bmatrix}$

(ii) $\lambda_2 = 14.620 \quad \leftrightarrow \quad \underline{h}_2 = \begin{bmatrix} 1 \\ 0.348 \end{bmatrix}$

The PMF using LL, LR data is specified by solution (ii) above. Note that the PMF weights the LL return much more heavily than the LR return.

The curves of Figure 11 indicate that the performance of the $|LL|^2$- only detector compares well with that of the matched filter (which requires prior knowledge of the target and clutter covariances). The $|LL|^2$-only-detector provides much better performance than the $|LR|^2$-only detector.

This is consistent with the observation that the armored target contains significant evenbounce (LL) return whereas the clutter is predominantly odd-bounce (LR). Also, the $|LL|^2$-only detector is also superior to the $|LL|^2 + |LR|^2$ detector (because the two channels are simply added without optimum weighting). Figure 11 shows that the best combination of polarization channels to use in a detector is dependent on the statistics (i.e., covariance matrices) of the particular target and clutter type. The relative performance of the detectors shown in Figures (9), (10), and (11) might be different for different targets and/or clutter types.

10.4 DETECTION PERFORMANCE WITH CORRELATED MULTI-LOOK DATA

Actual correlations calculated from polarimetric measurements of an armored target (as a function of frequency change between looks) are shown in Figure 12. The magnitude of the correlation coefficients for all three channels (HH, HV, and VV) is approximately 0.8 and follows closely the model defined in Equation (79). The cross-correlation between the complex VV and HH data also agreed with the model. Correlations calculated from polarimetric measurements of meadow clutter were very small (less than 0.1) for all the polarimetric channels. Thus, the results described below assume a frequency step of 10 MHz corresponding to correlation coefficients of 0.8 and 0.0 for the target and clutter, respectively.
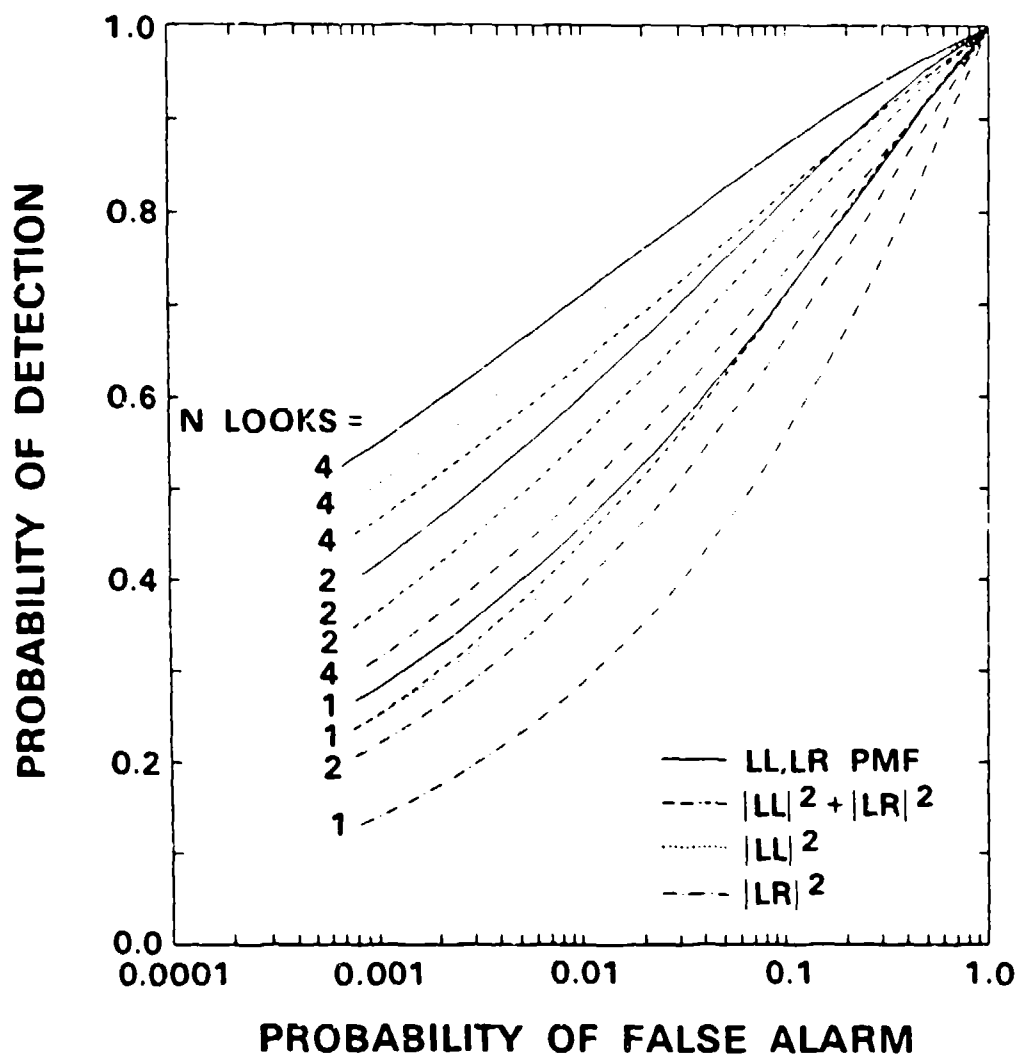
Figure 11. Algorithm performance comparison
[T/C = 6 dB, product models (α_t = 3 dB, α_c = 2 dB)].
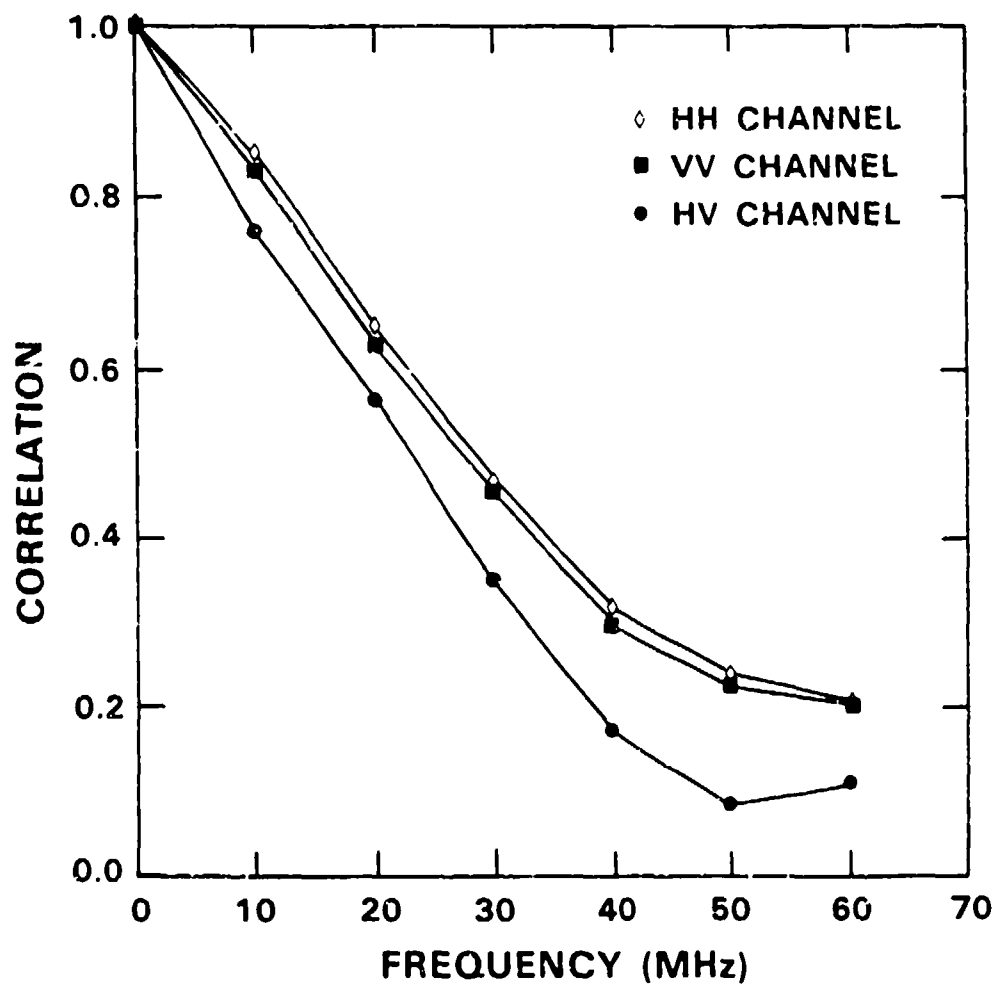
Figure 12. Correlation vs frequency for armored target.

Figures 13, 14, and 15 show the performance predictions for the same detection algorithms and cases given previously in Figures 9, 10, and 11, however, this time with correlated multi-look data. Comparing the curves of Figures 13 and 14 with Figures 9 and 10 shows that correlation between frequency measurements degrades algorithm performance slightly. Performance of the optimal quadratic detector using LL, LR data is again comparable with that of the OPD. The $|LL|^2 + |LR|^2$ algorithm is also shown to give the poorest performance.

Similar remarks can be made about the comparison of performance predictions of Figures 15 and 11. In general, the use of correlated measurement data has degraded the performance of the various algorithms. The relative performance of algorithms is consistent with the previous results shown in Figure 11.

Figure 13. Algorithm performance comparison vs T/C ratio
[single-look product model ($\alpha_t = 3$ dB, $\alpha_c = 1.5$ dB), correlated
looks ($r_t = 0.8$, $r_c = 0.0$)].

Figure 14. Algorithm performance comparison vs N looks [T/C = 6 dB, product models (α_t = 3 dB, α_c = 1.5 dB), correlated looks (r_t = 0.8, r_c = 0.0)].
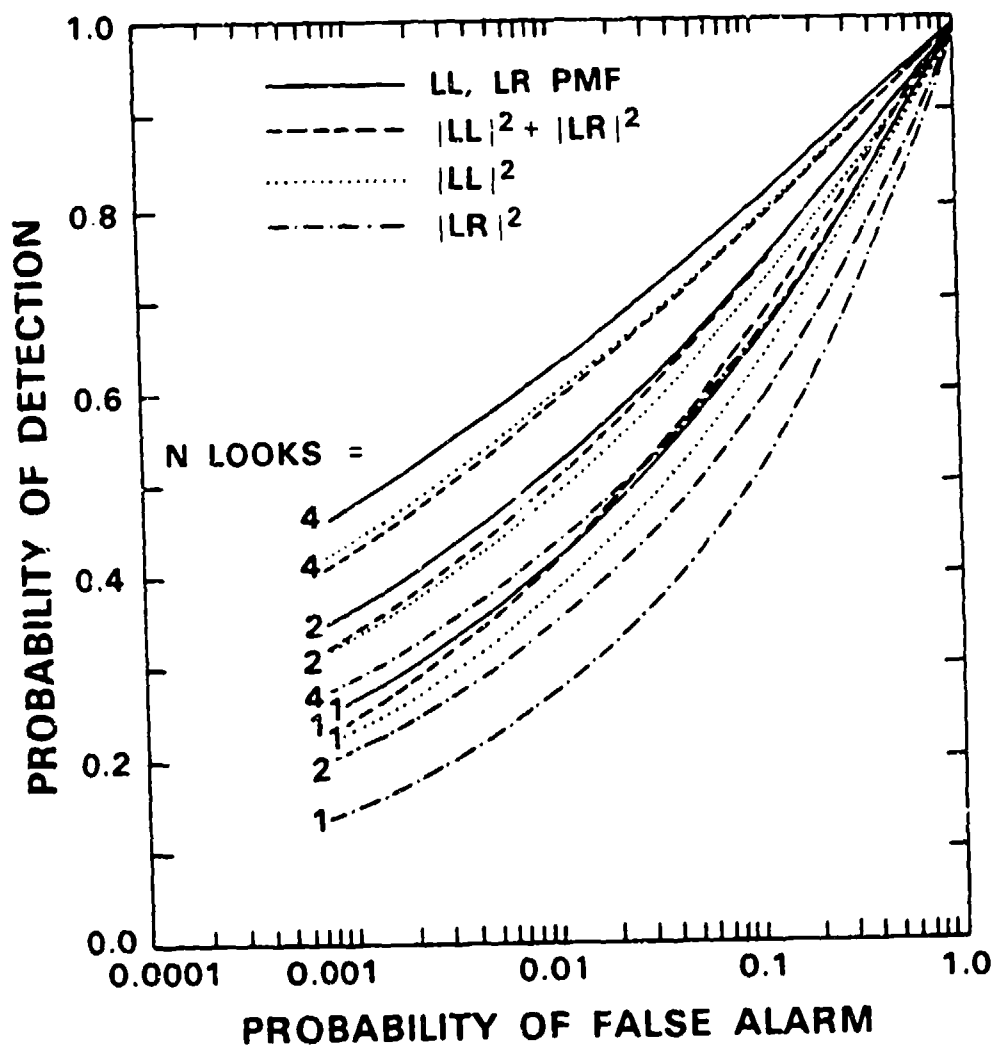
Figure 15. Algorithm performance comparison vs N looks
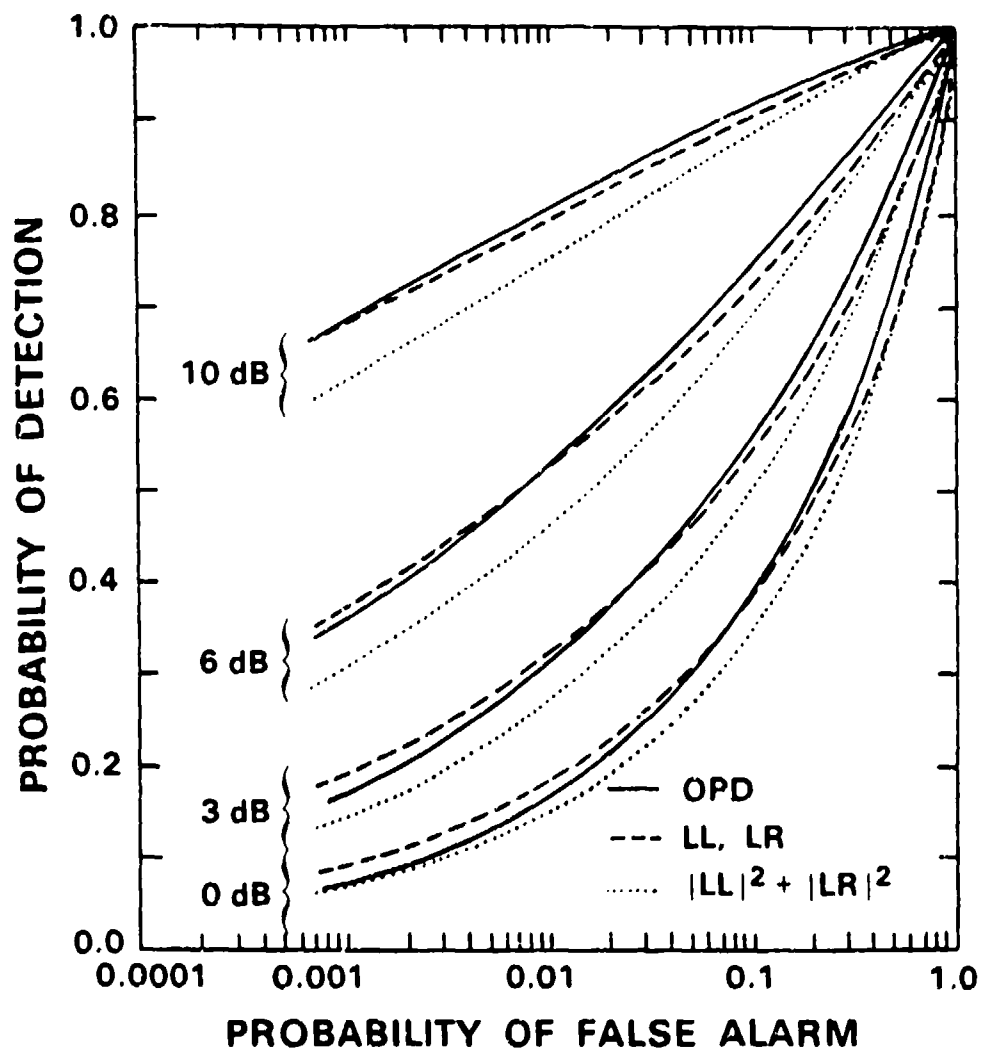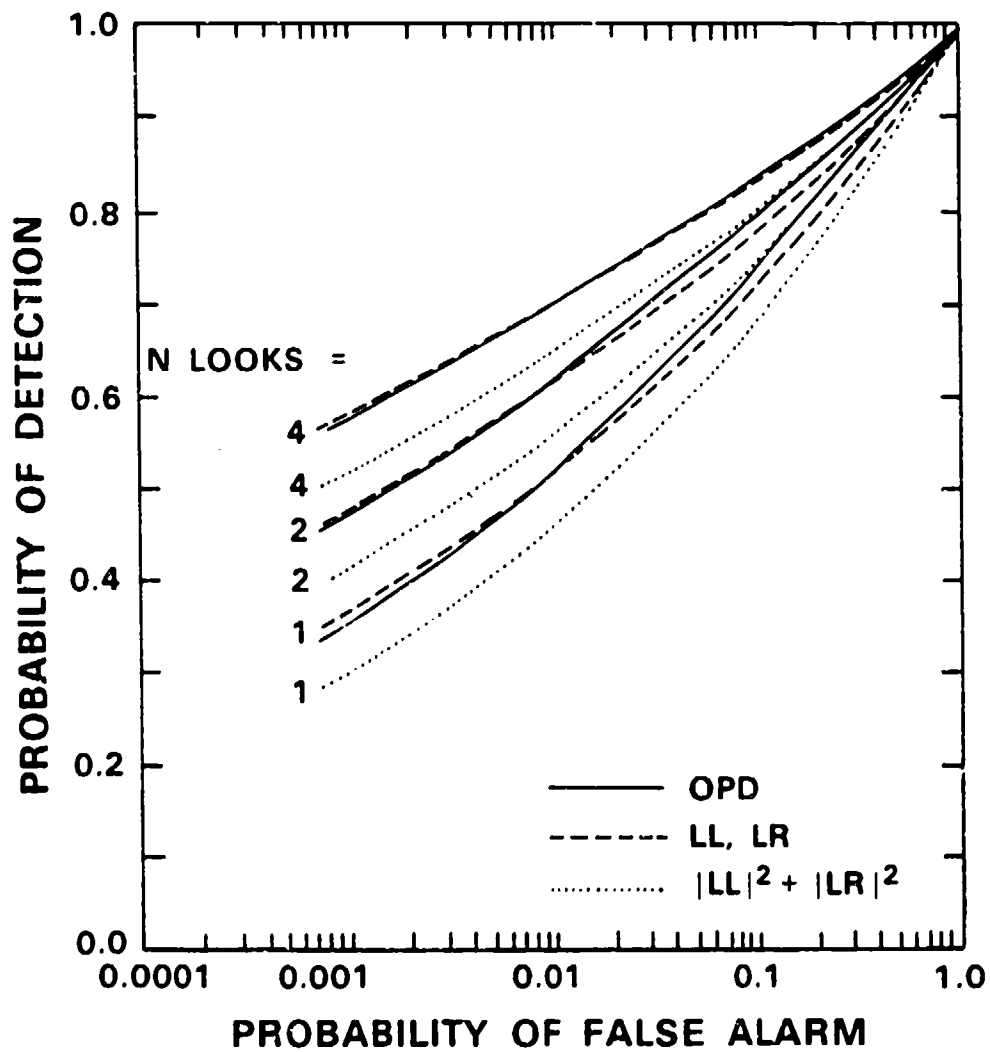[T/C = 6 dB, product models (α_t = 3 dB, α_c = 2 dB), correlated
looks (r_t = 0.8, r_c = 0.0)].

11.0 DISCRIMINATION PERFORMANCE OF THE OPD

Once a target has been detected, it may be important to discriminate between different target types (e.g., tank versus truck). The collected polarimetric data for various targets may contain information as to the type of target being observed, which may be used by a polarimetric classifier to achieve discrimination. This section presents the results of studies which used the OPD as a polarimetric classifier.

In our discrimination studies, we used normalized feature vectors having unit length. This has the advantage of removing the product scale factor from the data, so that classifier design becomes independent of absolute radar cross-section. Only the relative amplitude differences between the complex HH, HV, and VV elements, and the polarimetric phase $\phi_{HH} - \phi_{VV}$, are used to discriminate among target types. Table II shows average probability of classification error for the armored target versus the truck. The table includes results for various numbers of looks (i.e., various numbers of independent polarimetric measurements processed) and for target-to-clutter ratios of 0, 3, 6, and 10 dB for target 1 versus clutter. In each case, the target-to-clutter ratio for target 2 versus clutter is 10 dB higher due to the larger radar cross section of target 2 (see Table I).

TABLE II

Probability of Classification Error (%)

Number of Looks

T / C Ratio	1	2	4	8
10 dB	24.6	17.6	10.6	5.2
6 dB	26.0	19.2	12.0	6.2
3 dB	27.8	21.0	14.0	7.4
0 dB	30.2	24.3	17.1	10.0

The results shown in Table II suggest that polarimetric information is useful in discriminating between target types. However, to achieve reliable performance requires multi-look processing with reasonably high (6-10 dB) target-to-clutter ratios. Also good discrimination can only be achieved for targets exhibiting discernable differences in polarization characteristics (e.g., the values seen for ϵ and ρ in Table I).

12.0 SPECKLE REDUCTION USING POLARIMETRIC DATA

SAR radars produce imagery with considerable speckle. Indeed, speckle reduction has long been recognized as one of the main problems in coherent imaging [18], and many techniques have been proposed for reducing speckle. With the recent availability of coherent, fully polarimetric, high-resolution SAR data, it may be possible to optimally process the coherent scattering matrix into pixel intensity so as to reduce the speckle content of a SAR image.

It has been reported [19] that span SAR images appear to the eye to have less speckle than the usual single-polarimetric-channel SAR images. A span image is simply the noncoherent superposition of three single-polarimetric-channel images (see Equation 26); this noncoherent superposition produces a noticeable speckle reduction (relative to an $|HH|^2$ image). In this section we consider the optimal processing of the complex HH, HV, and VV elements into an intensity image which has the minimum possible amount of speckle.

In Section 2 we defined a Gaussian fully polarimetric clutter model, and used it to characterize homogeneous clutter regions. The same simple model is used in this section to derive and analyze the theoretical performance of various polarimetric speckle reduction algorithms including (1) the polarimetric whitening filter (PWF), (2) the span algorithm, (3) the optimally weighted sum of intensities ($k_1 |HH|^2 + k_2 |HV|^2 + k_3 |VV|^2$), and (4) other algorithms (which use partial polarimetric information). The theoretical speckle- reduction performance of these algorithms is calculated, and the amount of speckle reduction achievable in homogeneous clutter regions (the upper bound) is quantified.

In Section 6 we defined a non-Gaussian fully polarimetric clutter model, and used it to characterize nonhomogeneous regions of ground clutter (e.g., meadow and tree clutter) as well as spiky sea clutter. Spatial nonhomogeneity was incorporated by modeling the clutter as having a gamma spatially distributed intensity, modulated (i.e., multiplied) by an independent, complex-Gaussian speckle component. This clutter model (a "product" model) is consistent with the models developed by Lee [20], Oliver [21], and others [8,10]. Recent clutter studies by Watts and Ward [22] have shown that the gamma component (which characterizes the spatial variability of the clutter) exhibits correlation between neighboring pixels. Oliver and Tough [23] have developed approximate methods for simulating spatially correlated, K-distributed random clutter. In this section, we develop an exact method for simulating spatially correlated, K-distributed random clutter, by extending the approach used by Novak [24].

Finally, in this section we evaluate the performance of various speckle-reduction algorithms. To do this, we simulate 2-D, spatially correlated, K-distributed, fully polarimetric clutter scenes. These scenes are used to con-

struct various polarimetric images (e.g., $|HH|^2$ span, etc.), which are then used to evaluate the performance of the speckle-reduction algorithms. We also compare the target detection performance of an optimal polarimetric detector (OPD) with that of the polarimetric whitening filter (PWF), and the span and $|HH|^2$ detectors.

12.1 DERIVATION OF MINIMUM SPECKLE IMAGE

In this section we consider how to construct an optimal image from the three complex measurements HH, HV, and VV. We take as our performance measure the ratio of the standard deviation of the image pixel intensities to the mean of the intensities:

$$\frac{s}{m} = \frac{\text{st. dev}\{y\}}{E\{y\}}$$

(92)

where random variable y denotes pixel intensity. Given the measurements HH, HV, and VV, the most general construction of an image is the quadratic

$$y = \underline{X}^t A \underline{X}$$

(93)

where weighting matrix A is assumed to be Hermitian symmetric and positive definite (or perhaps semi-definite). To find the optimal weighting matrix A* (i.e., the one that results in an image whose pixel intensities have the minimum possible standard deviation-to-mean ratio) we make use of the following results from Barnes [4]:

$$E\{y\} = \text{tr}\,(\Sigma\,A) = \sum_{i=1}^{3} \lambda_i$$

(94)

$$\text{Var}\{y\} = \text{tr}\,(\Sigma\,A)^2 = \sum_{i=1}^{3} \lambda_i^2$$

(95)

where $\lambda_1, \lambda_2, \lambda_3$ are the eigenvalues of the matrix Σ A. Substituting Equations (94) and (95) into Equation (92) yields:

$$\frac{s}{m} = \frac{\sqrt{\sum_{i=1}^{3} \lambda_i^2}}{\sum_{i=1}^{3} \lambda_i}$$

(96)

We seek the optimal weighting matrix A*, the one that yields the eigenvalues $\lambda_1, \lambda_2, \lambda_3$ that minimize the s/m ratio. It is easy to show that matrix A* must be one that yields the eigenvalues

$$\lambda_1 = \lambda_2 = \lambda_3$$

(97)

Therefore, A^* is a whitening filter, which we shall call the polarimetric whitening filter (PWF). Thus, the minimum-speckle image is constructed as follows:

$$y = \underline{X}^\dagger \Sigma^{-1} \underline{X} \qquad (98)$$

For clutter having a covariance of the form shown in Equation (3) we obtain the solution

$$y = \frac{|HH|^2}{\sigma_{HH}\left(1 - |\rho|^2\right)} + \frac{|VV|^2}{\sigma_{HH}\left(1 - |\rho|^2\right)\gamma} + \frac{|HV|^2}{\sigma_{HH}\,\epsilon}$$

$$-\frac{2|\rho|}{\sigma_{HH}\left(1 - |\rho|^2\right)\sqrt{\gamma}}|HH|\,|VV|\,\cos\left(\phi_{HH} - \phi_{VV} - \phi_\rho\right) \qquad (99)$$

where ϕ_{HH}, ϕ_{VV}, and ϕ_ρ are the phases of the complex quantities HH, VV, and ρ.

The structure of the minimum-speckle image is such that the $|HH|^2$, $|VV|^2$, and $|HV|^2$ intensity images are optimally weighted, and then summed. Note, however, that the solution also incorporates a term that accounts for the information contained in the correlation of the HH and VV data. The POL-SAR (polarimetric SAR) image defined by Equation (99) yields a minimum standard deviation-to-mean ratio of

$$\left(\frac{s}{m}\right) = \frac{1}{\sqrt{3}} \quad \text{(-4.8 dB)} \qquad (100)$$

To summarize the major results of this section, we have shown that, given the three complex measurements HH, HV, and VV, the intensity image having the least speckle is constructed by (1) passing the polarimetric measurement vector $\underline{X}$ through a whitening filter to obtain $\underline{W} = \Sigma^{-1}\underline{X}$, which has unit covariance, and then (2) summing the powers contained in the elements of $\underline{W}$:

$$y = \underline{W}^\dagger \underline{W} = \underline{X}^\dagger \Sigma^{-1} \underline{X} \qquad (101)$$

The whitening filter provides the maximum achievable reduction in speckle: 4.8 dB relative to an image constructed from a single-polarmetric-channel radar.

12.2 OPTIMALLY WEIGHTED SUM OF INTENSITIES

In Section 12.1 we defined a measure of speckle and derived the processing of the three complex elements of a polarization measurement vector which minimized the amount of speckle in the intensity image. The optimal solution was

shown to be a weighted sum of $|HH|^2$, $|HV|^2$, and $|VV|^2$ plus a term which made use of the information contained in ρ, the complex correlation between the HH and VV terms. In this section we consider a simplified version of the optimal solution, one which ignores the correlation between HH and VV. Thus, we consider an intensity image

$$y = |HH|^2 + k_2|HV|^2 + k_3|VV|^2 \tag{102}$$

where the weights (k_2, k_3) are positive scale factors selected to minimize image speckle. Clearly, the span intensity image (see Equation (26)) is a special case of this more general solution.

Applying the approaches developed in Section 12.1, we first define the matrix $\Sigma\ A$:

$$\Sigma\ A = \sigma_{HH}\begin{bmatrix} 1 & 0 & k_3\,\rho\sqrt{\gamma} \\ 0 & k_2\varepsilon & 0 \\ k_3\,\rho*\sqrt{\gamma} & 0 & k_3\gamma \end{bmatrix} \tag{103}$$

The eigenvalues of this matrix are easily found to be

$$\lambda_1 = \sigma_{HH}\,k_2\varepsilon \tag{104}$$

$$\lambda_{2,3} = \sigma_{HH}\frac{(1+k_3\gamma) \pm \sqrt{(1+k_3\gamma)^2 - 4(1-|\rho|^2)\,k_3\gamma}}{2} \tag{105}$$

By substituting Equations (104) and (105) into Equation (96), we obtain an expression for the standard deviation-to-mean ratio

$$\frac{s}{m} = \frac{\sqrt{1+k_2^2\varepsilon_2^2 + k_3^2\gamma^2 + 2|\rho|^2k_3\gamma}}{(1+k_2\varepsilon + k_3\gamma)} \tag{106}$$

Omitting the details of the derivation, we now present the optimal solution. The minimum-speckle intensity image that can be constructed from $|HH|^2$, $|HV|^2$, and $|VV|^2$ data is

$$y = |HH|^2 + \frac{(1+|\rho|^2)}{\varepsilon}|HV|^2 + \frac{1}{\gamma}|VV|^2 \tag{107}$$

The standard deviation-to-mean ratio of the image constructed using the above combination of polarimetric intensities is given by

$$\frac{s}{m} = \frac{\sqrt{3 + 4\,|\rho|^2 + |\rho|^4}}{\sqrt{9 + 6\,|\rho|^2 + |\rho|^4}} \tag{108}$$

Two special cases are of particular interest. These are (1) $\rho = 0$, and (2) $\rho \to 1$.

When $\rho = 0$, Equation (107) is equivalent to the whitening filter, and yields the result

$$\frac{s}{m} = \frac{1}{\sqrt{3}} \quad (\text{-4.8 dB}) \tag{109}$$

which is the optimal performance obtained previously. Each intensity image $|HH|^2$, $|HV|^2$, and $|VV|^2$) provides an independent look at the clutter scene. Scaling the $|HV|^2$ intensities by ε^{-1} and the $|VV|^2$ intensities by γ^{-1} yields three polarimetric images which have the same average power; these three images are then noncoherently summed to obtain an average image having minimum speckle.

As $\rho \to 1$, the $|HH|^2$ and $|VV|^2$ images become identical and

$$\left(\frac{s}{m}\right) \to \frac{1}{\sqrt{2}} \quad (\text{-3 dB}) \tag{110}$$

which is equivalent to the noncoherent summation of two independent looks at the clutter scene. In this case, the $|HV|^2$ intensities are scaled by $2\varepsilon^{-1}$ and the $|VV|^2$ intensities are scaled by γ^{-1}. The independent $|HV|^2$ image is given twice the weight as the perfectly correlated $|HH|^2$ and $|VV|^2$ images.

The amount of speckle-reduction achieved by span processing can be easily calculated by letting $k_2 = 2$ and $k_3 = 1$ in Equation (102) and (106). This yields a standard deviation-to-mean ratio of

$$\frac{s}{m} = \frac{\sqrt{1 + 4\varepsilon^2 + \gamma^2 + 2\,|\rho|^2\gamma}}{(1 + 2\varepsilon + \gamma)} \tag{111}$$

Other intensity images may be constructed that use partial polarimetric information. For example, weather radars have been implemented which make use of complex HH and VV returns. Given complex HH and VV measurements, the optimal solution is obtained simply by letting HV = 0 in Equation (99). This gives

$$y = \frac{|HH|^2}{\sigma_{HH}(1-|\rho|^2)} + \frac{|VV|^2}{\sigma_{101}(1-|\rho|^2)\gamma}$$
$$- \frac{2|\rho|}{\sigma_{HH}(1-|\rho|^2)\sqrt{\gamma}} |HH| \, |VV| \cos\left(\phi_{HH} - \phi_{VV} - \phi_\rho\right)$$

(112)

Constructing a POL-SAR image using the above algorithm reduces the amount of image speckle by 3 dB relative to a single-polarimetric-channel image. Other dual-polarization measurement schemes (e.g., LL and LR or HH and HV) may be analyzed using the approaches described above.

12.3 NON-GAUSSIAN POLARIMETRIC CLUTTER SIMULATION

The results presented thus far assume a homogeneous clutter scene; with this assumption, each pixel of clutter in the scene has the same average polarimetric power and the same covariance between the polarimetric returns. A number of authors [8, 9] have stated that it is more realistic to assume that ground clutter, sea clutter, etc., are spatially nonhomogeneous. The non-Gaussian clutter model described in Section 6 is consistent with this more realistic assumption; the clutter model has a gamma-distributed intensity multiplied by an independent complex-Gaussian speckle component. This yields polarimetric clutter with a K-distributed PDF.

The non-Gaussian clutter model we shall use to simulate clutter scenes has the product-model structure $\underline{Y} = \sqrt{g}\ \underline{X}$ where g is a gamma-distributed intensity and $\underline{X}$ is an independent complex-Gaussian polarimetric vector.

Since the gamma variable (which characterizes the spatial variability of the clutter) is generally spatially correlated, we need to develop an exact method for simulating correlated K-distributed clutter scenes. The technique we will develop provides synthetic POL-SAR clutter scenes which have two desirable properties:

1. The gamma samples have the exact PDF specified by Equation (33).

2. The gamma samples are spatially correlated according to any specified 2-D correlation function (Gaussian, exponential, etc.).

Our approach is not restricted to the gamma random variable; any desired random variable (Rayleigh, Weibull, lognormal, etc.) can be simulated having any specified 2-D correlation function. Approximate solutions (such as proposed in Reference [25]) are not necessary.

Figure 16 shows a block diagram of the polarimetric clutter simulation. The following paragraphs provide a step-by-step description of the data transformations used to generate a synthetic 2-dimensional, spatially correlated, fully polarimetric clutter scene.
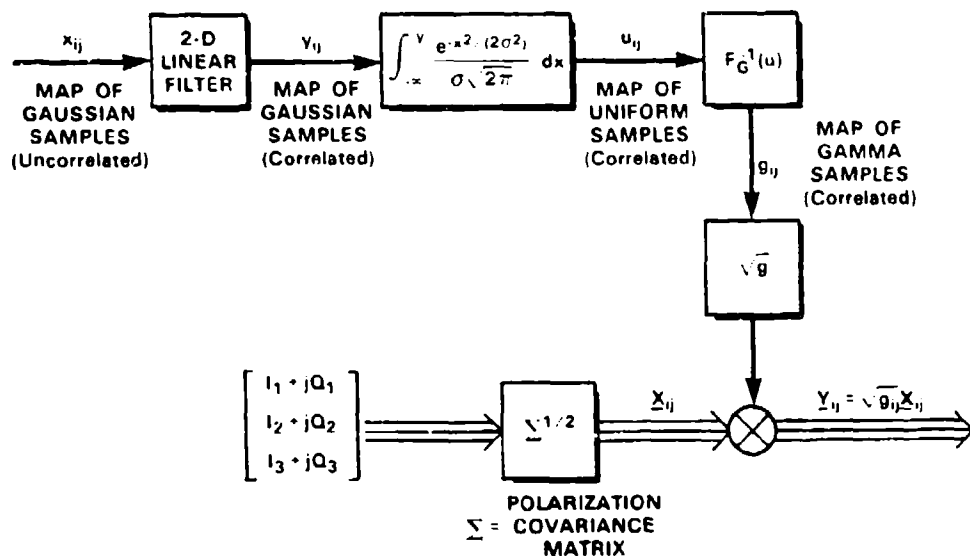
POLARIMETRIC CLUTTER SIMULATION

Figure 16. Block diagram of spatially correlated, K-distributed, fully polarimetric clutter simulation.

Step 1: A 2-dimensional array of independent, zero mean Gaussian random variables (denoted x_{ij}) is obtained; these data are processed in a 2-dimensional filter to obtain a spatially correlated Gaussian scene (y_{ij}).

Step 2: The correlated Gaussian samples (y_{ij}) are transformed into correlated uniformly distributed samples (u_{ij}) by the non-linear transformation.

$$u_{ij} = \int_{-\infty}^{y_{ij}} \frac{\exp\left\{-\frac{y^2}{2\sigma^2}\right\}}{\sqrt{2\pi}\,\sigma} \, dy \tag{113}$$

This transformation is simply the cumulative probability distribution function (the error function) of a Gaussian variable. Each input y_{ij} is converted into a uniform variable u_{ij}. Since the samples y_{ij} are correlated, the samples u_{ij} are correlated. The array denoted uij is therefore a spatially correlated set of random samples having a uniform PDF.

Step 3: The array u_{ij} is then transformed into an array of spatially correlated gamma variabies (g_{ij}) by the nonlinear transformation

$$g_{ij} = F_G^{-1}(u_{ij}) \tag{114}$$

where $F_G^{-1}(u_{ij})$ is the inverse cumulative distribution function of the gamma. Denoting the input and output by u_{ij} and g_{ij} respectively, we solve the expression

$$u_{ij} = \int_0^{g_{ij}} f_G(g) \, dg \tag{115}$$

Step 4: Finally, the fully-polarimetric measurement vectors $\underline{Y}i_j$ are obtained by multiplying the spatially correlated gamma array g_{ij} by independent complex Gaussian vectors $\underline{X}_{ij}$. The tech nique used to simulate these complex-Gaussian vectors is based on the method of Marsaglia [26]

$$\underline{Y}_{ij} = \sqrt{g_{ij}} \begin{bmatrix} 1 & 0 & 0 \\ 0 & \sqrt{\varepsilon} & 0 \\ \rho^*\sqrt{\gamma} & 0 & \sqrt{\gamma(1-|\rho|^2)} \end{bmatrix} \begin{bmatrix} r_0 + jr_1 \\ r_2 + jr_3 \\ r_4 + jr_5 \end{bmatrix} \tag{116}$$

where $r_0, r_1, r_2, r_3, r_4, r_5$ are statistically independent zero mean Gaussians, each having a variance of 0.5.

12.4 ANALYSIS OF CORRELATION TRANSFER FUNCTION

In this section we calculate a "correlation transfer function" for the system used to transform correlated Gaussian variables into correlated gamma variables (see Figure 16). The actual correlation function of the gamma data (g_{ij}) will be different from that of the correlated Gaussian data (y_{ij}) due to the nonlinear transformations used. The objective of the analysis that follows is to evaluate the output correlation (pout) as a function of the selected input correlation (pin) of the Gaussian variables. This will permit us to specify a correlation function for the Gaussian data which yields any desired 2-D correlation function for the gamma data.

Clearly, the samples g_{ij} have a first-order probability density which is gamma. Since the samples y_{ij} comprise a stationary Gaussian process, the samples g_{ij} are also stationary. To evaluate the correlation between any two gamma samples we must calculate $E\{g_{ij} \; g_{k\ell}\}$. To simplify notation, we define

$$y_1 \overset{\Delta}{=} y_{ij} \; ; \; y_2 \overset{\Delta}{=} y_{k\ell} \qquad \text{(Gaussian)} \qquad (117)$$

$$u_1 \overset{\Delta}{=} u_{ij} \; ; \; u_2 \overset{\Delta}{=} u_{k\ell} \qquad \text{(Uniform)} \qquad (118)$$

$$g_1 \overset{\Delta}{=} g_{ij} \; ; \; g_2 \overset{\Delta}{=} g_{k\ell} \qquad \text{(Gamma)} \qquad (119)$$

The expectation we must evaluate is written

$$E\{g_1, \; g_2\} = \int_0^\infty \int_0^\infty g_1 \; g_2 \; f_G(g_1, \; g_2) \; dg_1 \; dg_2 \qquad (120)$$

where $f_G (g_1, g_2)$ is the joint PDF of g_1 and g_2. This quantity is evaluated by calculating the expectation with respect to u_1 and u_2.

$$E\{g_1, \; g_2\} = \int_0^1 \int_0^1 F_G^{-1}(u_1) F_G^{-1}(u_2) \; f_u(u_1, u_2) \; du_1 \; du_2 \qquad (121)$$

where the joint PDF of the uniform samples is derived to be

$$f_u(u_1, u_2) = \frac{\exp\left\{-\dfrac{\text{pin}^2\left(y_1^2 + y_2^2\right) - 2 \, \text{pin} \, y_1 \, y_2}{2\sigma^2\left(1 - \text{pin}^2\right)}\right\}}{\sqrt{1 - \text{pin}^2}} \qquad (122)$$

Finally, the correlation between the two gamma samples g_1 and g_2 is determined from

$$\rho_{out} = \frac{E\{g_1\ g_2\} - E^2\{g_1\}}{E\{g_1^2\} - E^2\{g_1\}}$$

(123)

Typical clutter regions have clutter standard deviations(α_c) of approximately 1 dB (meadow clutter) to 3 dB (tree clutter). We have evaluated the parameters of the gamma PDF which yield these clutter standard deviations; Table III presents these results.

TABLE III:

GAMMA PARAMETER VERSUS CLUTTER ST. DEV (dB)

α_c	υ
1.0	19.3
1.5	8.9
2.0	5.2
2.5	3.5
3.0	2.6

For the clutter parameters of interest, we have calculated the correlation between gamma samples g_1 and g_2. To do this, it is necessary to evaluate Equation (121) using numerical integration. The results of the analysis are shown in Figure 17.

Given a specified Gaussian correlation function, the curves in Figure 17 may be used to obtain the corresponding output correlation function of the Gamma data. Likewise, given a specified correlation function for the gamma data (g_{ij}), the required input correlation function of the Gaussian data (y_{ij}) can be determined. In this case the problem becomes one of synthesizing a linear fil-ter which produces the required correlation function for the Gaussian samples (y_{ij}). Note that the curves of Figure 17 indicate that the out put correlation, pout, is only slightly less than the input correlation, rin. Therefore, for many applications one can simply generate correlated Gaussian variables by convolving the array (x_{ij}) with the impulse response of a 2-D digital filter and the resulting correlation function of the Gamma data will be approximately the same.

12.5 SPECKLE REDUCTION FOR NON-GAUSSIAN CLUTTER

In section 12.1 we derived the optimum processing of complex HH, HV, and VV data into an intensity image having minimum speckle; the derivation assumed homogeneous clutter. In the following paragraphs we evaluate the
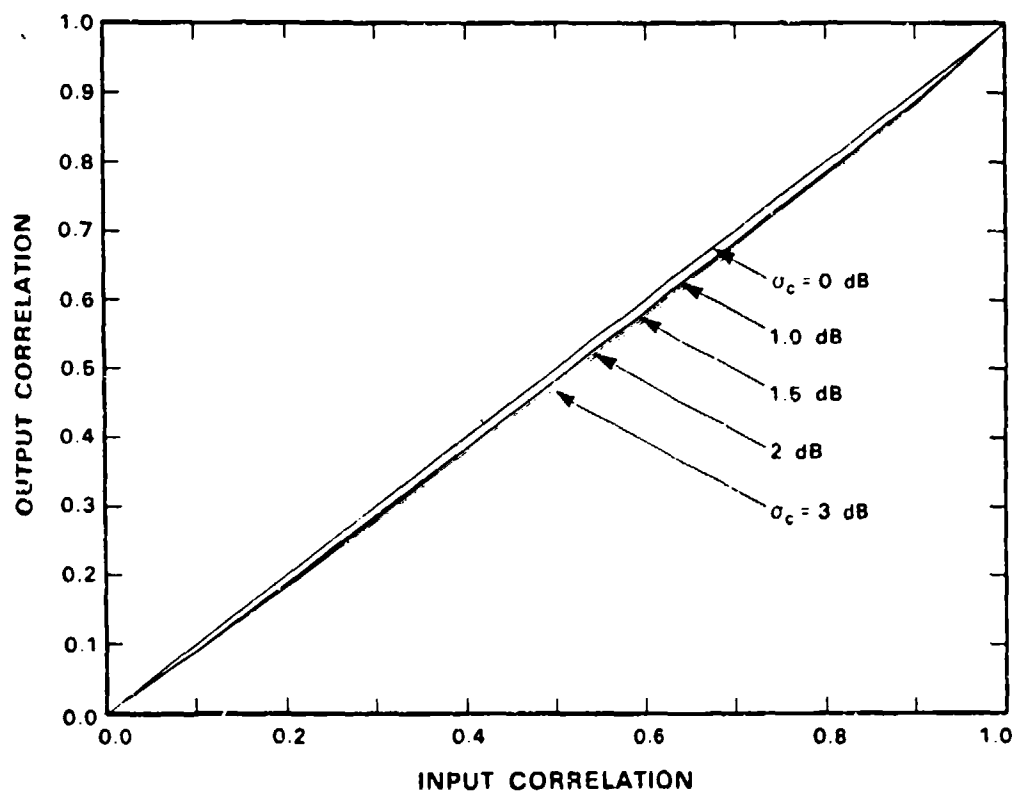
Figure 17. Correlation transfer function.

s/m ratio for nonhomogeneous clutter. We consider the case of spatially independent gamma variables (this implies the data g_{ij} have spatial correlation pout = 0). The standard deviation-to-mean ratio is derived and is shown to be only a function of the gamma parameter, v; the s/m ratio is independent of the gamma parameter, $\bar{g}$. Minimizing the s/m ratio we again find that the optimal solution is the polarimetric whitening filter (PWF) derived previously for homogeneous clutter. Finally the analysis shows that for clutter standard deviations of interest (α_c = 1.0 dB to 3.0 dB), the s/m ratio is somewhat larger than for the homogeneous clutter case.

Omitting the unnecessary details, it can be shown that

$$\frac{\text{Var}\{y\}}{\text{E}^2\{y\}} = \frac{v+1}{v}\left[\frac{\sum\limits_{i=1}^{3}\lambda_i^2}{\left(\sum\limits_{i=1}^{3}\lambda_i\right)^2}\right] + \frac{1}{v}$$

(124)

Note that the mean parameter $\bar{g}$ has cancelled out of the above expression. For large v, the s/m ratio reduces to the homogeneous clutter case (Equation (96)); this is reasonable since as $v \to \infty$ the random product multiplier becomes constant and the clutter becomes homogeneous.

The eigenvalues λ_1, λ_2, λ_3 which minimize the s/m ratio of Equation (124) are easily derived using the approach of Cadzow [7]. The numerator of Equation (124) is minimized subject to the constraint that the denominator is constant. As for the homogeneous clutter case, the solution is easily found to be $\lambda_1 = \lambda_2 = \lambda_3$. Therefore, the minimal-speckle intensity image is constructed by processing the complex HH, HV and VV measurements just as is done for homogeneous clutter. The resulting standard-deviation-to-mean ratio is, however, a function of the gamma parameter, v. Substituting for the eigenvalues, the s/m ratio becomes

$$\left(\frac{s}{m}\right) = \sqrt{\frac{1+\dfrac{4}{v}}{3}}$$

(125)

Note that as $v \to \infty$, the above Equation (125) reduces to the result derived previously for homogeneous clutter. The s/m ratio for a single-polarimetric-channel intensity image is easily shown to be

$$\left(\frac{s}{m}\right) = \sqrt{1+\frac{2}{v}}$$

(126)

Using Equations (125) and (126), the reduction in s/m ratio achieved using the polarimetric whitening filter (relative to a single-polarimetric-channel image) can be calculated. For a clutter standard deviation of 1 dB, total image speckle (s/m

ratio) is reduced by approximately 4.4 dB relative to the single-polarimetric-channel image. Thus, meadow regions should look considerably more homogeneous. For a clutter standard deviation of 3 dB, total image speckle (s/m ratio) is reduced by approximately 3.2 dB.

In Section 12.7 we will simulate spatially correlated, K-distributed, fully polarimetric clutter scenes and will verify these results, both numerically and visually by showing the various intensity images.

12.6 MINIMUM MEAN SQUARE ERROR

In Section 12.5 we showed that the polarimetric whitening filter will produce the POL-SAR intensity image with the minimum s/m ratio for both homogeneous and non-homogeneous clutter. In this section we consider processing the polarimetric measurements into an intensity image such that the mean square error between the intensity image and the gamma image (i.e., the "ideal" image) is minimized. We will show that the optimal processing is again accomplished using the polarimetric whitening filter.

Mathematically the problem is formulated as follows. The pixel intensity, y, is given by the quadratic:

$$y = g\underline{X}^{t} A \underline{X} \tag{127}$$

We wish to minimize the mean square error by selecting an appropriate weighting matrix, A, where:

$$M.S.E. = E\left[(y - g)^2\right] \tag{128}$$

Using Equations (94) and (95), the mean square error is calculated to be:

$$M.S.E. = \left[\sum_{i=1}^{3} \lambda_i^2 + \left(\sum_{i=1}^{3} \lambda_i - 1\right)^2\right] E\left[g^2\right] \tag{129}$$

The minimum mean square error occurs when all the eigenvalues, λ_i, equal 1/4. (This is easily shown by setting the partial derivatives with respect to λ_i equal to 0.) The resulting RMS error is:

$$R.M.S.E. = \frac{\sqrt{E\left[g^2\right]}}{2} = \frac{\sqrt{1 + 1/\upsilon}}{2} \tag{130}$$

and the optimal weighting matrix, A^*, is given by

$$A^* = \frac{1}{4} \Sigma^{-1} \tag{131}$$

71

Note that this matrix also minimizes the standard deviation-to-mean ratio. The mean square error resulting from other suboptimal combinations of the polarimetric data can also be determined from Equation (129).

12.7 SPECKLE-REDUCTION RESULTS

We simulated POL-SAR clutter scenes and calculated the amount of speckle reduction (i.e., the reduction in standard deviation-to-mean ratio) achieved with span and PWF intensity images. The following paragraphs describe the experiment and summarize the results obtained.

Three fully polarimetric synthetic clutter scenes were simulated, including: (1) a homogeneous clutter region, (2) a nonhomogeneous clutter region having $\alpha_c = 1$ dB, corresponding to typical meadow clutter and (3) a nonhomogeneous clutter region with $\alpha_c = 3$ dB, corresponding to typical tree clutter. In order to compare results we used the same polarimetric covariance (specified by $\varepsilon = 0.18$, $\gamma = 1.6$, and $\rho = 0.5$) for all scenes. The nonhomogeneous clutter scenes had spatially correlated gamma samples. These correlated gamma samples (g_{ij}) were generated by applying a 2-D digital filter (having a 16 x 16 uniform impulse response) to uncorrelated Gaussian samples (y_{ij}), as shown in Figure 16.

Figure 18 shows a side-by-side comparison of the gamma image with $|HH|^2$, span, and PWF images constructed from the homogeneous POL-SAR data. The under-lying gamma image corresponds to an "ideal" speckle-free image. In Figure 18, the gamma image is, of course, a constant. Table IV gives the s/m ratios which were calculated from the intensity images of Figure 18; these s/m ratios agree almost exactly with theoretical predictions.

Figures 19 and 20 present side-by-side comparisons of the gamma, $|HH|^2$, span, and PWF images constructed from the nonhomogeneous data. The spatially correlated gamma images correspond to "ideal" speckle-free images. Comparing the $|HH|^2$, span, and PWF images with the ideal gamma images, it is clear that the single-polarimetric-channel $|HH|_2$ images are speckle dominated, whereas the span and PWF images appear to the eye to be much clearer. The PWF intensity images are, of course, the best.

Tables V and VI present the corresponding s/m ratios which were calculated from the intensity images of Figures 19 and 20, respectively. From the data shown, it is found that the s/m ratio for $\alpha_c = 1$ dB has been reduced by 4.38 dB relative to the $|HH|^2$ data, and for $\alpha_c = 3$ dB the s/m ratio was reduced by 3.36 dB. These results also agree quite well with theoretical predictions.

Figure 18. Synthetic clutter images (homogeneous)
gamma image (upper left), HH image (upper right),
optimal image (lower left), span image (lower right).

Figure 19. Synthetic clutter images (nonhomogeneous, $\alpha_c = 1$ dB)
gamma image (upper image), HH image (upper right),
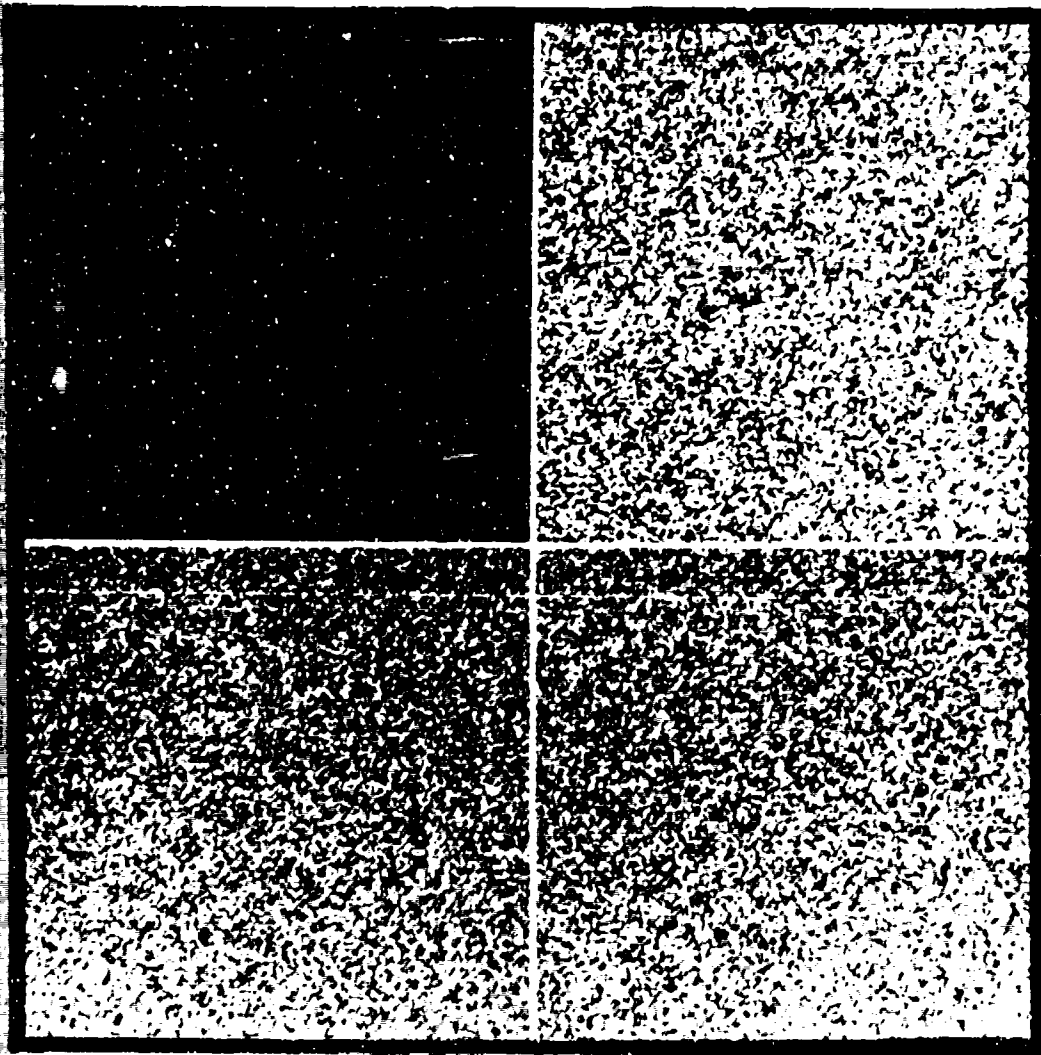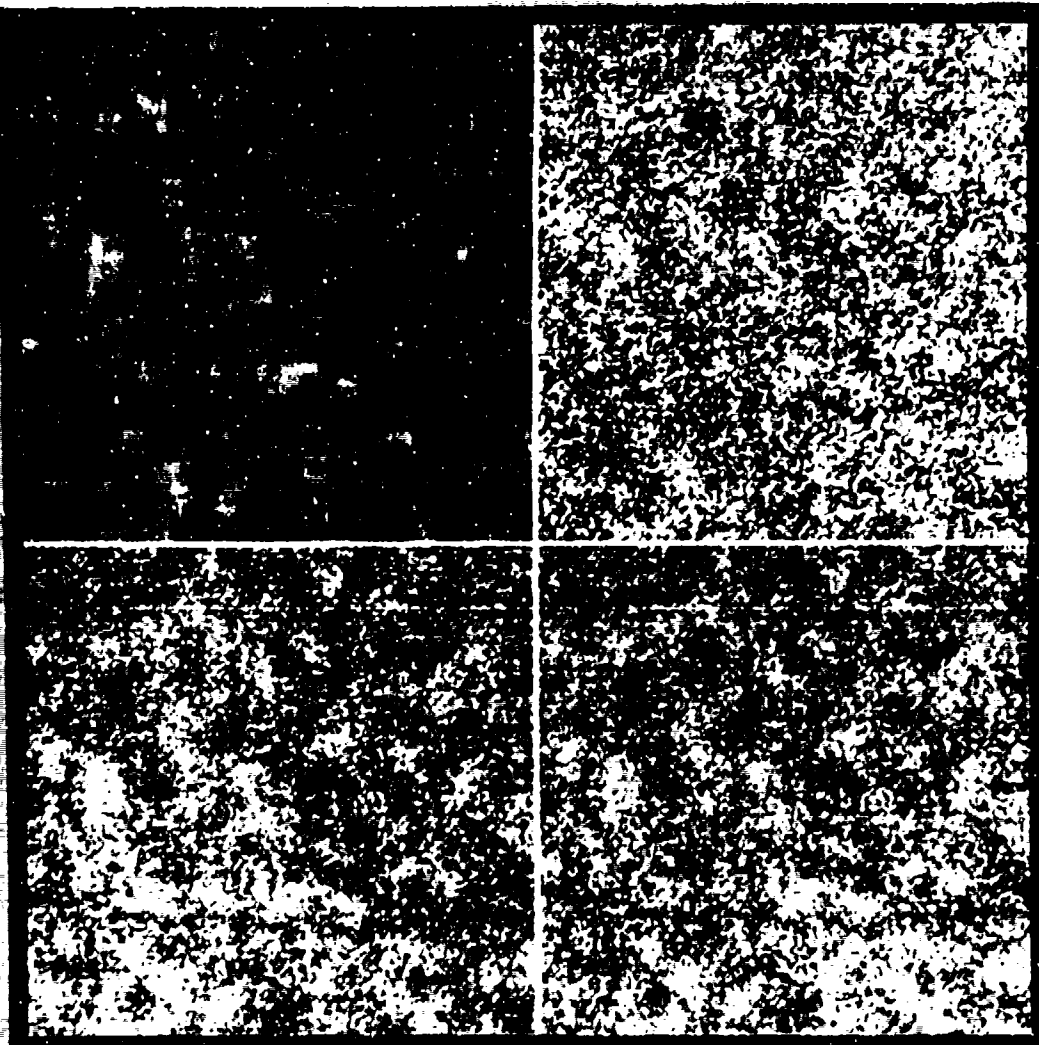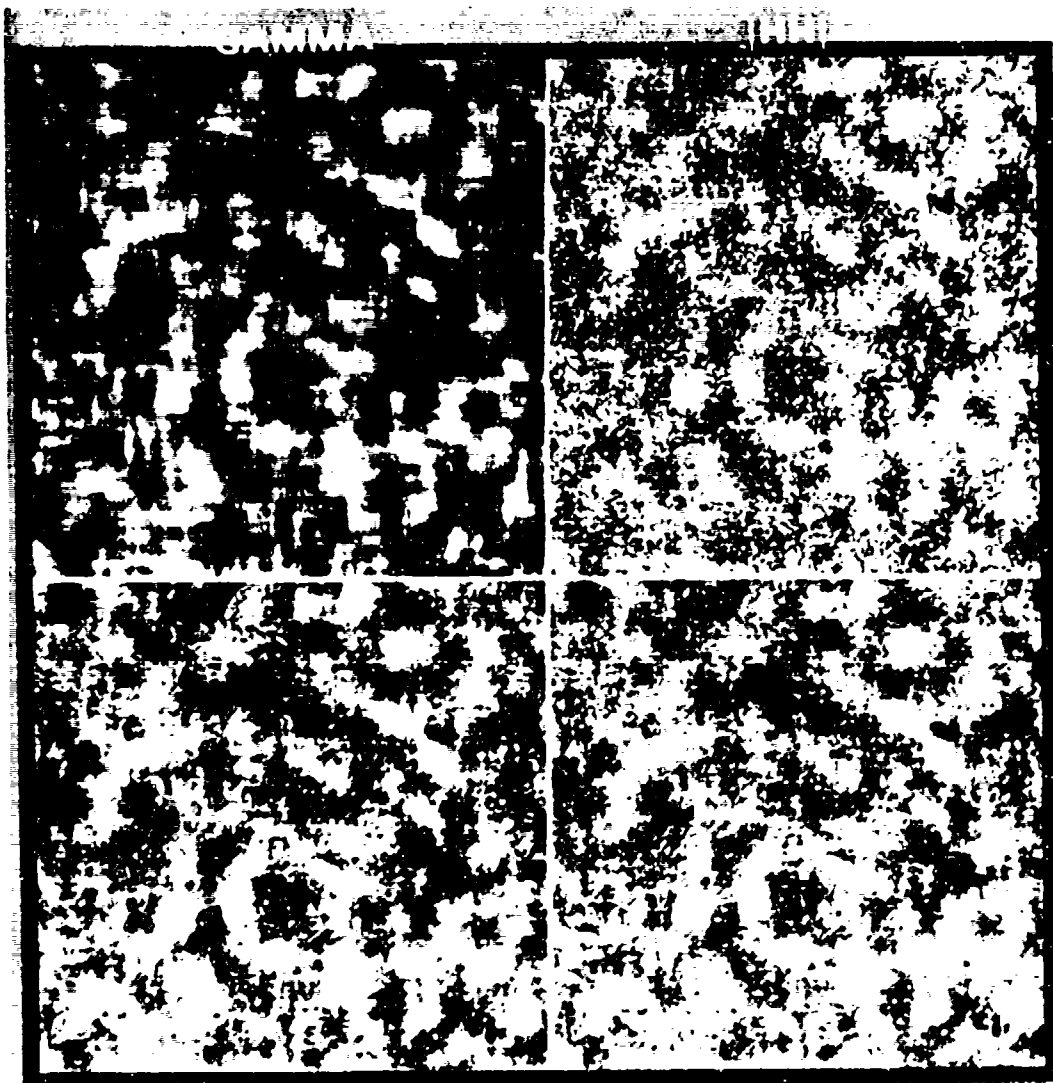optimal image (lower left), span image (lower right).

Figure 20. Synthetic clutter images (nonhomogeneous, $\alpha_c = 3$ dB)
gamma image (upper left), HH image (upper right),
optimal image (lower left), span image (lower right).

TABLE IV

s/m Ratio (dB)

	Measured	Theory
$|HH|^2$	0.19	0.00
span	-2.89	-2.90
PWF	-4.76	-4.77

TABLE V

s/m Ratio (dB)

	Measured	Theory
$|HH|^2$	0.44	0.43
span	-2.27	-2.29
PWF	-3.94	-3.95

TABLE VI

s/m Ratio (dB)

	Measured	Theory
$|HH|^2$	3.01	2.51
span	0.72	0.43
PWF	-0.35	-0.68

12.8 TARGET DETECTION USING THE PWF

The use of fully polarimetric HH, HV, and VV complex data for detection of targets in clutter was studied in previous sections of this report; it was shown that for Gaussian target and clutter models, the optimal polarimetric detector (OPD) was a quadratic algorithm:

$$y = \underline{X}'\left(\Sigma_c^{-1} - (\Sigma_c + \Sigma_t)^{-1}\right)\underline{X} > T \tag{132}$$

where Σ_t and Σ_c are the target and clutter covariances and T is the detection threshold. The polarimetric whitening filter, also derived previously, is a quadratic algorithm:

$$y = \underline{X}^t \Sigma_c^{-1} \underline{X} > T \qquad (133)$$

where Σ_c is the clutter covariance and T is a detection threshold.

The OPD is optimal in the likelihood ratio sense; that is, it yields the best probability of detection (P_D) for a given false alarm probability (P_{FA}). The PWF is therefore not optimal since it ignores the target (i.e., target-plus-clutter) covariance information. Detection performance using the PWF will be degraded relative to the OPD for Gaussian targets and clutter. For nonhomogeneous (non-Gaussian) targets and clutter, the OPD is not optimal; hence, we compared the detection performance of the PWF with that of the OPD. In addition, we also evaluated the detection performance achieved with $|HH|^2$ and span data.

Figure 21 presents the performance of the various detectors for nonhomogeneous product model target and clutter data. The curves shown for the OPD and span detectors were taken directly from Figure 4; the curves for the $|HH|^2$ and PWF detectors were calculated using the methods described previously. Note that in this section of the report, $|HH|^2$ detection performance is based on a look formed from a single-pulse return (in previous sections, $|HH|^2$ detection performance was based on two noncoherently integrated frequency-diverse pulse returns per look).

The detection performance results presented in Figure 21 indicate, for the armored target and clutter covariances given in Table I, that: (1) performance of the PWF is essentially identical to that of the OPD, (2) performance of the span detector is quite degraded, and (3) the $|HH|^2$ detector gives the worst performance. Thus, the PWF provides a simple alternative to the OPD (which requires prior knowledge of both the target and clutter covariances as well as the target-to-clutter ratio) for the detection of stationary targets in clutter. The PWF requires only knowledge of the polarization covariance of the clutter; this could be estimated from the complex HH, HV and VV data and then used to construct the minimum speckle image.
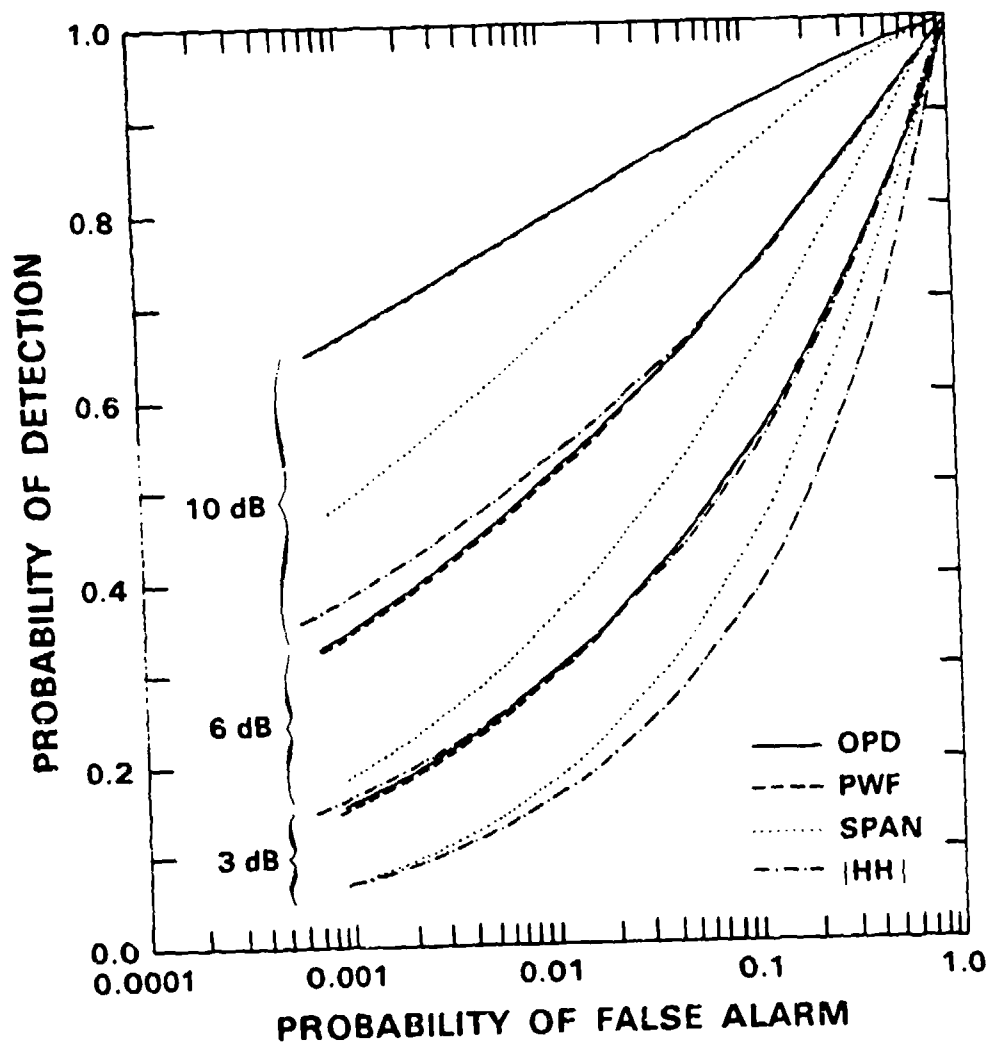
Figure 21. Detection performance versus T/C ratio
(product-models, α_c = 1.5 dB, u_1 = 3 dB).

12.9 ANALYSIS OF THE ADAPTIVE PWF

In Section 12.8 we compared the target detection performance of an optimal polarimetric detector (OPD) with the performance of PWF, span, and $|HH|^2$ detectors; the OPD and PWF gave comparable performance, and were significantly better than the span and $|HH|^2$ detectors. Since the PWF requires only the polarimetric covariance of the clutter, it is possible that an adaptive PWF could be implemented. Such an algorithm would estimate the polarization covariance matrix of the clutter, use this to construct the minimum-speckle image, and then test for the presence of targets. The algorithm could be made adaptive to the local clutter statistics, as is done in a standard amplitude CFAR detector. In this section we present an analysis of the detection performance of an adaptive PWF. We also determine the number of independent clutter samples required to estimate the polarization covariance matrix.

In order to evaluate the detection and false alarm probabilities (P_D and P_{FA}) for the quadratic detector defined in Equation (133) it is necessary to calculate its probability density function (PDF). When the clutter polarization covariance Σ_c is known exactly (i.e., is a constant matrix), this calculation is easily performed using the techniques developed in Section 7. When the polarization covariance matrix of the clutter is adaptively estimated from the local clutter, the PDF of random variable y is more difficult to calculate; this section provides the derivation.

It is well known that the sample covariance

$$\hat{\Sigma}_{X_c} = \frac{1}{N} \sum_{i=1}^{N} \underline{X}_{c_i} \underline{X}'_{c_i}$$

(134)

has a Wishart distribution; we do not, however, have to make direct use of this result in the following derivation. The derivation which follows is an extension of the approach described in Anderson [27] for deriving the PDF of the T^2 statistic. The major difference between our derivation and that of Anderson is that we treat the more complicated case where the test vector $\underline{X}$ is an independent measurement of target plus clutter.

Consider the adaptive PWF that we have defined by the quadratic expression

$$y = \underline{X}' \hat{\Sigma}_{X_c}^{-1} \underline{X}$$

(135)

where $\underline{X} \sim N(\underline{0}, \Sigma_t + \Sigma_c)$, and $\hat{\Sigma}_{X_c}$ is the sample covariance matrix defined in Equation (134). Following the approach of Anderson [27] we assume that the vectors $\underline{X}_{c_i}$ are independent clutter samples, thus $\underline{X}_{c_i} \sim N(\underline{0}, \Sigma_c)$. First we

whiten the clutter measurements by transforming the data vectors $\underline{X}$ and $\underline{X}_{c_1}$, $\underline{X}_{c_2}, \ldots, \underline{X}_{c_N}$ as follows:

$$\underline{Y} = \Sigma_c^{-\frac{1}{2}} \underline{X} \tag{136}$$

$$\underline{Y}_{c_i} = \Sigma_c^{-\frac{1}{2}} \underline{X}_{c_i} \qquad ; \; i = 1, 2, \ldots, N \tag{137}$$

The whitening transformation (from Fukunaga [5]) is of the form

$$\Sigma_c^{-\frac{1}{2}} = \Lambda_c^{-\frac{1}{2}} \Phi_c \tag{138}$$

where matrix Φ_c consists of the eigenvectors of the covariance matrix Σ_c, and Λ_c is diagonal (with the corresponding eigenvalues of Σ_c along the diagonal). When the test vector is target-plus-clutter, $\underline{Y}$ has Gaussian statistics:

$$\underline{Y} \sim N\left(\underline{0}, \; \Sigma_c^{-\frac{1}{2}}(\Sigma_t + \Sigma_c)\Sigma_c^{-\frac{1}{2}t}\right) \tag{139}$$

Next, examine the expression $\Sigma_c^{-\frac{1}{2}} \hat{\Sigma}_{\underline{X}_c} \Sigma_c^{-\frac{1}{2}t}$, which can be manipulated as follows

$$\begin{aligned}
\Sigma_c^{-\frac{1}{2}} \hat{\Sigma}_{\underline{X}_c} \Sigma^{-\frac{1}{2}t} &= \Sigma_c^{-\frac{1}{2}}\left(\frac{1}{N} \sum_{i=1}^{N} \underline{X}_{c_i} \underline{X}^t_{c_i}\right)\Sigma_c^{-\frac{1}{2}t} \\
&= \frac{1}{N} \sum_{i=1}^{N} \left(\Sigma_c^{-\frac{1}{2}}\underline{X}_{c_i}\right)\left(\Sigma_c^{-\frac{1}{2}}\underline{X}_{c_i}\right)^t \\
&= \frac{1}{N} \sum_{i=1}^{N} \underline{Y}_{c_i}\underline{Y}^t_{c_i}
\end{aligned} \tag{140}$$

The clutter data vectors $\underline{Y}_{c_1}, \underline{Y}_{c2}, \ldots, \underline{Y}_{c_N}$ are white, since

$$\underline{Y}_{c_i} = \Sigma_c^{-\frac{1}{2}} \underline{X}_{c_i} \sim N(0, I) \qquad ; i = 1, 2, \ldots, N \tag{141}$$

The sample covariance of the whitened clutter measurements is defined as

$$\hat{\Sigma}_{\underline{Y}_c} = \frac{1}{N} \sum_{i=1}^{N} \underline{Y}_{c_i}\underline{Y}^t_{c_i} \tag{142}$$

Next, we write the transformed test vector from Equation (136) in terms of its scalar components:

$$\underline{Y} = \left(y_1, y_2, \ldots, y_p\right)^t \tag{143}$$

and we construct linear transformation matrix Q, where the first row of Q consists of the samples

$$q_{1i} = \frac{y_i}{\sqrt{\underline{Y}^t \underline{Y}}} \quad ; \quad i = 1, 2, \ldots p \tag{144}$$

and the remaining (p-1) rows of Q are selected to be orthogonal to the first row. This can always be done (for a simple proof, see Lemma 2 in the appendix of refe: ~ce [27]). Matrix Q is an orthogonal matrix; i.e.,

$$Q^t Q = Q Q^t = I \tag{145}$$

We note that matrix Q is a function of the measurements; thus, Q is a random matrix. We now transform the data vectors $\underline{Y}$ and $Y_{c_1}, \underline{Y}_{c_2}, \ldots, Y_{c_N}$ (using the linear transformation Q) as follows:

$$\underline{Z} = Q\underline{Y} \tag{146}$$

$$\underline{Z}_{c_i} = Q\underline{Y}_{c_i} \quad ; \quad i = 1, 2, \ldots N \tag{147}$$

The detection statistic (Equation (37)) can now be written

$$y = \underline{Z}^t \left[Q \hat{\Sigma}_{\underline{Y}_c} Q^t \right]^{-1} \underline{Z} \tag{148}$$

Next, we examine the expression $Q \hat{\Sigma}_{\underline{Y}_c} Q^t$, which can be manipulated as follows:

$$\hat{\Sigma}_{\underline{Z}_c} = Q\hat{\Sigma}_{\underline{Y}_c}Q^t = \frac{1}{N} \sum_{i=1}^{N} (Q\underline{Y}_{c_i})(Q\underline{Y}_{c_i})^t$$
$$= \frac{1}{N} \sum_{i=1}^{N} \underline{Z}_{c_i}\underline{Z}_{c_i}^t \tag{149}$$

The clutter measurement vectors $\underline{Z}_{c_1}, \underline{Z}_{c_2}, \ldots, \underline{Z}_{c_N}$ are also white, since they are obtained by an orthogonal transformation of whitened data.

Summarizing the derivation thus far, we have shown that the detection statistic (Equation (135)) can be written as

$$y = \underline{Z}^t \hat{\Sigma}_{\underline{Z}_c}^{-1} \underline{Z} \tag{150}$$

where the sample covariance of the whitened clutter measurements is

$$\hat{\Sigma}_{Z_c} = \frac{1}{N} \sum_{i=1}^{N} \underline{Z}_{c_i} \underline{Z}^t{}_{c_i}$$

(151)

Continuing with the derivation, we now write the test vector $\underline{Z}$ in terms of its scalar components and obtain the following results:

$$
\begin{aligned}
\Sigma_1 &= \frac{\sum_{i=1}^{P} |y_i|^2}{\sqrt{\sum_{i=1}^{P} |y_i|^2}} &= \sqrt{\sum_{i=1}^{P} |y_i|^2} \\
\vdots &= \vdots \\
\Sigma_2 &= \sum_{i=1}^{P} q_{2i} y_i &= 0 \\
\Sigma_P &= \sum_{i=1}^{P} q_{Pi} y_i &= 0
\end{aligned}
$$

(152)

Thus, the detection statistic y is of the form

$$
y = (Z_1\, 0\, 0\, 0 \cdots 0)\, \hat{\Sigma}_{Z_c}{}^{-1}
\begin{bmatrix}
Z_1 \\ 0 \\ 0 \\ \cdot \\ \cdot \\ 0
\end{bmatrix}
$$

(153)

Next, we borrow a useful lemma from partitioned-matrix theory. If we write covariances $\hat{\Sigma}_{Z_c}$ and $\hat{\Sigma}_{Z_c}^{-1}$ as follows:

$$
\hat{\Sigma}_{Z_c} = \left[\begin{array}{c|c} b^{11} & \underline{b'}_{12} \\ \hline \underline{b}_{12} & B_{22} \end{array} \right]
$$

(154)

$$
\hat{\Sigma}_{Z_c}{}^{-1} = \left[\begin{array}{c|ccc} b^{11} & b^{12} & \cdots & b^{1P} \\ b^{12} & b^{22} & \cdots & b^{2P} \\ \vdots & & & \\ b^{1P} & b^{2P} & \cdots & b^{PP} \end{array} \right]
$$

(155)

then the element b^{11} can easily be shown to be

$$b^{11} = \left(b_{11} - \underline{b}_{12}' B^{-1}{}_{22} \underline{b}_{12} \right)^{-1} \tag{156}$$

Finally, evaluating the detection statistic, we find that

$$y = \frac{N \sum\limits_{i=1}^{p} |y_i|^2}{\left(b_{11} - \underline{b}_{12} B_{22}^{-1} \underline{b}_{12} \right)} = \frac{N\eta}{\delta} \tag{157}$$

Equation (157) expresses random variable y as the ratio of two statistically independent random variables, η and δ. The denominator random variable, δ, is conditionally distributed as chi-square with $N - p + 1$ degrees of freedom [27]. Since the conditional distribution of δ does not depend upon the linear transformation Q, then it is unconditionally distributed as chi-square with $N - p + 1$ degrees of freedom.

The numerator random variable η, where

$$\eta = \sum\limits_{i=1}^{p} |y_i|^2 = \underline{Y}^\dagger \underline{Y} \tag{158}$$

is a quadratic function of the complex-Gaussian vector $\underline{Y}$, where

$$\underline{Y} \sim N\left(\underline{0}, \Sigma_c^{-\frac{1}{2}}(\Sigma_t + \Sigma_c)\Sigma_c^{-\frac{1}{2}\dagger} \right) \tag{159}$$

There are two cases of interest: (1) when the test vector is an independent clutter sample, and (2) when the test vector is a target-plus-clutter sample.

For case (1), we have the solution from Anderson [27] which we summarize as follows: We know that $\underline{Y} \sim N(\underline{0}, I)$ and that the numerator random variable

$$\eta = \sum\limits_{i=1}^{p} |y_i|^2 \tag{160}$$

is chi-square with p degrees of freedom. Thus, when the test vector is an independent clutter sample, the detection statistic has a PDF which is calculated as the ratio of two independent chi-square-distributed variables.

For case (2), the test input $\underline{Y}$ is not white; therefore, the solution is more complicated. Using the methods of section 7, we calculate the characteristic function of the numerator random variable η:

$$\phi_\eta(jw) = \int .. \int e^{jwY'Y} \frac{e^{-Y'\left[\Sigma_c^{-\frac{1}{2}}(\Sigma_i+\Sigma_c)^{-1}\Sigma_c^{-\frac{1}{2}}\right]Y}}{\pi^p |\Sigma_c^{-\frac{1}{2}}(\Sigma_i + \Sigma_c)\Sigma_c^{-\frac{1}{2}}|} dY$$

(161)

The solution is obtained by calculating the eigenvalues $\lambda_1, \lambda_2, \lambda_3$ of the matrix $\Sigma_c^{-1/2}(\Sigma_i + \Sigma_c)\Sigma_c^{-1/2\dagger}$. This yields the result

$$\phi_\eta(jw) = \prod_{i=1}^{p} \frac{1}{(1-j\lambda_i w)} = \sum_{i=1}^{p} \frac{A_i}{(1-j\lambda_i w)}.$$

(162)

where the A_i are residues obtained by performing the partial fraction expansion. Since the eigenvalues are all positive, inverting the characteristic function yields the following PDF for random variable η:

$$f_\eta(\eta) = \sum_{i=1}^{p} \left(\frac{A_i}{\lambda_i}\right) \exp\left(-\frac{\eta}{\lambda_i}\right)$$

(163)

Next we will use of the formula for calculating the PDF of the ratio of two independent variables. If we have the ratio $y = N\eta/\delta$ then the PDF of y is obtained by calculating the integral

$$f_y(y) = \frac{1}{N} \int_0^\infty \delta \, f_\eta\left(\frac{y\delta}{N}\right) f_\delta(\delta) \, d\delta$$

(164)

where $f_\eta(\eta)$ and $f_\delta(\delta)$ are the PDFs of random variables η and δ, respectively.

For case (1), the numerator and denominator variables are both chi-square-distributed. Evaluating Equation (164) yields

$$f_y(y) = \frac{\Gamma(N+1)\,(N)^{(N-p+1)}}{\Gamma(p)\,\Gamma(N-p+1)} \frac{y^{(p-1)}}{(y+N)^{(N+1)}}$$

(165)

Thus, the detection statistic for this case has a PDF which is the F-Distribution [27]. False alarm probability for the detector is easily shown to be

$$P_{FA} = \frac{1}{\left(1+\dfrac{T}{N}\right)^N} \sum_{k=0}^{p-1} \binom{N}{k}\left(\frac{T}{N}\right)^k$$

(166)

where T is the detection threshold. For large N, this expression becomes

$$P_{FA} = e^{-T} \sum_{k=0}^{p-1} \frac{T^k}{k!}$$

(167)

The covariance estimate used in the adaptive PWF becomes exact for large N, and the algorithm reduces to the ideal PWF. Thus, Equation (167) is the corresponding PFA formula for the PWF.

For case 2, the numerator variable has a PDF which is a sum of three exponentials. Each exponential term is equivalent to a chi-square variable with 2 degrees of freedom. Omitting the details of the derivation, we obtain

$$f_y(y) = \sum_{i=1}^{p} A_i \frac{(N-p+1)(N\lambda_i)^{(N-p+1)}}{(y + N\lambda_i)^{(N-p+2)}}$$

(168)

Detection probability for the adaptive PWF is easily calculated using the above PDF. We obtain the result

$$P_D = \sum_{i=1}^{p} A_i \frac{1}{\left(1 + \dfrac{T}{N\lambda_i}\right)^{N-p+1}}$$

(169)

For large N, the expression for detection probability becomes

$$P_D = \sum_{i=1}^{p} A_i \exp\left\{-\frac{T}{\lambda_i}\right\}$$

(170)

For large N, the covariance estimate used in the adaptive PWF becomes exact and the algorithm reduces to the ideal PWF. Thus, Equation (170) is the corresponding P_D formula for the PWF.

12.10   PWF DETECTION PERFORMANCE PREDICTIONS

Figure 22 shows PWF detection performance for Gaussian target and clutter models. The curves shown are for T/C ratios of 0, 3, 6 and 10 dB; for comparison, the corresponding OPD detection performance curves are also shown. Recall that we showed earlier that PWF and OPD performance was nearly identical for non-Gaussian product-model targets and clutter (Figure 21); Figure 22 shows that, for Gaussian target and clutter models, the PWF again performs almost as well as the OPD.

If the clutter polarization covariance is adaptively estimated from local clutter, using the adaptive PWF, detection performance will depend upon the accuracy of the covariance estimate. In order to gain insight into the sensitivity of the adaptive PWF, we evaluated the detection performance of the algorithm using 16, 32, and 64 complex (HH, HV, and VV) clutter samples to estimate the
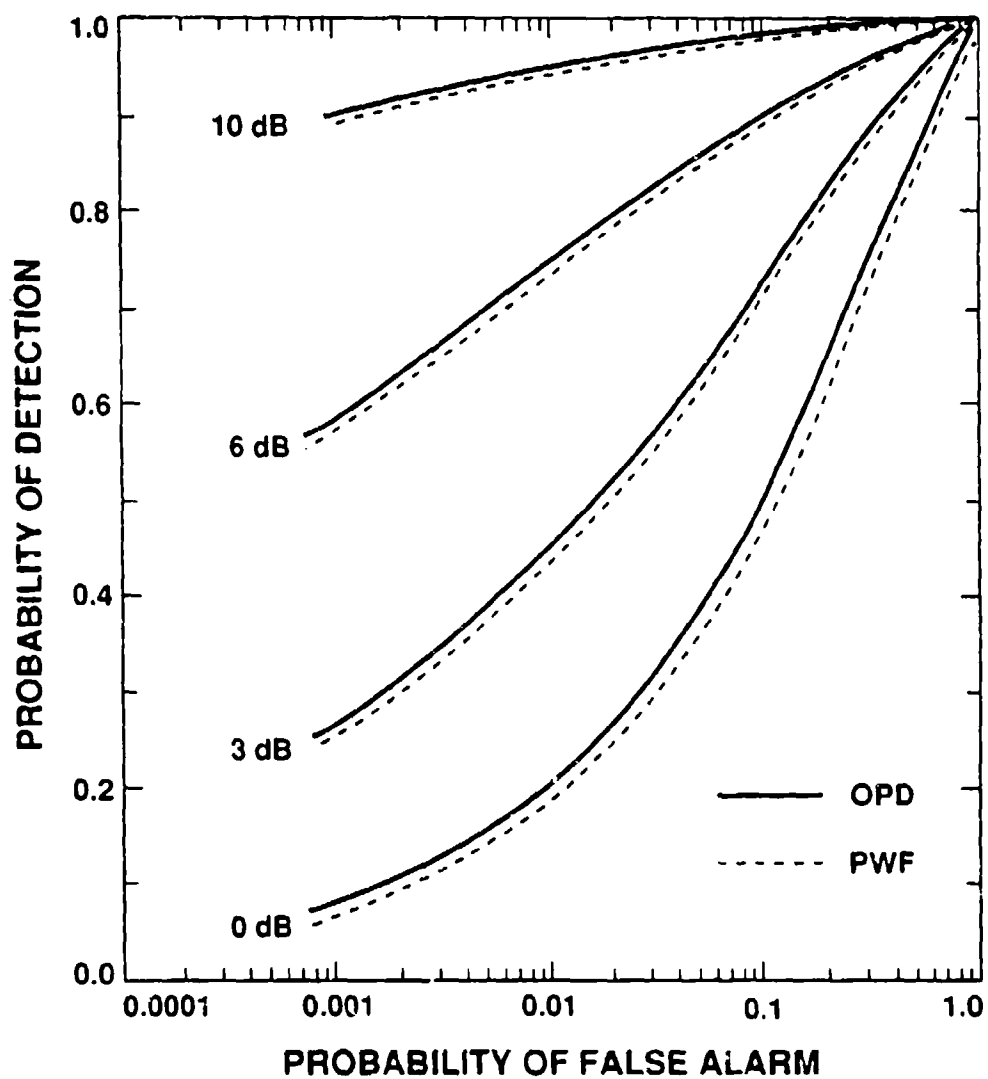
Figure 22. OPD and PWF detection performance versus
target-to-clutter ratio (Gaussian target and clutter models).

polarization covariance. The detection performance curves for these three cases are shown in Figure 23. Comparing the results of Figure 23 with the exactly known case (Figure 22) shows that only a small loss in detection performance (usually referred to as CFAR loss) is incurred when a reasonable number of independent clutter samples are used to estimate the polarization covariance (e.g., 64 samples). When only 16 independent samples were used to estimate the polarization covariance matrix, the CFAR loss was larger (about 2 dB).

In radar detection it is customary to characterize the performance of an adaptive CFAR detector (in this case the adaptive PWF) by using a set of ideal, fixed-threshold detection performance curves plus an additive CFAR loss which depends upon the number of clutter samples (N) used to estimate the clutter covariance. We evaluated CFAR loss (versus N) for the adaptive PWF by calculating the target-to-clutter ratio required to achieve $P_D = 0.5$ with $P_{FA} = 10^{-3}$ for two situations, (1) with Σ_c known exactly, and, (2) with Σ_c estimated. Figure 24 shows the loss (in dB) versus the number of independent clutter samples used to estimate $\hat{\Sigma}_c$. The CFAR loss is approximately 1 dB with N=24 and increases rapidly when fewer than 24 samples are used. At least 50 independent samples are required to reduce the CFAR loss to 0.5 dB.
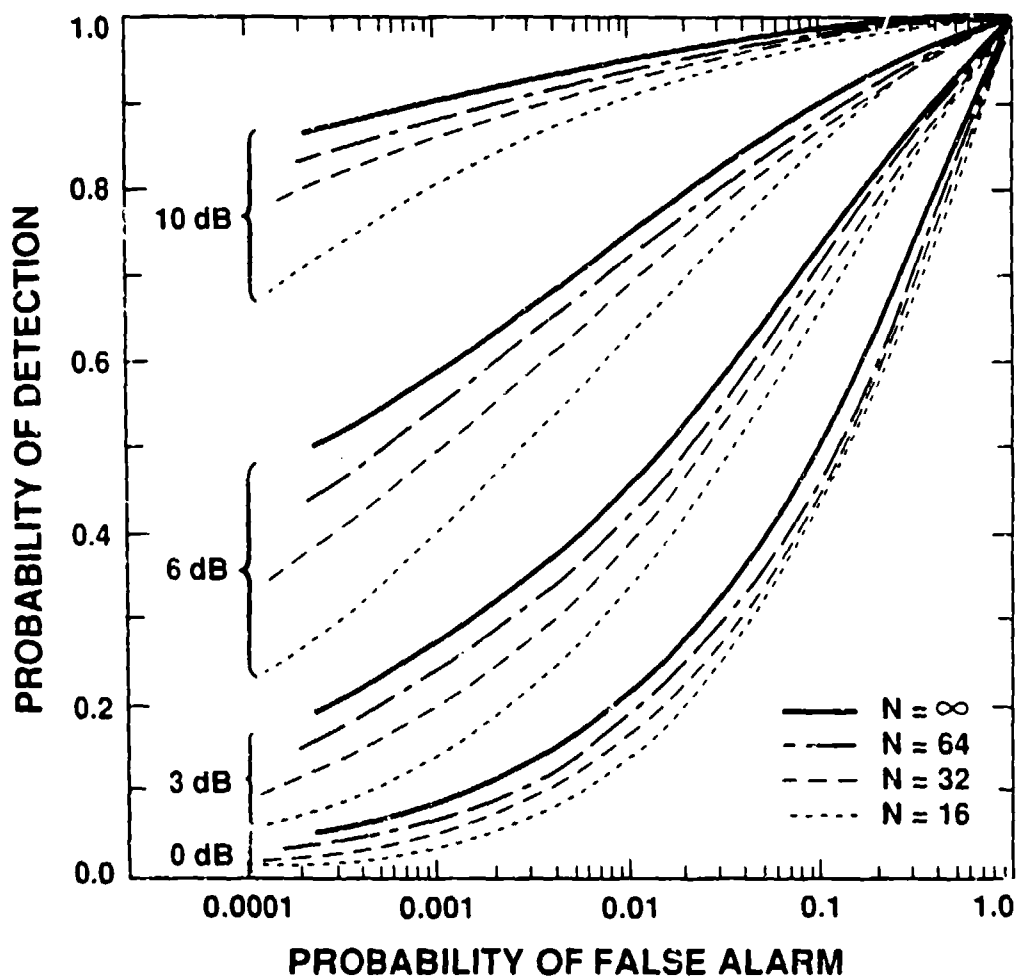
Figure 23. Detection performance of the adaptive PWF versus
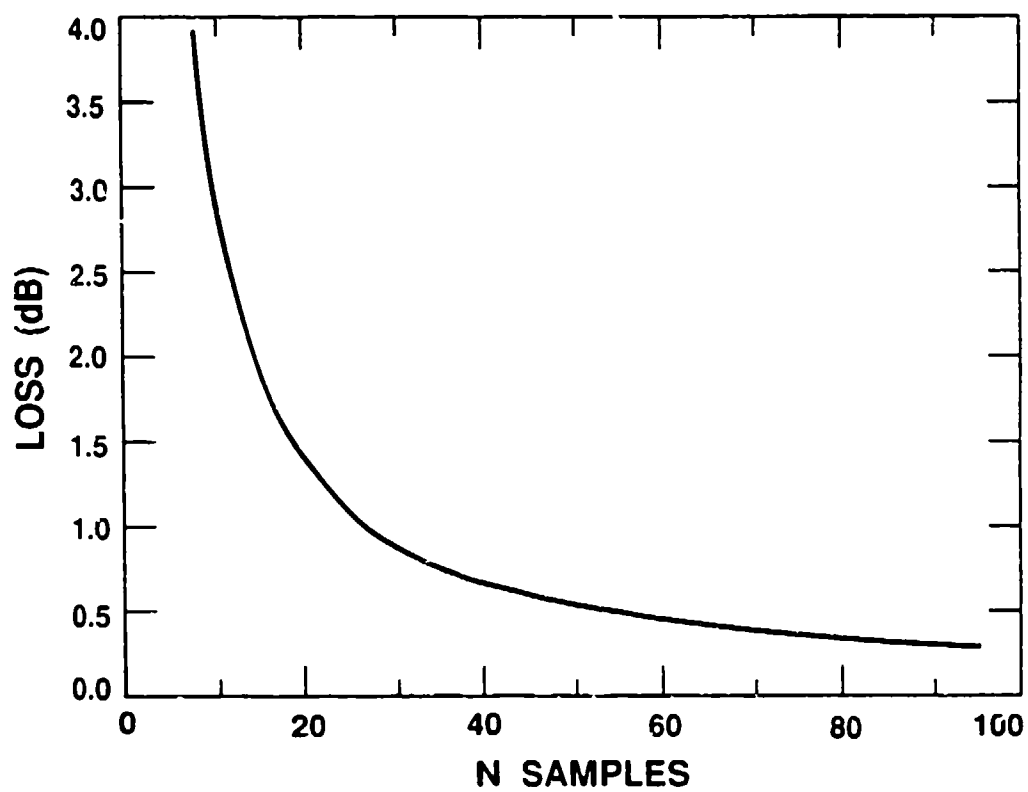target-to-clutter ratio (Gaussian target and clutter models).

Figure 24. CFAR loss (dB) versus N for the adaptive PWF.

13.0 SUMMARY AND CONCLUSIONS

This report summarizes a study of target detection, target classification, and radar imaging algorithms that use polarimetric radar data. A model which includes the effects of the spatial nonhomogeneity of ground clutter and the aspect angle variability of targets was developed, and then used to evaluate the performance of various detection, classification, and imaging algorithms.

Our target detection studies found that the additional information provided by the full PSM measurement, even when processed in an optimal fashion, did not aid significantly in target detection. That is, a radar which transmits and receives a single polarization (e.g., LL or HV) will obtain almost as good performance as the optimal polarimetric detector (OPD), which measures the full PSM. Furthermore, to achieve the additional performance improvement from the OPD, one must have a priori knowledge of the target and clutter polarization covariances, as well as the target-to-clutter ratio. When these covariances are not known, a single-polarimetric-channel detector (e.g., LL or HV) provides nearly optimal performance. Therefore, independent, multi-look, single-polarization algorithms appear to be the best approach to target detection.

Our target detectior studies showed that, when a single polarization was used, $|LL|^2$ (even-bounce) circular polarization provided slightly better performance than $|HV|^2$ or $|HH|^2$ (linear) polarizations. However, the clutter data base used in these studies was limited, and further study of this problem using various types of clutter (for example, snow clutter) will be necessary.

Once a target is detected, information contained in the PSM may be useful for classifying between target types (e.g., armored target versus truck). Our preliminary results indicate that, for classification to be effective, many independent looks at the target are required and the target-to-clutter ratio must be fairly high. This area will require further study using a variety of target types.

Another area in need of further investigation is the development of more realistic statistical target models. Some targets have different polarimetric properties at different aspect angles. Thus a more realistic statistical target model would be one which uses different covariance matrices to characterize a target at different aspect angles.

We derived the optimal method of processing the complex HH, HV, and VV elements of the PSM to minimize speckle in a polarimetric SAR image; the solution was shown to be the polarimetric whitening filter (PWF). For homogeneous clutter, this algorithm was shown to reduce the standard deviation-to-mean ratio by 4.8 dB (relative to that of single-polarimetric-channel data); this is 1.9 dB better than the span algorithm.

A comparison of the target detection performance of the OPD with PWF, span, and $|HH|^2$ detectors showed that the OPD and PWF gave comparable performance, and were significantly better than the span and $|HH|^2$ detectors.

Since the PWF (unlike the OPD) requires only the polarimetric covariance of the clutter, an adaptive PWF was implemented. This algorithm estimates the polarization covariance matrix from the local clutter, uses the estimated covariance to construct the minimum speckle image, and then tests for the presence of targets. This algorithm was found to produce detection performance comparable to that of the OPD.

ACKNOWLEDGMENTS

REFERENCES

1. V.L. Lynn, "HOWLS Radar Development," Millimeter Wave Radar, Ed. Stephen L. Johnson (Artech House, Inc, Dedham, MA, 1980).

2. L.M. Novak and F.W. Vote, "Millimeter Airborne Radar Target Detection and Selection Techniques," Proc. NAECON 1979 Conference, Dayton, OH, 15-17 May 1979.

3. L.M. Novak, M.B. Sechtin and M.J. Cardullo, "Studies of Target Detection Algorithms That Use Polarimetric Radar Data," Proc. 21st Asilomar Conference on Signals, Systems and Computers, Pacific Grove, CA. 2-4 November 1987.

4. R.M. Barnes, "Detection of a Randomly Polarized Target," PhD Thesis, Northeastern University, Department of Electrical Engineering (June 1984).

5. K. Fukunaga, Introduction to Statistical Pattern Recognition (Academic Press, New York, 1972).

6. J. Kong, A. Swartz, H. Yueh, L.M. Novak, and R. Shin, "Identification of Terrain Cover Using the Optimal Polarimetric Classifier," J. Electromagn. Waves Appl. Vol. 2, No. 2 (1988).

7. J. Cadzow, "Generalized Digital Matched Filtering," Proc. 12th Southeastern Symposium on System Theory," Virginia Beach, VA, 19-20 May 1980.

8. E. Jakeman and P. Pusey, "A Model for Non-Rayleigh Sea Clutter," IEEE. Trans. Antennas Propag. (November 1976).

9. D. Lewinski, "Nonstationary Probabilistic Target and Clutter Scattering Models," IEEE Trans. Antennas Propag. (May 1983).

10. J. Jao, "Amplitude Distribution of Composite Terrain Clutter and the K-Distribution," IEEE Trans. Antennas Propag. (October 1984).

11. I. Gradshteyn and I. Ryzhik, Table of Integrals, Series, and Products (Academic Press, New York, 1980).

12. K. Fukunaga and T. Krile, "Calculation of Bayes Recognition Error for Two Multivariate Gaussian Distributions," IEEE Trans. Comput. (March 1969).

13. L.M. Novak, "On the Sensitivity of Bayes and Fisher Classifiers in Radar Target Detection," Proc. 18th Asilomar Conference on Circuits, Systems, and Computers, Pacific Grove, CA, November 1984.

14. MACSYMA Reference Manual, Vol. 1, M.I.T., Cambridge, MA, 1983.

15. L.M. Novak and M.B. Sechtin, "On the Performance of Linear and Quadratic Classifiers in Radar Target Detection," Proc. 20th Asilomar Conference on Circuits, Systems, and Computers, Pacific Grove, CA, November 1986.

16. A. Oppenheim and A. Willsky, Signals and Systems (Prentice Hall, New Jersey, 1983), p. 772.

17. H. Yueh, A. Swartz, J. Kong, R. Shin, and L.M. Novak, "Bayes Classification of Terrain Cover Using Normalized Polarimetric Data," Journal of Geophysical Research, Vol 93, No. B12, 1988.

18. J.C. Dainty, "Laser Speckle and Related Phenomena," Topics in Applied Physics, Vol. 9, Springer Verlag, Herdelberg (1975).

19. H.A. Zebker, J.J. Van Zyl, and D.N. Held, "Imaging Radar Polarimetry from Wave Synthesis," J. Geophysics Research, Vol. 9 (1987), pp. 683-701

20. J. Lee, "Speckle Analysis and Smoothing of Synthetic Aperature Radar Images," Computer Graphics and Image Processing, Vol. 17, pp. 24-32, 1981.

21. C.J. Oliver, "Correlated K-distributed Clutter Models, Optica Acta, Vol. 32, No. 12, pp. 1515-1547, 1985.

22. S. Watts and K.D. Ward, "Spatial Correlation in K-distributed Sea Clutter," IEEE Proceedings, Vol. 13, Pt. F, No. 6, pp. 526-532, Oct. 1987.

23. C.J. Oliver and R.J.A. Tough, "On the Simulation of Correlated K-distributed Random Clutter," Optica Acta, Vol.33, No. 3, pp. 223-250, 1986.

24. L.M. Novak, "Generating Correlated Weibull Random Variable for Digital Simulations," Proceedings IEEE Decision and Control Conference, San Diego, CA. 1973.

25. W.A. Czarnecki, "Generation of Multi-Dimensional Stationary Discrete Random Signals With Given Probability Density and Autocorrelation Functions," IEEE ASSP Spectrum Estimation Workshop, No. 2, pp. 136-138, Tampa, FL. November 10-11, 1983.

26. G. Marsaglia, "A Note on the Construction of a Multivariate Normal Sample", I.R.E. Trans. Info. Theory, VOL. IT-3, June 1957.

27. T.W. Anderson, An Introduction To Multivariate Statistical Analysis, Wiley, New York, NY 1962.

APPENDIX

This appendix provides the solution for the calculation of the eigenvalues of the matrix product $\Sigma_3(\Sigma_1^{-1} - \Sigma_2^{-1})$. Equivalently, we may simultaneously diagonalize the following two matrices:

$$\Sigma_1^{-1} - \Sigma_2^{-1} \;\rightarrow\; \Lambda \tag{A-1}$$

$$\Sigma_3^{-1} \;\rightarrow\; I \tag{A-2}$$

When this is done, the diagonal elements of the matrix Λ are the desired eigenvalues. These eigenvalues are required in the performance evaluation of the optimal polarimetric detector. In this appendix, we assume the polarimetric measurement vector to be a real, 6-dimensional zero-mean, Gaussian vector

$$\underline{X} = \left(HH_I, HH_Q, HV_I, HV_Q, VV_I, VV_Q\right)' \tag{A-3}$$

with real 6×6 covariances Σ_1, Σ_2, Σ_3 of the form

$$\Sigma_i = \frac{\sigma_{HH}}{2}
\left[
\begin{array}{cc|cc|cc}
1 & 0 & 0 & 0 & \sqrt{\gamma}\,\mathrm{Re}(\rho) & -\sqrt{\gamma}\,\mathrm{Im}(\rho) \\
0 & 1 & 0 & 0 & \sqrt{\gamma}\,\mathrm{Im}(\rho) & \sqrt{\gamma}\,\mathrm{Re}(\rho) \\
\hline
0 & 0 & \varepsilon & 0 & 0 & 0 \\
0 & 0 & 0 & \varepsilon & 0 & 0 \\
\hline
\sqrt{\gamma}\,\mathrm{Re}(\rho) & \sqrt{\gamma}\,\mathrm{Im}(\rho) & 0 & 0 & \gamma & 0 \\
-\sqrt{\gamma}\,\mathrm{Im}(\rho) & \sqrt{\gamma}\,\mathrm{Re}(\rho) & 0 & 0 & 0 & \gamma
\end{array}
\right] ; \; i = 1, 2, 3 \tag{A-4}$$

This solution is general in that we have assumed the correlation parameter ρ, to be complex. The real 6×6 matrix has 3 eigenvalues, each of multiplicity two. We present the analytical solution for these eigenvalues λ_1, λ_2, λ_3 in the following FORTRAN subroutine.

```fortran
        subroutine eigvals(e1,g1,r1,s1,e2,g2,r2,s2,e3,g3,r3,s3)

c------------------------------------------------------------------------
c
c       This program generates the eigenvalues of an input matrix in
c       the form (sigma.3)x(sigma.1.inverse - sigma.2.inverse) where
c       sigma.1, sigma.2, and sigma.3 are all 6x6 covariance matrices
c       whose elements are determined by the parameters contained in
c       the input data file.  The equations for the eigenvalues were
c       obtained using MACSYMA.
c
c------------------------------------------------------------------------

        parameter(inlu=12,outlu=21)

c       DATA STRUCTURES
        double precision e1,e2,g1,g2,s1,s2
        double precision l1,l2,l3,l4,l5,l6,lam(3)
        double precision a1,a2,a3,b1,b2,b3,den1,den2
        double precision e3,g3,s3
        complex*16 r1,r2,r3

c       CHARACTER STRINGS
        character*50 infil,filname,gettext

c------------------------------------------------------------------------

        a1=(g1**0.5)*dreal(r1)
        b1=(g1**0.5)*dimag(r1)
        a2=(g2**0.5)*dreal(r2)
        b2=(g2**0.5)*dimag(r2)
        a3=(g3**0.5)*dreal(r3)
        b3=(g3**0.5)*dimag(r3)

        den1=(g1-(b1**2)-(a1**2))*s1
        den2=(g2-(b2**2)-(a2**2))*s2

        x=(g1/den1)-(g2/den2)
        y=(a2/den2)-(a1/den1)
        z=(b2/den2)-(b1/den1)
        v=(1/den1)-(1/den2)
        w=(1/(e1*s1))-(1/(e2*s2))

c-------Compute the eigenvalues of the matrix
c       (sigma.3) x (sigma.1.inverse - sigma.2.inverse)

        l1=(s3*(x-sqrt(g3*(4*z**2+4*y**2-2*v*x)+a3**2*(4*v*x-4*z**2)+a3*
     1   (8*b3*y*z+4*x*y+4*g3*v*y)+b3*(4*x*z+4*g3*v*z)+b3**2*(4*v*x-4*
     2   y**2)+x**2+g3**2*2*v**2))+2*b3*s3*z+2*a3*s3*y+g3*s3*v)/2.0


        l2=(s3*(sqrt(g3*(4*z**2+4*y**2-2*v*x)+a3**2*(4*v*x-4*z**2)+a3*
     1   (8*b3*y*z+4*x*y+4*g3*v*y)+b3*(4*x*z+4*g3*v*z)+b3**2*(4*v*x-4*
     2   y**2)+x**2+g3**2*2*v**2)+x)+2*b3*s3*z+2*a3*s3*y+g3*s3*v)/2.0

        l3=e3*s3*w

        lam(1)=l1
        lam(2)=l2
        lam(3)=l3
```

REPORT DOCUMENTATION PAGE			Form Approved OMB No. 0704-0188

1. AGENCY USE ONLY *(Leave blank)*	2. REPORT DATE 6 November 1989	3. REPORT TYPE AND DATES COVERED Project Report

4. TITLE AND SUBTITLE

Algorithms for Optimal Processing of Polarimetric Radar Data

5. FUNDING NUMBERS

6. AUTHOR(S)

Leslie M. Novak, Michael B. Sechtin, and Michael C. Burl

7. PERFORMING ORGANIZATION NAME(S) AND ADDRESS(ES)

Lincoln Laboratory, MIT
P.O. Box 73
Lexington, MA 02173-9108

8 PERFORMING ORGANIZATION REPORT NUMBER

TT-73

9. SPONSORING/MONITORING AGENCY NAME(S) AND ADDRESS(ES)

Defense Advanced Research Projects Agency
1400 Wilson Blvd.
Arlington, VA 22209

10. SPONSORING/MONITORING AGENCY REPORT NUMBER

ESD-TR-89-236

11. SUPPLEMENTARY NOTES

12a. DISTRIBUTION/AVAILABILITY STATEMENT

Approved for public release; distribution is unlimited.

12b. DISTRIBUTION CODE

13. ABSTRACT *(Maximum 200 words)*

This report describes algorithms that make optimal use of polarimetric radar information to detect and classify targets in a ground clutter background. The optimal polarimetric detector (OPD) is derived; this algorithm processes the complete polarization scattering matrix (PSM) and provides the best possible detection performance from polarimetric radar data. Also derived is the best linear polarimetric detector, the polarimetric matched filter (PMF); the structure of this detector is shown to be related to simple polarimetric target types. Finally, the polarimetric whitening filter (PWF) is derived; this constant false alarm rate (CFAR) detector provides a simple alternative to the OPD for detecting targets in clutter. New K-distributed polarimetric target and clutter models are described; these models are used to predict the performance of the OPD, the PMF, and the PWF. The performance of these three algorithms is compared with that of simpler detectors that use only amplitude information to detect targets. The ability to classify target types by exploiting differences in polarimetric scattering properties is also discussed.

14. SUBJECT TERMS

polarimetric radar	clutter models	polarimetric matched filter
target detection	optimal polarimetric	target models
target classification	detector	

15. NUMBER OF PAGES
108

16. PRICE CODE

17. SECURITY CLASSIFICATION OF REPORT Unclassified	18. SECURITY CLASSIFICATION OF THIS PAGE Unclassified	19. SECURITY CLASSIFICATION OF ABSTRACT Unclassified	20. LIMITATION OF ABSTRACT None